Mechanisms of Neuronal Activity-Dependent Transcription

Mechanisms of Neuronal Activity-Dependent Transcription

A dissertation presented

by

Nicholas Regis DeStefino

to

The Department of Neurobiology

in partial fulfillment of the requirements

for the degree of

Doctor of Philosophy

in the subject of

Neurobiology

Harvard University

Cambridge, Massachusetts

March 2019

Dissertation Advisor: Jesse Gray Nicholas DeStefino

Mechanisms of Neuronal Activity-Dependent Transcription

Abstract

Experience-dependent neural activity initiates cascades of activity-regulated gene expression that produce long-lasting changes in the adult brain. Different patterns of activity can produce opposing synaptic changes that each require transcription, but whether these different patterns of activity produce distinct programs of ARG transcription is not known. We addressed this question in Chapter 2, where we find that in both *in vivo* and *in vitro* studies, brief activity selectively induces a subset of the activity-regulated gene program that corresponds to the initial, rapid wave of transcription that is induced by sustained activity. This selective transcriptional response to brief activity requires MAPK/ERK signaling, which functions to mediate the rapid recruitment of RNAPII to promoters. Genes induced by brief activity are further differentiated from other inducible genes by a baseline open-chromatin state, higher levels of promoter-occupied RNAPII, binding of the MAPK-sensitive transcription factor SRF, and proximity to rapidly activated enhancers. These rapid enhancers are occupied at baseline by SRF and activate in response to brief depolarization by increasing histone acetylation and eRNA transcription, as detected by eRNA-sequencing and H3K27ac ChIP-seq. MAPK/ERK is required for eRNA synthesis but not increases in enhancer histone acetylation, suggesting that MAPK/ERK acts on a specific stage of enhancer activation and implicating MAPK/ERK-dependent eRNA synthesis in the transcriptional response to brief activity. Overall, these results identify changes in the epigenome that enable different neuronal activity patterns to induce distinct gene expression programs. In Chapter three, we further evaluate candidate transcriptional regulatory mechanisms

differentiating differently patterned genes. In using small-molecule inhibitors to test the contribution of DNA-damage response proteins to activity-dependent transcription, we find that NMS-873, an allosteric inhibitor of the AAA ATP-ase, p97/VCP, acts acutely and selectively to inhibit stimulus-dependent transcription. This transcription inhibition proceeds through a mechanism that is upstream of RNAPII initiation. We next generate and validate inhibitor-resistant mutant cell lines to test the on-target activity of NMS-873. Experiments in these cell lines suggest that NMS-873 suppresses transcription through an off-target mechanism of action.

Table of Contents

List of Figures

Attributions

Chapter 2:

Modified from:

> Tyssowski, K. M.*, DeStefino, N. R.*, Cho, J. H., Dunn, C. J., Poston, R. G., Carty, C. E., Jones, R.D., Chang, S.M., Romeo, P., Wurzelmann, M.K., Ward, J.M., Andermann, M.L., Saha, R.N.#, Serena, M.D.#, Gray, J. M.# (2018). Different Neuronal Activity Patterns Induce Different Gene Expression Programs. *Neuron, 98*(3), 530-546 e511. doi:10.1016/j.neuron.2018.04.001 , * denotes co-equal author, # denotes co-senior author
>
> K.M.T. and J.M.G originally designed the part of the study using KCl/visual stimulation. RNS. and S.M.D. separately designed the bicuculline experiments. K.M.T. performed and analyzed all RNA-seq experiments, H3K27ac ChIP-seq, ERK western blotting, high-throughput qPCR, and enhancer RT-qPCR, and analysis of published single-cell sequencing and ChIP-seq data. N.R.D. performed and analyzed RNA polymerase ChIP-seq, p-Elk1 western blotting, triptolide experiments, STO-609 qPCR. J.-H.C. performed visual stimulation experiments. R.N.S., P.R., and M.K.W. performed the bicuculline experiments including Nanostring and western blots of nuclear extracts. J.M.W. with K.M.T. analyzed the Nanostring data. S.M.C. performed 11e experiments. R.D.J. performed the luciferase assay. K.M.T. and J.M.G. wrote the manuscript with input from NRD and other authors.

Chapter 3: N.R.D. performed experiments and analysis.

Chapter 1: Introduction

One of the most remarkable aspects of the adult brain is its capacity to undergo structural and functional plasticity in response to sensory experiences. This plasticity underlies the ability to form new long-term memories and to adaptively respond to new demands imposed by the environment. The cellular mechanisms that produce the long-term plasticity that shapes the development and function of neural circuits require activity-dependent transcription and the translation of new protein products (Leslie & Nedivi, 2011; West & Greenberg, 2011; Whitney et al., 2014). Underscoring the importance of activity-dependent transcription to human disease, mutations in the genes encoding many molecular components of this transcriptional process (e.g. the L-type calcium channel and CREB-binding protein, CBP) are known genetic causes of human neuropsychiatric and developmental disorders of cognitive (Ebert & Greenberg, 2013; Ripke et al., 2013).

Since the initial discovery that the Immediate Early Gene (IEG) Fos is induced by neural depolarization (Greenberg, Greene, & Ziff, 1985; Greenberg & Ziff, 1984; Greenberg, Ziff, & Greene, 1986), it has become clear that neural activity induces the expression of dozens of other IEGs and hundreds of other activity-regulated genes. Like *Fos,* many, but not all, IEGs are themselves transcription factors that regulate the subsequent induction of the downstream genes—collectively referred to as delayed response genes (DRGs) (West & Greenberg, 2011). The number and types of genes that are activated in response to changes in neuronal activity are of critical importance, then, to specifying the types of long-term changes that neurons undergo. The spatial and temporal activity of these genes—their patterns of activation—is governed by the activity of enhancers—regulatory DNA loci that are positioned in *cis* to target gene promoters.

This work addresses a number of unknown questions concerning the mechanisms by which the neuronal genome responds to changes in activity by initiating gene expression. Specifically, this work first tests the hypothesis that the neuronal genome possesses the ability to transduce different patterns of neuronal activity into different gene expression programs. Unique activity-regulated programs could theoretically coordinate unique forms of adaptive changes to neuronal circuits. We next interrogate the molecular mechanisms that endow the neuronal genome with this capability of transducing patterned activity into patterned gene expression responses. Specifically, we study whether gene programs are specified through the activation of subsets of enhancers. We uncover a signaling mechanism that defines a set of rapidly activating enhancers and genes, and we explore the mechanisms of enhancer and promoter activation that are regulated by this signaling mechanism. We next investigate the mechanisms governing the duration of activation of the rapidly expressed IEGs. A defining feature of IEGs, in contrast to DRGs, is their rapid transcriptional down-regulation in the continued presence of the activating stimulus. Early nuclear-run on experiments, which precisely monitor active transcription, demonstrated that IEG transcription ceases fully and rapidly after stimulus onset—in some cases returning to basal levels within as quickly as thirty minutes (Rivera, Sheng, & Greenberg, 1990; Thompson, Ginty, Bonni, & Greenberg, 1995). Despite these early observations, there have been few comprehensive studies of negative regulatory mechanisms of inducible gene expression (Amit et al., 2007) and the specific mechanisms that deactivate IEGs remain unknown**.** This IEG-specific negative transcriptional regulation has critical functional cellular consequences, as the concentration of IEG protein products specifies the delayed-response genes that coordinate long-term cellular changes (Yuan et al., 2009). Moreover, the precise levels of certain IEG protein products, such as ARC, (Shepherd et al., 2006; Smith-Hicks et al., 2010) determine the

strength of synaptic connections within neural networks. Therefore, deactivation of IEG expression is critically important for shaping cellular plasticity.

The initial discovery that extracellular stimuli initiates the rapid induction of transcription was made over thirty years ago in fibroblasts that were treated with growth factors (Greenberg & Ziff, 1984). This work soon led to observations demonstrating the importance of this immediate early gene transcription to neuronal development and activity. Nerve growth factor (NGF) and epidermal growth factor (EGF) were independently shown to induce *Fos* immediate-early gene (IEG) transcription in neuroendocrine PC12 cells (Greenberg et al., 1985). And cholinergic activation of nicotinic acetylcholine receptors was shown to initiate calcium-dependent immediate early gene expression (Greenberg, Ziff, et al., 1986) raising the possibility that neuronal activity operates to initiate gene expression changes *in vivo.*

Since this time, an enormous amount of work has been performed to uncover the mechanisms allowing neurons to initiate gene expression changes in response to activity and to understand the functional relevance of this transcription to neuronal plasticity. It is now well accepted that much of the synaptic activity-induced gene expression arises from calcium signaling (West & Greenberg, 2011). Specifically, synaptic activity leads to neuronal depolarization and stimulates the influx of calcium ions through somatic L-type voltage dependent calcium channels. This calcium subsequently activates cytoplasmic and nuclear signaling kinases that then produce changes in gene expression by activating transcription factors. Two well-studied signaling kinase pathways that transduce neuronal depolarization into gene expression changes are the Calcium-Calmodulin Activated Kinases (CaMKs) and the MAPK/ERK kinase pathways, both of which

phosphorylate and activate a large number of transcription factors, including CREB and SRF (Greer & Greenberg, 2008). A third signaling enzyme is the phosphatase Calcineurin, which is activated by both Ca2+ and by CAMKII and acts to dephosphorylate and activate a number of neuronal transcription factors, such as NFATc and MEF2 (Crabtree, 2001; Greer & Greenberg, 2008).

Since these initial observations concerning the activity-dependent expression of *Fos*, it has become clear that neuronal depolarization induces the expression of a large and complex network of transcription factors (TFs) then then specify the expression of particular downstream genes. Numerous studies have led to the identification of hundreds of neuronal activity-regulated genes(West & Greenberg, 2011). The expression of these hundreds of genes is best characterized by two core phases of gene expression: An initial rapid and transient induction of approximately 50 immediate-early genes (IEGs)(Saha & Dudek, 2013) and a subsequent, delayed phase of prolonged transcription of hundreds of delayed response genes (DRGs). IEGs are typically described as being primary response genes because their stimulus-dependent induction does not require protein translation. In contrast, DRGs include both a set of delayed primary genes (dPRGs) that also do not require new protein synthesis for their transcription and a set of delayed secondary-response genes that require stimulus-dependent protein synthesis for their induction.

The functional necessity of distinct sets of early and late genes is unknown, but many of the immediate-early genes are transcription factors that are thought to coordinate the expression of the downstream, delayed genes. This complexity might hardwire flexibility within the inducible gene expression network that allows for cell-type specific inducible gene expression responses

(Ramirez-Carrozzi et al., 2009; Spiegel et al., 2014) and for stimulus-specific patterns of gene expression changes (Dolmetsch, Lewis, Goodnow, & Healy, 1997; Sheng, Fields, & Nelson, 1993).

1.1 Enhancer Regulatory Mechanisms of Inducible Expression

Considerable attention has been applied to understanding the DNA regulatory elements that regulate inducible gene expression. An emerging consensus is that enhancers specify the temporal and spatial properties of these gene expression cascades. The discovery that enhancers can be identified by the presence of the mono-methylation of the N-terminal residue of H3K4 (H3K4me) and, in particular, that they may be distinguished from other active promoter elements by the relative absence of H3K4-me3 (trimethylation) (Heintzman et al., 2007) has unleashed numerous studies uncovering cell-type and -specific enhancers.

Two additional key insights have provided the tools to comprehensively identify active enhancers in mammalian cells. These include the recent discovery that H3K27 acetylation (H3K27ac) denotes active enhancer elements (Rada-Iglesias et al., 2011) and the discovery of genome-wide polymerase-II driven transcription of enhancer RNAs (eRNAs) at active enhancers (T. K. Kim et al., 2010). This has allowed for the global annotation of active enhancers in neurons using ChIP-seq, by mapping the genome-wide distributions of histone acetylation and methylation, as well as the binding of key activity-regulated transcription factors, including CREB-Binding Protein (CBP), the immediate-early gene product NPAS4, SRF, and FOS (T. K. Kim et al., 2010; Malik et al., 2014).

Together, this published work has characterized a large-set of distal-acting enhancers that activate in response to neuronal depolarization, capturing information about enhancer activation occurring two hours after the onset of continuous depolarization. These results therefore provide a snapshot of the active regulatory elements in neurons occurring in response to neuronal depolarization. Given the clear complexity of the activity-dependent gene expression cascades and the fact that the transcription of many IEGs has ended by 60-120 minutes of stimulation, there are likely additional enhancers acting outside this time-point to regulate gene expression. It is possible that enhancers are the targets of negative regulatory mechanisms causing the delayed transcriptional down-regulation of IEGs in response to prolonged depolarization, Recent results demonstrate the functional importance of eRNAs to stimulus-dependent enhancer activity (Hah et al., 2011; Lam, Li, Rosenfeld, & Glass, 2014; Wang et al., 2011), suggesting that transcriptional processes at some enhancers have a direct impact on mRNA production. This is also evidenced by observations that eRNAs may release paused proximal RNA Pol-II at immediate early gene promoters (Schaukowitch et al., 2014), suggesting that eRNAs regulate a critical step in the induction of IEGs (Saha et al., 2011; Schaukowitch et al., 2014). Moreover, work in primary macrophages has shown that TLR4 signaling activates transcriptional repressors which bind to distal enhancer sequences to repress eRNA transcription and that this repression functionally reduces nearby mRNA transcription (Lam et al., 2013). These results provide proof of principle evidence that some enhancers are the targets of stimulus-dependent negative regulatory mechanisms. This raises the possibility that prolonged neuronal depolarization acts to repress subsets of neuron-specific enhancers and that this repression underlies the transcriptional repression of nearby target genes. This is perhaps supported by the observation that the induction of eRNAs at neuronal IEG enhancers for *Arc* and *Gadd45b* declines after approximately sixty

minutes, suggesting that the activity of these enhancers wanes under prolonged stimulation (Schaukowitch et al., 2014).

1.2 Transcriptional Regulatory Differences between IEGs and DRGs

Much of the work that has addressed the mechanistic basis for these two temporal waves of expression has been studied in mouse macrophages and mouse embryonic fibroblasts and has focused on the architecture of promoters from each gene class(Escoubet-Lozach et al., 2011; Ramirez-Carrozzi et al., 2009; Tullai et al., 2007). One possible framework for understanding the differences between immediate and delayed responses is provided by studies of LPS-driven activation of TLR4-receptor signaling in mouse macrophages. In these studies, IEG promoters were found to have higher CpG content and lower nucleosomal occupancy compared to DRG promoters. Correspondingly, only DRG promoters required the recruitment of specialized transcription factors to remodel these nucleosomes for proper stimulus-dependent activation (Ramirez-Carrozzi et al., 2009). Conceptually, this is consistent with parallel observations that only primary-response genes have preassembled RNA polymerase II (Pol-II) positioned at their core promoters under basal conditions(Escoubet-Lozach et al., 2011; Foster, Hargreaves, & Medzhitov, 2007; Gilmour & Lis, 1986; Hargreaves, Horng, & Medzhitov, 2009; Saha & Dudek, 2013; Saha et al., 2011). Together, these results may support a model in which core promoters differentiate IEGs from DRGs, suggesting that they may be candidate sites for the negative regulation that rapidly deactivates IEG expression. Little of this work, though, has examined differences in the genomic architectures of enhancers regulating the two classes of genes—although distal enhancers are known to show enrichment for similar stimulus-dependent transcription factor motifs as the IEGs (Ghisletti et al., 2010). None of this work has examined

differences in the sensitivity of these different classes of promoters and their proximal enhancers to different patterns of neuronal activity.

1.3 Rapid Transcriptional Shut-Off of Immediate Early Genes

A defining feature of immediate-early genes is their rapid transcriptional down-regulation in the continued presence of the activating stimulus (Rivera et al., 1990). Nuclear run-on experiments, which quantify ongoing transcription by using radiolabeling of actively RNAPII complexes, have demonstrated that depolarization-dependent transcription of IEGs is rapidly down-regulated soon after stimulus onset. Specifically, while transcription of the *Fos* gene is initiated within 15 minutes of depolarization, it then returns fully to baseline, lowly detectable levels of transcription after sixty minutes of depolarization (Rivera et al., 1990). Early work on *FOS* suggested that its transcriptional down-regulation was initiated, in part, by the binding of the newly-synthesized FOS to an auto-regulatory AP-1 binding site nearby the serum response element in the proximal *FOS* promoter(Sassone-Corsi, Sisson, & Verma, 1988). However, follow up work in 3T3 cells failed to demonstrate AP-1 binding to this site and demonstrated the sufficiency of the proximal 14bp core serum-response element (SRE)—known to bind SRF—in conferring both the rapid induction and rapid down-regulation properties of transcription to the *FOS* gene and to the human *B-GLOBIN* gene in a transfected plasmids(Rivera et al., 1990). These results suggest that the mechanism of transcriptional de-activation may at the *cis*-regulatory level be inseparable from the mechanism of transcriptional activation. They also implicate SRF, a transcription factor enriched at IEGs compared to DRGs (T. K. Kim et al., 2010), in the negative regulation of this gene class.

Since this time, there have been few comprehensive studies of negative regulatory mechanisms on inducible gene expression. One such study was performed in human HeLa cell lines treated with epidermal growth factor (EGF), and this work provides a conceptual framework for understanding how cells terminate the inducible responses to environmental stimuli. Specifically, Amit *et al.* used microarrays to profile the genes that are induced in response to EGF in the presence or absence of protein synthesis inhibitors and observed that genes with peak mRNA inductions occurring with delayed kinetics are enriched for putative negative regulators—including protein products that negatively regulate signaling pathways, transcription, and mRNA stability (Amit et al., 2007). EGF therefore initiates a stimulus-specific program of gene expression that functions via multiple mechanisms to negatively regulate the transcription of immediate early genes. These results are consistent with earlier observations that hypothesized that transcriptional down-regulation of inducible genes is achieved via the actions of newly synthesized protein products(Greenberg, Hermanowski, & Ziff, 1986). A number of early studies demonstrated that the transcriptional time course of immediate early gene induction could be extensively prolonged by the application of protein synthesis inhibitors, such as cyclohexamide and anisomycin (Edwards & Mahadevan, 1992; Lau & Nathans, 1987). Protein synthesis inhibitors were found to produce 'superinduction,' or the prolonged and accelerated induction, of immediate early genes when applied to cells that also receive other types of stimuli, such as treatment with serum. These results suggested that stimulation activates the formation of a newly translated protein product or products that subsequently play critical roles in terminating the stimulus-induced transcriptional response. Additional work suggested that these repressive mechanisms involve the actions of labile proteins, as treatment with cycloheximide was sufficient to induce expression from an SRE (Subramaniam, Schmidt, Crutchfield, & Getz, 1989)

and was shown to independently activate IEG expression, such as *FOS* and *JUN* family members, in the absence of serum stimulation (Cochran, Reffel, & Stiles, 1983; Edwards & Mahadevan, 1992; Hazzalin, Cuenda, Cano, Cohen, & Mahadevan, 1997; Mahadevan & Edwards, 1991; Wall et al., 1986). However, this original interpretation is also complicated by the observation that multiple other effects of these drugs—other than intended inhibition of new protein synthesis—are likely to contribute to the prolonged IEG mRNA time course. For example, translation inhibition stabilizes mRNAs by a still-unknown mechanism (Edwards & Mahadevan, 1992; Lau & Nathans, 1987) and two protein synthesis inhibitors, anisomycin and cyclohexamide, activate nuclear signaling pathways and transcription at concentrations below those that are required to block translation (Edwards & Mahadevan, 1992; Hazzalin et al., 1997). Therefore, the prolonged kinetics (i.e. superinduction) of IEGs in response to translational inhibitors may be a consequence of (1) increased mRNA stability, (2) the loss of labile translated transcriptional repressors, or (3) pharmacological activation of signal transduction cascades (*e.g.,* MAPKs).

One possible model then for the transcriptional inactivation of immediate early genes is that these loci are restored to their pre-stimulus repressed status, either by the negative regulation of specific signaling pathways that function to eliminate trans-activators or by the recruitment of negative regulators to these DNA loci. The pre-stimulus transcriptional regulation of immediate early gene promoters has been studied for select IEGs in neurons. The *FOS* IEG promoter is bound, at least to some extent, by Pol-II (Qiu & Ghosh, 2008; Saha et al., 2011) in a proximally paused position which prevents productive elongation through the gene body (Saha et al., 2011; Schaukowitch et al., 2014). This quiescent state may be maintained by the presence of HDACs,

which at *FOS* are recruited to the SRF-ELK1 heterodimer at the SRE and to the SP1 transactivator by a retinoblastoma (Rb) –BRG1-CREST nucleosomal remodeling complex (Qi and Ghosh 2008). Following activation of calcium-dependent signaling pathways, activated Calcineurin has been shown to release the HDACs allowing for IEG induction (Qi and Ghosh 2008). Thus, it is possible that the rapid transcriptional down-regulation of IEGs is achieved by returning promoters or other regulatory regions to their basal state. This model does not rule out an involvement of other regulatory regions in restoring the promoter to a quiescent state nor does it rule out the involvement of other, activity-induced HDACs from participating in this negative regulation.

Discovery of basally paused RNAPII and permissive chromatin states at IEG, but not DRG promoters suggests that promoters may coordinate differences between the transiently expressed IEGs and persistently expressed DRGs. However, an alternate hypothesis is that similarly, different classes of enhancers exist to coordinate the transcriptional downregulation of IEGs in response to prolonged depolarization. Consistent with the key function of enhancers in driving cascades of mRNA production is the recent genome-wide observation that transcription at enhancers precedes the transcription of mRNAs during the development of numerous cell types under diverse biologic stimuli (Agalioti et al., 2000). The specific hypothesis that enhancers coordinate the downregulation of IEGs is supported by (i) the previous identification of a *Fos* promoter proximal enhancer that functions to regulate both rapid induction and downregulation (Rivera et al., 1990) and (ii) recent observations that enhancer RNAs (eRNAs) produced at distal neuronal IEG enhancers for *Arc* and *Gadd45b* decline in abundance after approximately sixty minutes, suggesting that the activity of these enhancers wanes under prolonged stimulation

(Schaukowitch et al., 2014).

This eRNA decline may well be consequential. Numerous recent studies have demonstrated the functional importance of eRNA transcription (Hah et al., 2011; Kaikkonen et al., 2013; Lam et al., 2014; Wang et al., 2011) and the eRNA transcripts (Lam et al., 2013; Li et al., 2013; Melo et al., 2013; Mousavi et al., 2013) to stimulus-dependent enhancer activity (Hah et al., 2011; Lam et al., 2014; Wang et al., 2011), demonstrating that the transcriptional processes occurring at some enhancers have a direct impact on mRNA production. In fact, some appear to be required to release paused proximal RNA Pol-II at IEG core promoters(Schaukowitch et al., 2014), suggesting that eRNAs regulate the critical regulatory step of IEG induction(Saha et al., 2011; Schaukowitch et al., 2014). Moreover, recent work in LPS-treated macrophages has revealed the existence of transcriptional repressors that downregulate mRNA expression primarily by binding to distal enhancers to repress eRNA transcription (Lam et al., 2013). These results therefore provide evidence that enhancers can be the targets of stimulus- dependent negative regulatory mechanisms that downregulate mRNA production. They thus strengthen the idea that enhancers may deactivate neuronal IEG induction.

1.4 Role of DNA-damage in regulating activity-dependent transcription

Madabhushi et al., 2015 found that neuronal immediate early genes (IEGs) recruit Topoisomerase-IIBeta (TOP2B) to their promoters in response to NMDA stimulation and that IEG activation requires TOP2B. This work raises the possibility that TOP2B-dependent double-stranded DNA breaks (DSBs) are required for transcription neuronal immediate early genes (IEGs) and that the repair of these DSBs functions in the termination of IEG transcription. *Madabhishi et al., 2015* found that histone H2AX phosphorylation, a signature of DNA-damage,

is deposited at IEG promoters in a TOP2B-dependent manner. Moreover, inhibition of IEG transcription by TOP2B knockdown could be rescued by delivery of a Cas9 nucleus to the IEG promoter. This data is supportive of a model in which neuronal stimulation initiates a TOP2B-dependent DNA cleavage at these promoters and that this cleavage is required for gene activation. This work is supported by other studies which have found TOP2B-dependent regulation of genes, including IEGs, in neuronal cell types (Lutz, Nguyen, Joswig, Rau, & Laube, 2019; Tiwari et al., 2012). Other studies in neurons have linked DSBs to neuronal activity (Crowe, Movsesyan, Jorgensen, & Kondratyev, 2006; Madabhushi, 2018; Suberbielle et al., 2013). The mechanism by which TOP2B activity regulates IEG transcription is unknown. The initial work which discovered that activating transcription factor complexes, such as nuclear hormone receptors and AP1, stimulate gene expression through the recruitment of TOP2B and the initiation of DSBs, also found that this process led to the eviction of transcriptional repressor complexes such as NCoR1 and to the exchange of repressive histone H1 for activating histone HMGB1 (Ju et al., 2006). This work suggests that TOP2B might function to directly regulate the local chromatin environment at promoters to be permissive to activation by transcription factors. Other work has linked TOP2B to the regulation of the release of paused RNAPII (Bunch et al., 2015)—a feature of IEGs (Saha et al., 2011; Tyssowski et al., 2018). *Madabhushi et al., 2015* found that sites of activity-dependent DNA damage and TOP2B peaks were also enriched for CTCF binding, and TOP2B has been shown to interact with CTCF and cohesin at anchors of looped chromatin which may aid in the establishment of these loops through the relief topological stress through DSBs. (Bunch et al., 2015; Canela et al., 2017; Uuskula-Reimand et al., 2016) Therefore, this TOP2B activity could be essential to the formation of enhancer-promoter loops which enable transcription.

Chapter 2
Distinct neuronal activity patterns activate unique gene expression programs

2.1 Summary

A vast number of different neuronal activity patterns could each induce a different set of activity-regulated genes. Mapping this coupling between activity pattern and gene induction would allow inference of a neuron's activity-pattern history from its gene expression and improve our understanding of activity-pattern-dependent synaptic plasticity. In genome-scale experiments comparing brief and sustained activity patterns, we reveal that activity-duration history can be inferred from gene expression profiles. Brief activity selectively induces a small subset of the activity-regulated gene program that corresponds to the first of three temporal waves of genes induced by sustained activity. Induction of these first-wave genes is mechanistically distinct from that of the later waves because it requires MAPK/ERK signaling but does not require de novo translation. Thus, the same mechanisms that establish the multi-wave temporal structure of gene induction also enable different gene sets to be induced by different activity durations.

2.2 Introduction

Neurons induce hundreds of activity-regulated genes (ARGs) in response to elevations in their activity(Flavell & Greenberg, 2008), suggesting that a vast number of different neuronal firing patterns could each be coupled to a different gene expression profile. Consistent with this idea, distinct neuronal activity patterns differentially induce the expression of several individual genes (Douglas, Dragunow, & Robertson, 1988; Greenberg, Ziff, et al., 1986; Sheng et al., 1993; Worley et al., 1993). However, single-gene studies are inadequate for creating a complete coupling map that relates each neuronal activity pattern to a corresponding gene expression profile. This coupling map would be powerful because it would allow inference of a neuron's activity history from its gene expression profile. This kind of inference could enable single-cell-RNA-sequencing (scRNA-seq)-based assessment of the activity histories of thousands of

neurons at a time, far more than can be assessed with electrical recording or calcium imaging (Hrvatin et al., 2018; Hu et al., 2017; Jun et al., 2017; Mohammed et al., 2016; Y. E. Wu, Pan, Zuo, Li, & Hong, 2017). To generate a coupling map, it will be necessary to make genome-scale comparisons of the ARGs induced by different activity patterns (Lee, Cohen, Iacobas, Iacobas, & Fields, 2017).

Transcriptional regulators could establish the coupling map, as they can both define specific ARG subsets and respond differentially to different activity patterns. Regulators that define ARG subsets include transcription factors, such as CREB and SRF, that bind the promoters and enhancers of only some ARGs (T. K. Kim et al., 2010). Regulators that respond differentially to different activity patterns include calcium-dependent cell-signaling pathways, such as the MAPK/ERK pathway (De Koninck & Schulman, 1998; Dolmetsch et al., 1997; Dudek & Fields, 2001; Eshete & Fields, 2001; Fields, Eshete, Stevens, & Itoh, 1997; Fujii et al., 2013; H. Ma, Groth, Wheeler, Barrett, & Tsien, 201, G. Y. Wu, Deisseroth, & Tsien, 2001). Thus, each of the many inducible signaling pathways could regulate a distinct subset of ARGs, creating gene modules that are each independently coupled to activity patterns. Identifying the regulators of these gene modules would enable manipulation of the coupling map to investigate its contribution to firing-pattern-specific, gene-induction-dependent synaptic plasticity, such as long-term potentiation, long-term depression, and synaptic scaling (Ahn et al., 1999; Ibata et al., 2008; Nguyen et al., 1994).

One example of a regulatory mechanism that could couple stimulation patterns to induction of different gene modules comes from non-neuronal cells, where it has been proposed that brief and

sustained stimulation differentially induce two of the best-defined gene modules in inducible systems: primary and secondary response genes (PRGs and SRGs) (Fowler et al., 2011). These gene modules are defined by their requirement for de novo translation. PRGs can be induced rapidly and do not require de novo translation for their induction, whereas SRGs are induced slowly, require de novo translation for their induction, and are regulated by PRG protein products (Fowler et al., 2011; Herschman, 1991). Brief stimulation is sufficient to induce PRGs, but sustained cell-signaling pathway activation, which is induced by sustained stimulation, is required to stabilize PRG protein products and induce SRGs (Fowler et al., 2011). In neurons, brief activity could similarly induce only PRGs while sustained activity could be required to induce SRGs. Therefore, defining PRGs and SRGs in neurons and determining their responsiveness to different activity durations could reveal a basic principle underlying the coupling map between activity patterns and gene expression.

In a step toward generating this coupling map, we performed genome-scale comparisons of gene induction in response to neuronal activity patterns of varying duration. We found that different durations of activity induce different sets of genes, allowing us to infer neuronal activity duration from gene expression data. We further reveal that the coupling between activity duration and gene expression is determined in part by MAPK/ERK signaling, enabling future manipulation of the coupling map.

2.3 Results

Rapid but not delayed PRGs are induced by brief activity

We investigated the possibility that different patterns of neuronal activity induce different subsets of ARGs by varying just one aspect of neuronal activity: its duration. We activated

neurons briefly (10s-5min.) or continuously (for up to 6h) using three methods of stimulation that allowed us to precisely control the duration of neuronal firing or calcium influx (Figure 1A).

We primarily stimulated mouse cultured cortical neurons with KCl-mediated membrane depolarization and assessed the resulting gene induction using either total RNA-seq, which allowed to assess both mRNA and pre-mRNA transcription (Gaidatzis et al., 2015; Gray et al., 2014), or targeted sequencing of 251 ARG mRNAs (ARG-seq), which allowed us to reduce the number of reads needed per experiment (Figure 2A, see methods).

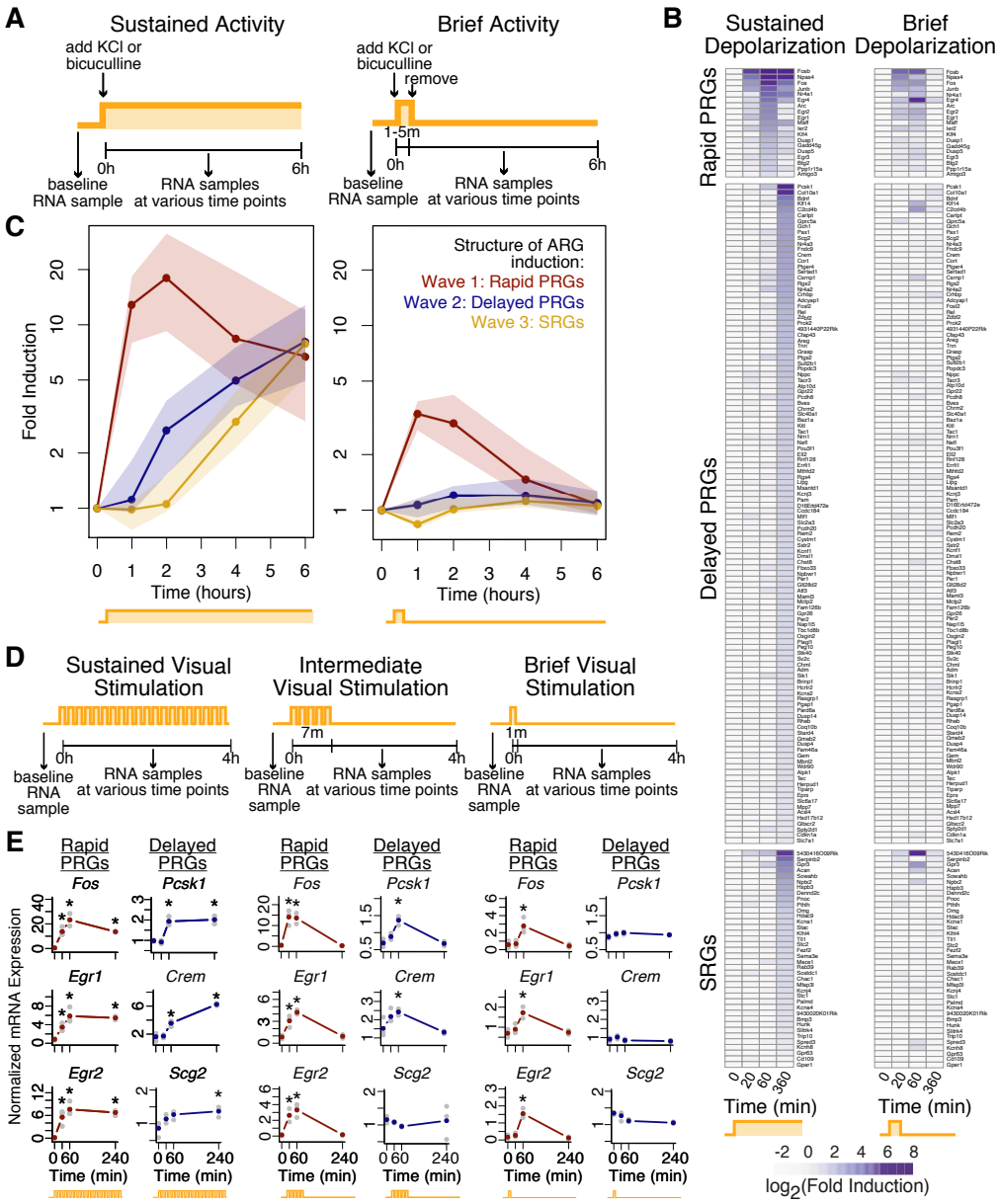

Figure 1. Brief neuronal activation selectively induces the first of three waves of gene induction.

(A) Experimental system for comparing sustained and brief neuronal activation in vitro. Except where indicated otherwise, neuronal activation is accomplished with brief (1-min) or sustained KCl-depolarization of cortical neurons silenced 14-16h before stimulation with APV and NBQX. (B) Comparison of gene induction upon sustained or brief neuronal activation using activity-regulated-gene-capture-based RNA-sequencing (ARG-seq) (means, n=3-6 biological replicates). Only induced genes are shown. Gene categories are defined based on kinetics of gene induction, as well as induction in the presence of the translation-inhibitor cycloheximide (Figure S1B).

Figure 1. (Continued) Brief neuronal activation selectively induces the first of three waves of gene induction.
PRG = primary response gene. SRG = secondary response gene. Genes induced by brief neuronal activation are enriched for rapid PRGs (rPRGs) ($p<10^{-13}$, Fisher's exact test).
(C) Three kinetically distinct temporal waves of gene induction as detected by high-throughput microfluidic qPCR. Points represent the mean expression of the median gene for each class. Shading covers the middle quartiles of mean expressions (25%-75%) (n=6 biological replicates). Each wave is kinetically distinct from the other waves (rPRG vs. delayed PRG (dPRG)/SRG induction at 1h, dPRG vs. SRG induction at 2h, $p<0.003$, rank-sum test). Plotted are 15, 37, and 9 genes from waves 1-3, respectively.
(D) Experimental system for comparing the duration of neuronal activation in the visual cortex in vivo. Mice were dark-housed for three days prior to visual stimulation consisting of lights flashing in a repeated pattern: 60s on, 20s off.
(E) Gene induction in the visual cortex following visual stimulation, as measured by qPCR. Colored points are means of n=3 biological replicates. Grey points are values from individual biological replicates. Gene categories defined as in (B). *significant induction compared to 0h time point, $p<0.05$ unpaired, two-sided t-test, fold induction>1.5.

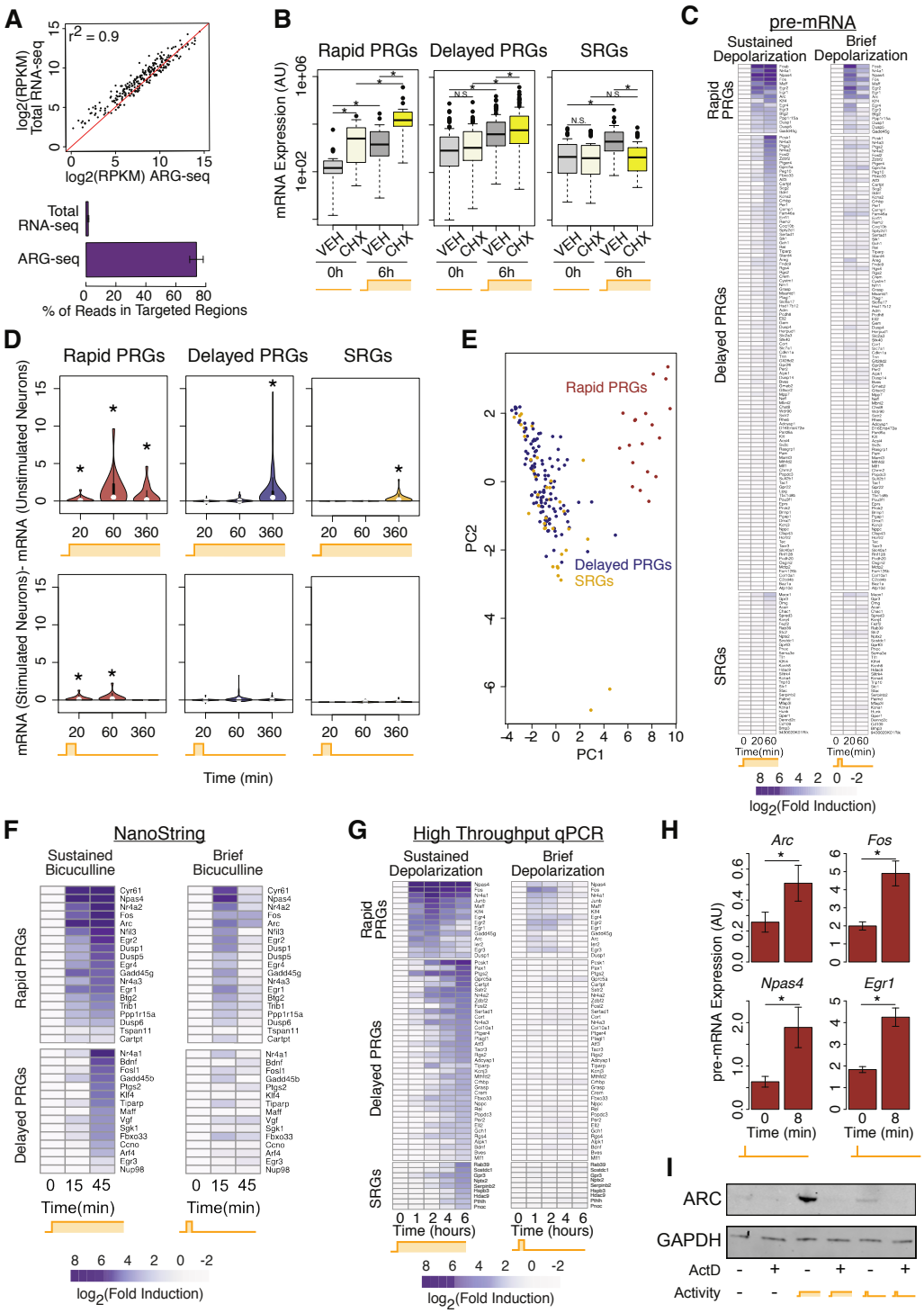

Figure 2. Brief neuronal activation induces only the first of three waves of gene induction – Part II.

Figure 2 (Continued). Brief neuronal activation induces only the first of three waves of gene induction – Part II.

(A) Top: Gene induction from total RNA-seq and ARG-seq are highly correlated (r^2 by Pearson correlation). Shown is one representative comparison of one biological sample prepared with total RNA-seq and ARG-seq. Bottom: ARG-seq provides ~76-fold enrichment of reads in targeted regions. Error bars are +/- S.E.M. from n=12 libraries. ARG-seq is targeted capture of 251 mRNAs previously shown (Kim et al., 2010) to be induced >3.5 fold by KCl and 47 control mRNAs whose expression does not change with KCl.

(B) Summary of primary response gene (PRG) and secondary response gene (SRG) sensitivity to the translational inhibitor cycloheximide (CHX), after distinguishing SRGs from PRGs based on >50% reduction in expression in the presence of CHX at 6 hours of stimulus and FDR<0.05 by edgeR (*p<0.01, paired rank-sum test, means for each gene from n=2 biological replicates).
(C) There is little pre-mRNA induction of delayed PRGs (dPRGs) with brief neuronal activation, based on total RNA-seq comparison of pre-mRNA induction using reads that align to annotated introns. Shown are means from n=2 biological replicates. No dPRG or SRG pre-mRNAs are significantly induced in response to brief activity (FDR>0.05). Genes induced by brief membrane depolarization are enriched for rapid PRGs (rPRGs) at the pre-mRNA level ($p<10^{-8}$, Fisher's exact test). Gene classes as in Figure 1.
(D) The greater response of rPRGs to brief stimulation is unlikely to be an artifact of their greater induction overall, as shown in violin plots. Note in particular the 360-minute time point for dPRGs at top (sustained) and bottom (brief), and compare to the 60-minute time point for rPRGs at top and bottom. Same data as in Figure 1B, with biological replicates averaged prior to plotting.
(E) Principal component analysis of the kinetics of gene induction distinguishes rPRGs from dPRGs and SRGs. Based on data shown in Figure 1B, see methods for details.
(F) Bicuculline/4AP treatment in rat neurons recapitulates rPRG and dPRG differences observed in mouse neurons with KCl-depolarization, based on NanoString comparison of gene induction upon sustained or brief neuronal activation using bicuculline/4AP treatment in rat cortical neurons. Shown are means from n=3 biological replicates. Only genes induced >2 fold at any time point are shown. Genes induced by brief membrane depolarization are enriched for rPRGs ($p = 0.001$, Fisher's exact test). rPRGs were defined based on reaching 50% of their maximum induction by 15 minutes or having greater than 4-fold induction by 15 minutes. Delayed genes are mostly dPRGs, based on their classification in mouse, although we did not confirm this via translational inhibition in rat neurons.
(G) Validation of RNA-seq and ARG-seq results using a high-throughput qPCR (Fluidigm)-based comparison of gene induction in response to sustained or brief neuronal activation with KCl-mediated depolarization. Shown are means from n=4 biological replicates. Genes induced by brief membrane depolarization are enriched for rPRGs ($p < 10^{-7}$, Fisher's exact test). Gene classes as in Figure 1, and this data is the same as that shown in Figure 1C.
(H) 10-second treatment with bicuculline/4AP followed by TTX induces rPRG pre-mRNA. Plotted is means from n=5 biological replicates. Error bars are +/- S.E.M. *p<0.05, paired student's t-test.
(I) ARC protein is induced by brief neuronal activation in a transcription-dependent manner. Representative western blot of ARC protein expression two hours after sustained or brief KCl-

Figure 2 (Continued). Brief neuronal activation induces only the first of three waves of gene induction – Part II.

depolarization in the presence or absence of the transcriptional inhibitor Actinomycin D (ActD) (10μg/mL). n=1 of 3 biological replicates.

We first used ARG-seq to characterize the gene induction in response to sustained activity. We found that sustained activity induces 173 ARGs, 114 of which also show significant induction in at least one of three in vivo studies (Cho et al., 2016; Lacar et al., 2016; Spiegel et al., 2014) (significant overlap, p=0.0002, Fisher's exact test). We observed that these 173 ARGs are induced in two waves, as expected (Flavell and Greenberg, 2008): a rapid wave that includes 19 genes and a delayed wave that includes 154 genes (Figure 1B-C, 2C-E, see methods for details of classification). We hypothesized that the first wave corresponds to the de-novo-translation-independent PRGs and the second to SRGs, which require PRG protein products for their induction. Indeed, after defining PRGs and SRGs based on their requirement for de-novo-translation, we found that the first wave of gene induction is entirely comprised of PRGs (Figures 1B, 2B). However, the second wave includes both PRGs and SRGs, similar to findings in human cancer cell lines and macrophages (Ramirez-Carrozzi et al., 2006; Tullai et al., 2007). Thus, neurons also induce two kinetically distinct classes of PRGs: rapid PRGs (rPRGs) and delayed PRGs (dPRGs). A finer-grained time course using high-throughput qPCR revealed that dPRGs are actually induced earlier than SRGs, suggesting that rPRGs, dPRGs, and SRGs represent three temporally distinct waves of transcription (Figures 1C, 2G).

We next measured gene induction in response to brief (KCl-mediated) activity using ARG-seq. Remarkably, rPRGs comprise 14 of the 15 genes significantly induced by brief activity (FDR<0.05, mean fold change>1.5) (Figures 1B-C, 2E,G). Pre-mRNA expression assessed in total RNA-seq data recapitulated these mature mRNA findings (Figure 2C), suggesting that the differential responsiveness to brief activity between rPRGs and dPRGs is due to transcriptional rather than post-transcriptional mechanisms. The selective induction of rPRGs but not dPRGs by

brief activity is not specific to KCl-mediated depolarization, as it also occurs following brief (5-min) bicuculline-induced activity in rat primary cortical neurons, as detected by NanoString (Figure 2F). rPRGs are also induced by just ten seconds of bicuculline-induced synaptic activity (Figure 2H), equivalent to a single burst of firing (Yu et al., 2017). These findings indicate that de-novo-translation-independence is not the only requirement for induction in response to brief activity. Instead, rPRGs in neurons may be distinguished from dPRGs by transcriptional mechanisms that allow them to respond both rapidly and to brief activity.

To confirm that rPRGs but not dPRGs are induced in response to brief activity in vivo, we assessed gene induction in the visual cortex in response to a visual stimulus consisting of bright, flashing lights (Figure 1D). Using photometry-based *in vivo* recordings of calcium activity, we first confirmed that neuronal activity in primary visual cortex increases with the onset of each flash of light, even for repeated flashes presented for several hours (Figure 3A-B).

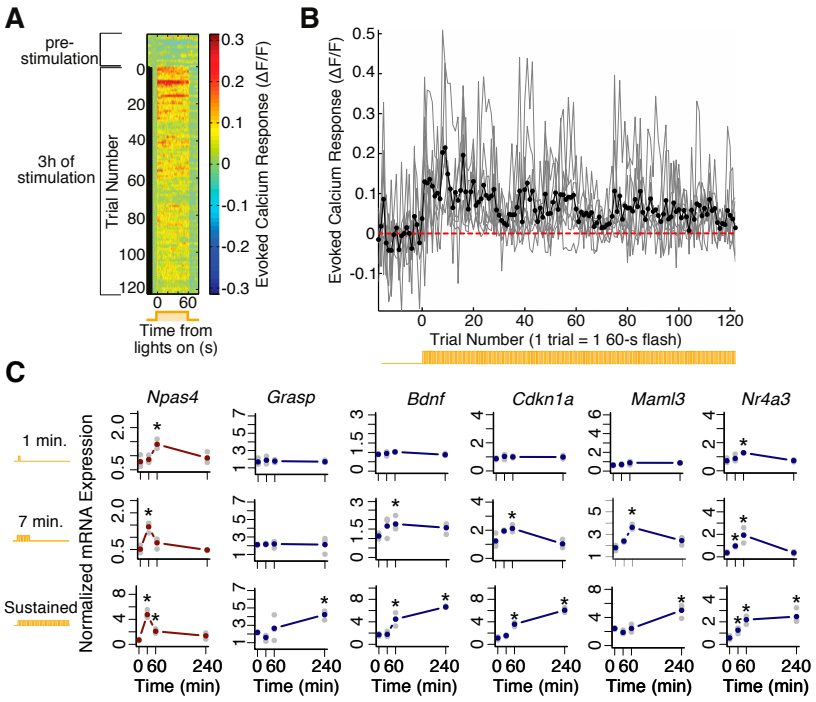

Figure 3. Brief visual stimulation induces only the first of three waves of gene induction in vivo.

(A) In vivo fiber photometry recording of light-evoked changes in bulk neuronal calcium activity in primary visual cortex (V1). Mice were exposed to up to 3 hours of a repeated visual stimulus of lights-on for 60s followed by lights-off for 20s. Each row represents a time course of activity (fractional change in fluorescence; ΔF/F; positive signals indicate net increase in calcium activity in V1 neurons) during presentation of a single lights-on stimulus, averaged across 8 sessions (8 mice, 1 session/mouse). There was a significant, ~13% increase in activity for the first trial ($p = 0.04$) compared to the pre-stimulus no-light trials (trials lacking a black bar at right and numbered less than 0 in the plot). Visual stimulation in the first hour of stimulation evoked a 9.3% average increase in activity ($p = 0.0005$). Visual stimulation in the second hour evoked a 6.1% average increase in activity ($p = 0.0005$). Visual stimulation in the third hour evoked a 4.7% average increase in activity ($p = 0.00007$). p-values: one-sided Student's t-test ($n = 8$ mice).

(B) Same data as in (A). Gray lines indicate mean ΔF/F for each trial (from 0-60 s post stimulus onset compared to the 10 s prior to stimulus onset) for each of the eight individual mice. Black line is the mean evoked response across mice, with each dot representing the mean evoked response for a single trial.

(C) Additional genes beyond those shown in Fig. 1E, showing ARG induction in the visual cortex following visual stimulation, as measured by qPCR. Colored points are mean of 3 biological replicates. Gray points are values from individual biological replicates. Gene categories defined as in Figure 1. *significant induction compared to 0h time point, $p<0.05$ Student's t-test, fold induction>1.5.

We assessed mRNA induction using qPCR with primers for four rPRGs and eight dPRGs, as classified using our in vitro data. The rPRGs are all induced rapidly and in response to one minute of visual stimulation, consistent with in vitro findings (Figure 1E, 3C). Most of the dPRGs (7/8) have delayed induction kinetics and no induction in response to one minute of stimulation, again consistent with our in vitro results. The exception, *Nr4a3*, is induced rapidly and by brief activity, thus behaving as a rPRG in vitro but a dPRG in vivo. The concordance between our in vitro and in vivo results suggests that activity duration is coupled to gene expression similarly in primary cortical neurons and in the cortex.

Our finding that dPRGs are induced in response to sustained but not brief activity suggests that there is a minimum activity duration required to induce dPRGs. To determine whether this minimum is the same for every dPRG, we assessed PRG expression in response to an intermediate duration of visual stimulation. This intermediate (7-min) stimulus is sufficient to induce only a subset (five) of the seven dPRGs (Figure 1E, S2C), indicating that different dPRGs have different minimum-activity-duration thresholds. The observation that there are three distinct ARG induction profiles for one-minute, seven-minute, and sustained activity suggests that ARG induction has a graded response to the duration of activity and hints at the potential complexity of the coupling between activity pattern and ARG induction.

We next investigated whether the genes in each of the three waves of ARG induction differ in their known or annotated gene function. Most (17/19) rPRGs that we identified in mouse cortical neurons are directly or indirectly involved in regulating transcription. rPRGs are also more likely

than dPRGs or SRGs to be stimulus-induced in macrophages ($p = 0.0004$, Fisher's exact test) (Escoubet-Lozach et al., 2011) and human cancer cell lines ($p=0.0001$, Fisher's exact test) (Tullai et al., 2007), consistent with the idea that transcription factors are re-used in many cell types. Therefore, most (112/114) of the effector (i.e., non-transcription-regulating) ARGs, which are thought to orchestrate transcription-dependent neuronal plasticity, are dPRGs or SRGs. A major exception is the rPRG effector gene *Arc* (Shepherd and Bear, 2011). We found that brief activity induces ARC protein in a de-novo-transcription-dependent manner (Figure 2I), consistent with the idea that ARC could mediate the synaptic changes driven by brief activity. These results suggest that any transcription-dependent synaptic changes caused by brief activity are driven by the protein products of only a few genes, including *Arc*.

Neuronal activity history is encoded in gene expression profiles

Given that brief and sustained activity induce different gene sets, we asked whether we could infer neurons' past activity duration from their ARG expression profiles. Indeed, a nearest-neighbor classifier correctly identified in vitro samples as having been stimulated with brief or sustained KCl-mediated depolarization, using normalized expression values from all significantly induced genes or all captured genes but not constitutively active control genes (Figure 4A). For such classification to be broadly useful, it should be robust to the method of stimulation. We therefore aimed to classify our in vivo visual stimulation samples using our in vitro KCl-mediated depolarization data as a training set. A classifier using 11 ARGs that have similar expression profiles between in vitro and in vivo experiments was able to correctly classify 100% of visual cortex samples as having undergone either brief, sustained, or no

stimulation (Figure 4B). Thus, the duration of past neuronal activity is indeed encoded in the ARG expression profile, and this information can be used to infer in vivo activity histories.

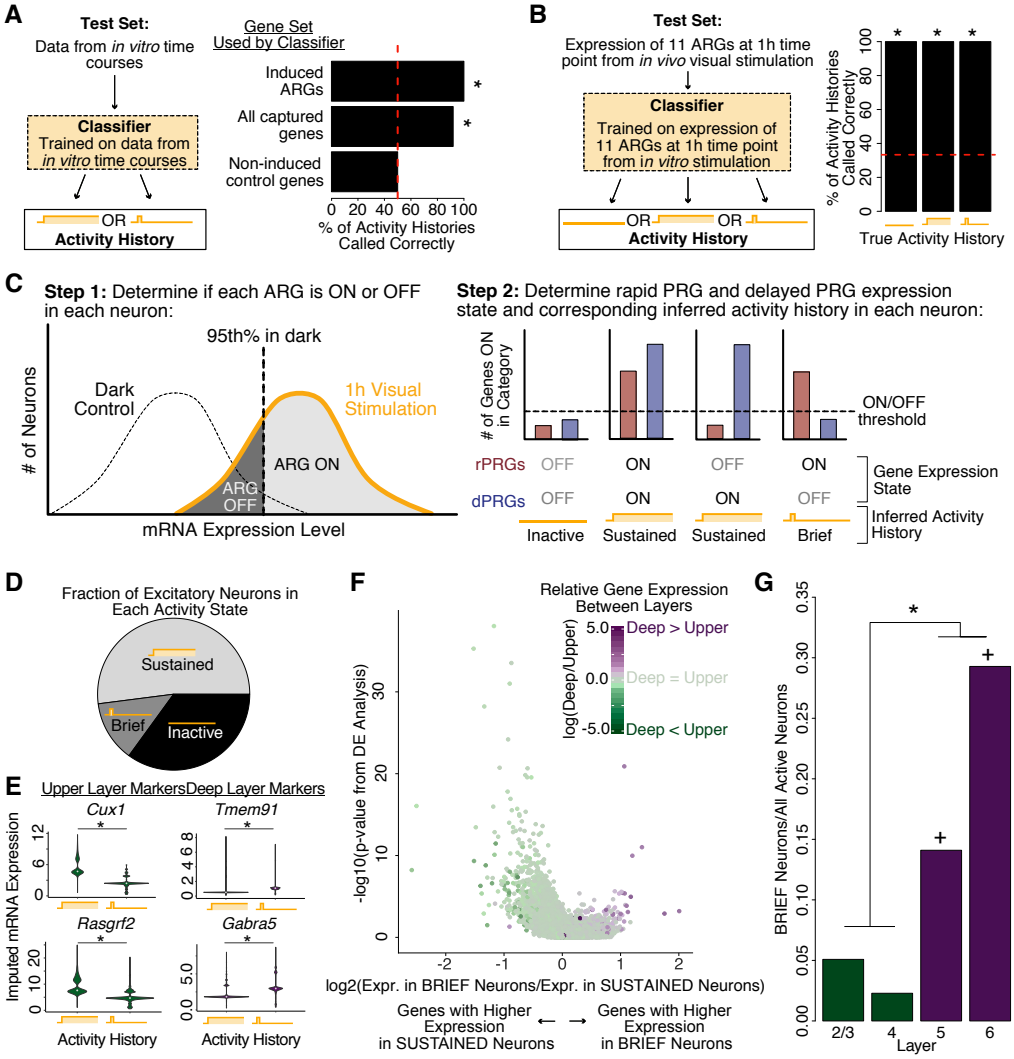

Figure 4. Neuronal activity patterns can be inferred from ARG expression.

(A) A classifier trained on in vitro gene expression data to infer activity histories of 12 in vitro samples (6 brief, 6 sustained). The classifier identified test samples as having undergone either brief or sustained activity based on based on Euclidean distance to training samples. *p = 0.007, exact binomial test.

Figure 4. (Continued) Neuronal activity patterns can be inferred from ARG expression.
(B) A similar (in vitro-trained) classifier used to infer the activity histories of 12 in vivo visual cortex samples (3 brief, 3 sustained, and 6 unstimulated). *$p<0.04$, exact binomial test.
(C) Method for scRNA-seq-based inference of BRIEF and SUSTAINED activity histories of individual visual cortex excitatory neurons from mice exposed to 1h of sustained visual stimulation. scRNA-seq data from Hrvatin et al., 2017.
(D) 1h of visual stimulation significantly increased the fraction of excitatory neurons with BRIEF and SUSTAINED inferred activity states ($p<10^{-15}$, Fisher's exact test).
(E) Expression of four layer markers in BRIEF and SUSTAINED neurons in scRNA-seq data. Data plotted are imputed mRNA reads after using DECENT (Ye et al., 2017) to account for the presence of technical zeroes. *FDR<0.1, rank-sum test.
(F) Differential expression (DE) of all genes (excluding ARGs) in BRIEF compared to SUSTAINED neurons. P-value determined using the rank-sum test. Color of the points represent the log of the ratio of gene expression in deep layers (Layers 5 and 6) to that in upper layers (Layers 2/3 and 4).
(G) Fraction of stimulated neurons in each layer that are BRIEF. *More BRIEF neurons in deep vs. upper layers, $p<10^{-15}$, Fisher's exact test. $^{+}$Significant population of brief neurons, $p<0.001$ based on a Fisher's exact test comparing the number of rPRG-ON neurons among dPRG-OFF neurons in the stimulated cortex to the number of rPRG-ON neurons in unstimulated cortex.

We therefore considered the possibility of using scRNA-seq data to infer the activity histories of thousands of individual neurons in a single experiment (Hrvatin et al., 2017; Hu et al., 2017; Wu et al., 2017). We asked whether we could use scRNA-seq-based detection of ARG expression to identify a population of visual cortex neurons that are activated only briefly in response to sustained visual stimulation. We analyzed published data collected one hour after the onset of visual stimulation (Hrvatin et al., 2017). We found that both rPRGs and dPRGs are robustly induced by one hour when compared to control mice left in the dark (Figure 5A). We classified neurons that induced rPRGs but not dPRGs as having been putatively briefly active ("BRIEF neurons"), whereas those that induced dPRGs were predicted to have had a history of sustained activity ("SUSTAINED neurons") (Figure 4C, 5B). We found that the majority (52%) of neurons were putative SUSTAINED neurons. However, we found a small (13%), but significant, population of putative BRIEF neurons (Figure 4D). The remaining 35% of neurons showed no PRG induction and were therefore classified as putatively inactive. We therefore predict that a subset of neurons in the mouse visual cortex undergoes brief activity in response to sustained visual stimulus.

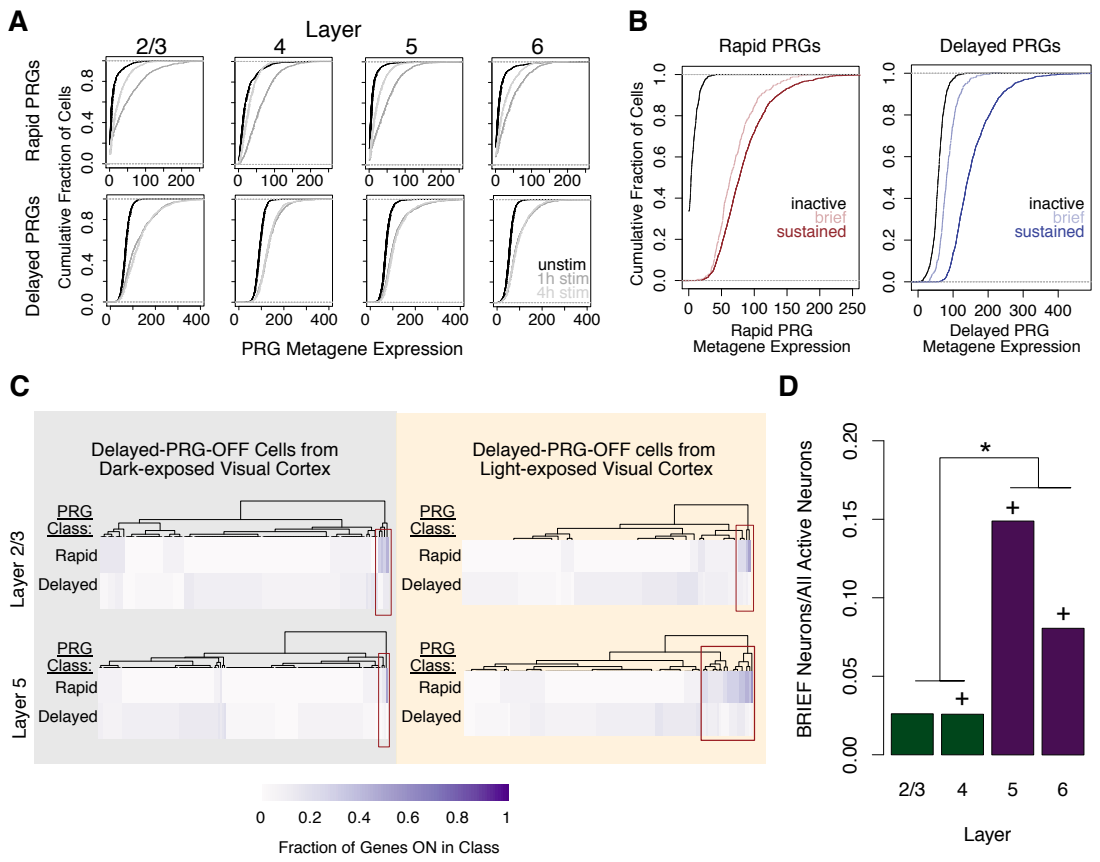

Figure 5. Neuronal activity pattern can be inferred from ARG expression.
(A) Both rPRGs and dPRGs are induced by 1h of visual stimulation in all cortical layers ($p<10^{-7}$, rank-sum test). Metagene expression is average expression of all rPRGs (19) or dPRGs (116) from read-depth-normalized data for each timepoint in each layer. scRNA-seq data (Hrvatin et al., 2017) is from the visual cortex of mice exposed to sustained visual stimulus. Evidence of induction of dPRGs in all layers suggests that our gene list is not biased toward any layer. The consistent dPRG induction across layers does not invalidate our finding of more putative BRIEF neurons in deeper layers, since the BRIEF neurons we found are a relatively small minority population.
(B) Expression of rPRG and dPRG metagenes in BRIEF, SUSTAINED, and inactive neurons, as classified in Figure 2. Metagene expression was computed as in (A), except that they were made from cell populations defined based on activity state instead of layer.
(C) Layer 5 has more putative BRIEF (rPRG-expressing dPRG OFF neurons) in the light than in the dark ($p = 0.002$, $OR = 0.47$, Fisher exact test), suggesting that rPRG expression in BRIEF neurons in the light is due to visual cortex simulation (see methods). The number of putative BRIEF neurons in the light and dark is similar in layer 2/3 ($p = 0.4$, $OR=1.6$, Fisher exact test). Each box in the heatmap represents a neuron. The color of the box represents the fraction of either rPRGs (top) or dPRGs (bottom) that are induced in that neuron (out of all rPRGs or dPRGs induced in that layer). The dendrogram represents hierarchical clustering using Euclidean distance. Red boxes indicate clusters of neurons that have large number of rPRGs induced.

Figure 5. (Continued) Neuronal activity pattern can be inferred from ARG expression.
(D) Deep compared to upper layers are enriched for BRIEF neurons (*$p < 10^{-15}$, Fisher exact test). Similar to Figure 2G, but BRIEF and SUSTAINED neurons defined using dPRG lists made specifically for each layer. $^{+}$significant population of BRIEF neurons; $p < 0.001$, Fisher exact test comparing the number of rPRG ON neurons among dPRG OFF neurons in the stimulated cortex to the number of rPRG ON neurons among unstimulated neurons.

To determine the identity of these BRIEF neurons, we performed differential gene expression analysis comparing BRIEF and SUSTAINED neurons. We found that the genes expressed significantly more in BRIEF neurons include deep layer (5 and 6) markers such as *Tmem91*, *Gabra5, Rprm*, and *Crym*. In contrast, genes with greater expression in SUSTAINED neurons included upper layer (2/3 and 4) markers, such as *Calb1*, *Cux1*, and *Rasgrf2* (fold change>2, FDR<0.1, Figure 4E) (layer markers from Hrvatin et al., 2017; Tasic et al., 2016). Impressively, almost all of the genes differentially expressed between BRIEF and SUSTAINED neurons show similar layer-specific trends in expression, suggesting that the major genetic differences between BRIEF and SUSTAINED neurons arise from their layer positions (Figure 4F). We therefore directly asked whether deep layers of the cortex have a greater enrichment for BRIEF neurons than upper layers, using gene-expression-based layer definitions (Hrvatin et al., 2017). We indeed found that deep layers of the cortex have more BRIEF neurons than upper layers, with only deep layers having a statistically significant population of BRIEF neurons (Figure 4G, Figure 5C). We were concerned about being biased toward detecting BRIEF neurons in deep layers if upper layer neurons induce more of the dPRGs on our in-vitro-defined list than deep layers, which is possible given that different layers of cortex induce different dPRGs (Hrvatin et al., 2017). To control for this alternative possibility, we used the scRNA-seq data to define dPRGs for each layer individually and confirmed that we still found an enrichment of BRIEF neurons in deep layers using the layer-specific dPRGs (Figure 5D). This analysis therefore predicts that upon sustained visual stimulation, a population of neurons in layers 5 and 6 of the primary visual cortex exhibits only brief elevations in activity.

Rapid PRG promoters are distinguished by open, active chromatin and the presence of pre-bound transcription regulators

We next investigated what might enable rPRGs both to be induced rapidly and by brief activity. The faster mRNA induction of rPRGs could be facilitated in part by their shorter gene length compared to dPRGs and SRGs (median ~13 kb shorter, Figure 6A). However, we found that rPRG first exons are induced before those of dPRGs or SRGs (Figure 6B), indicating that rPRG promoters are also activated more rapidly. We hypothesized rPRG promoters might be primed for faster promoter activation due to an open chromatin state prior to stimulation. To assess this hypothesis, we evaluated three marks of open chromatin: high DNaseI hypersensitivity (data from ENCODE Project Consortium et al., 2012), high CpG (and GC) content, and high levels of active chromatin marks, including H4K16ac, H3K4me2, and H3K27ac (data from Kim et al., 2010; Telese et al., 2015). We found that by all three of these criteria, unstimulated rPRG promoters have more open chromatin than unstimulated dPRG or SRG promoters (Figures 3A, 6C-D). Importantly, the histone acetylation signals extend across a wider promoter-proximal region and are more bimodal at rPRG promoters, indicative of reduced nucleosome occupancy at or near transcription start sites prior to stimulation (Figures 7A, 6C-D).

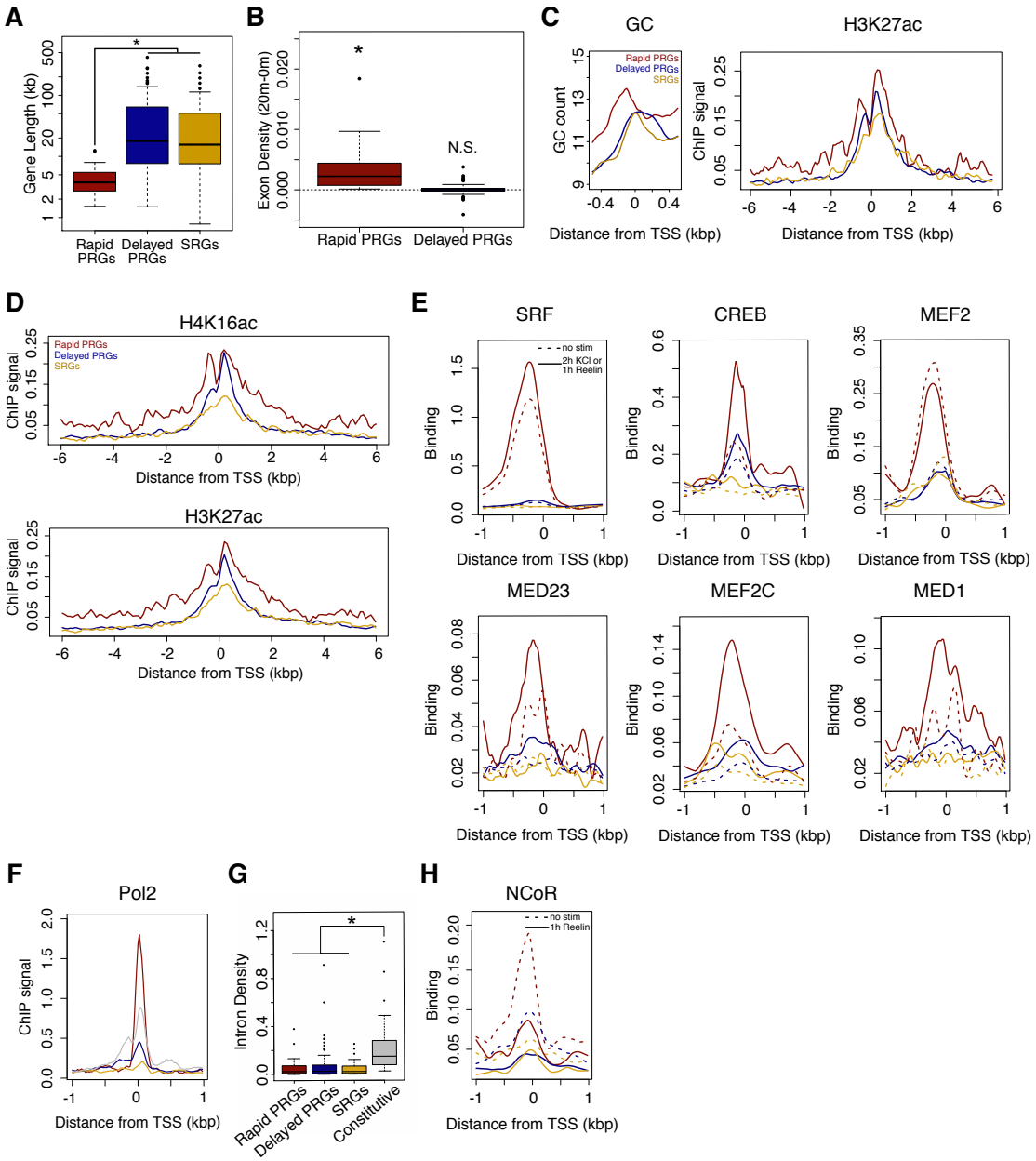

Figure 6. Rapid PRGs have open chromatin and pre-bound transcription factors.
(A) rPRGs are shorter than dPRGs and SRGs ($p<10^{-6}$, rank-sum test). Genes classified as in Figure 1.
(B) Reads from total RNA-seq that map to first exons of genes in each category shown on the y-axis as the increase from 0 to 20 minutes of KCl-depolarization, normalized by the length of the exon (read density) (show is one of n=2 biological replicates), *p<0.01, rank-sum test for both biological replicates, difference from zero.

Figure 6 (Continued). Rapid PRGs have open chromatin and pre-bound transcription factors.

(C) Chromatin state at rPRGs, dPRGs, and SRGs, shown as metaplots of the geometric mean by gene category. ChIP-seq data is from unstimulated mouse neurons. GC content and H4K27ac are significantly different (sum of the region shown) between rPRGs and dPRGs or SRGs ($p<0.01$, rank sum test).

(D) rPRGs have a more active chromatin state than dPRGs or SRGs in vivo. Chromatin state at rPRGs, dPRGs, and SRGs is shown as metaplots as in (C). ChIP-seq data is from mouse hippocampus without specific hippocampal activation. H4K16ac and H3K27ac are significantly different between rPRGs and dPRGs (or SRGs, $p<10^{-5}$, rank sum test on area under the curve). ChIP-seq data from Telese et al., 2015.

(E) Transcription factor binding in unstimulated and stimulated mouse neurons from ChIP-seq, shown as metaplots as in (C). MED23 and MED1 binding is greater at rPRGs than dPRGs in unstimulated neurons ($p<0.009$, rank sum test, for significance of SRF, MEF2, and CREB in unstimulated neurons see figure 3B). For SRF and CREB stimulation was with 2h of KCl-mediated depolarization (Kim et al., 2010). For MEF2, MEF2C, MED1, and MED23 stimulation was with 1h of reelin (Telese et al., 2015). SRF, CREB, MEF2, MEF2C, MED1, and MED23 binding is greater at rPRGs than dPRGs or SRGs in stimulated neurons ($p<0.0014$, rank-sum test). Stimulated signal shown for comparison.

(F) rPRGs and constitutively expressed control genes have more Pol2 binding in unstimulated neurons from ChIP-seq than dPRGs or SRGs ($p<0.04$, rank-sum test for area under the curve shown). Data from Kim et al., 2010.

(G) There is no difference in transcription of rPRG, dPRG, and SRG classes in unstimulated neurons based on pre-mRNA expression levels from RNA-seq ($p>0.5$, rank sum test). * = $p<10^{-5}$, rank-sum test.

(H) NCoR is selectively bound to rPRGs in unstimulated neurons, and its binding is reduced with stimulation ($p<0.009$, rank sum test). Stimulation was with 1h of reelin (Telese et al., 2015).

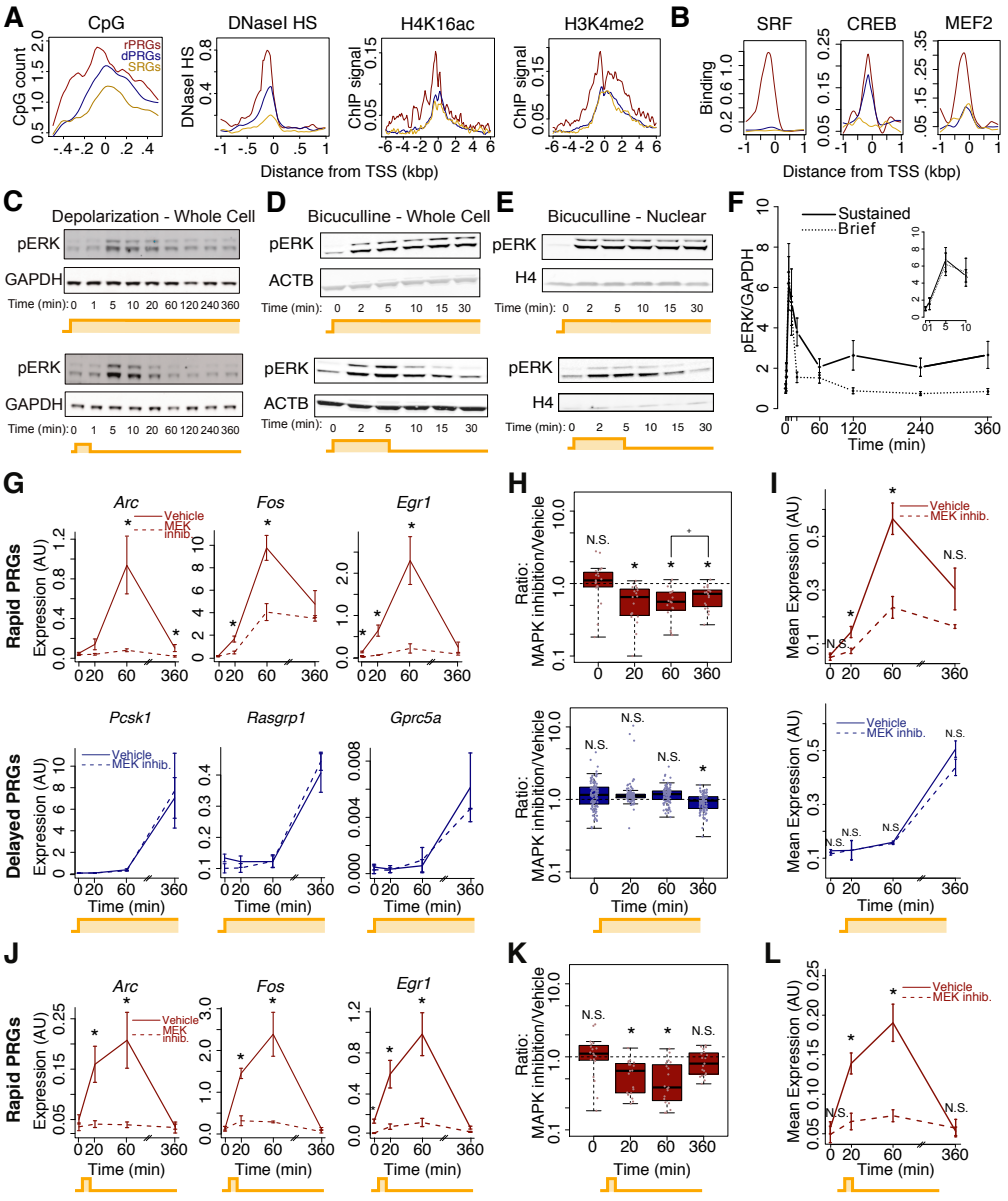

Figure 7. Requirement for MAPK/ERK signaling and an open chromatin state distinguish first and second waves of gene induction.

(A) Chromatin state in unstimulated neurons shown in metaplots of the geometric mean signal for all genes in each category. All measures of chromatin state are significantly different between rPRGs and dPRGs or SRGs ($p<0.009$, rank sum test on the area under the curves shown). ChIP-seq data are from cultured cortical neurons, Telese et al., 2015. DNaseI hypersensitivity data are from the 8w cerebrum (Consortium et al., 2012).

Figure 7. (Continued) Requirement for MAPK/ERK signaling and an open chromatin state distinguish first and second waves of gene induction.

(B) Transcription factor binding in unstimulated neurons from ChIP-seq, shown in metaplots as in (A). SRF and MEF2: significantly different between rPRGs and dPRGs or SRGs; CREB: not significantly different between rPRGs and dPRGs ($p=0.2$), but is different between rPRGs and SRGs ($p<0.009$, rank sum test). Data from cultured cortical neurons, Kim et al., 2010; Telese et al., 2015.
(C) ERK activation kinetics with KCl-mediated depolarization. Representative (1 of n=3) western blot for phosphorylated ERK (pERK). Phosphorylation of ERK paralogs, p44 and p42 (upper and lower bands), is kinetically similar ($r^2 = 0.97$, Pearson correlation).
(D) Similar to (C), but rat cortical neurons treated with sustained or brief bicuculline/4AP. One of n=3-4 representative biological replicates is shown.
(E) Same as (D), but from isolated nuclei.
(F) Quantification of (C), n=3 biological replicates. The inset is a magnified version of the first ten minutes. pERK induction at its peak (five minutes) is not different between brief and sustained stimulus ($p=0.3$, paired, two-sided t-test). Error bars represent +/- SEM.
(G) rPRG but not dPRG induction in response to sustained activity is dependent on MAPK/ERK. ARG-seq-based gene expression of three representative rPRGs and three representative dPRGs following sustained KCl depolarization of mouse neurons with and without 10μM of the MEK inhibitor, U0126. n=3-7 biological replicates. Error bars are +/- S.E.M. *$p<0.01$, rank-sum test.
(H) Data from the same experiment as (G), showing all ARGs. *significantly different from 1, $p<0.01$, rank-sum test; +$p = 0.02$, rank-sum test. Expression of rPRGs is more affected by MEK inhibition than expression of dPRGs ($p = 0.002$; rank-sum test on 17 rPRGs versus 110 dPRGs using the mean for each gene across n=3-7 biological replicates at its most induced time point).
(I) Data the same as in (H), but showing the geometric mean of gene expression. Error bars are +/- SEM from each of n=3-7 biological replicates of all genes in the category. *$p<0.03$, rank-sum test.
(J) rPRG but not dPRG induction in response to brief activity is dependent on MAPK/ERK. Same as (G), top row, but with 1-min KCl depolarization.
(K) Same as (H), top row, but with 1-min KCl depolarization.
(L) Same as (I), top row, but with 1-min KCl depolarization.

These differences in average DNase hypersensitivity and histone marks could be due to the greater number of neuronal and non-neuronal brain cell types that induce rPRGs compared to dPRGs and SRGs (Hrvatin et al., 2017) rather than to differences in chromatin accessibility in the neurons that actually induce each class. However, the observation that that rPRGs have more open chromatin than dPRGs and SRGs in homogenous non-neuronal cell populations (Hargreaves et al., 2009; Ramirez-Carrozzi et al., 2009, 2006) leads us to favor the idea that rPRG promoters in neurons are also distinguished by a relatively open chromatin state, potentially poising them for rapid activation in response to brief activity.

The open chromatin state at rPRG promoters in unstimulated neurons prompted us to ask whether these promoters might be selectively pre-bound to transcriptional regulators prior to neuronal activation. We found that RNA Polymerase 2 (Pol2) occupancy in unstimulated neurons is higher at the promoters of rPRGs and constitutively active genes compared to dPRGs and SRGs (Figures 6F, 8E) data, despite the finding that rPRGs, dPRGs and SRGs have similar levels of transcription in unstimulated neurons (Figure 6G).

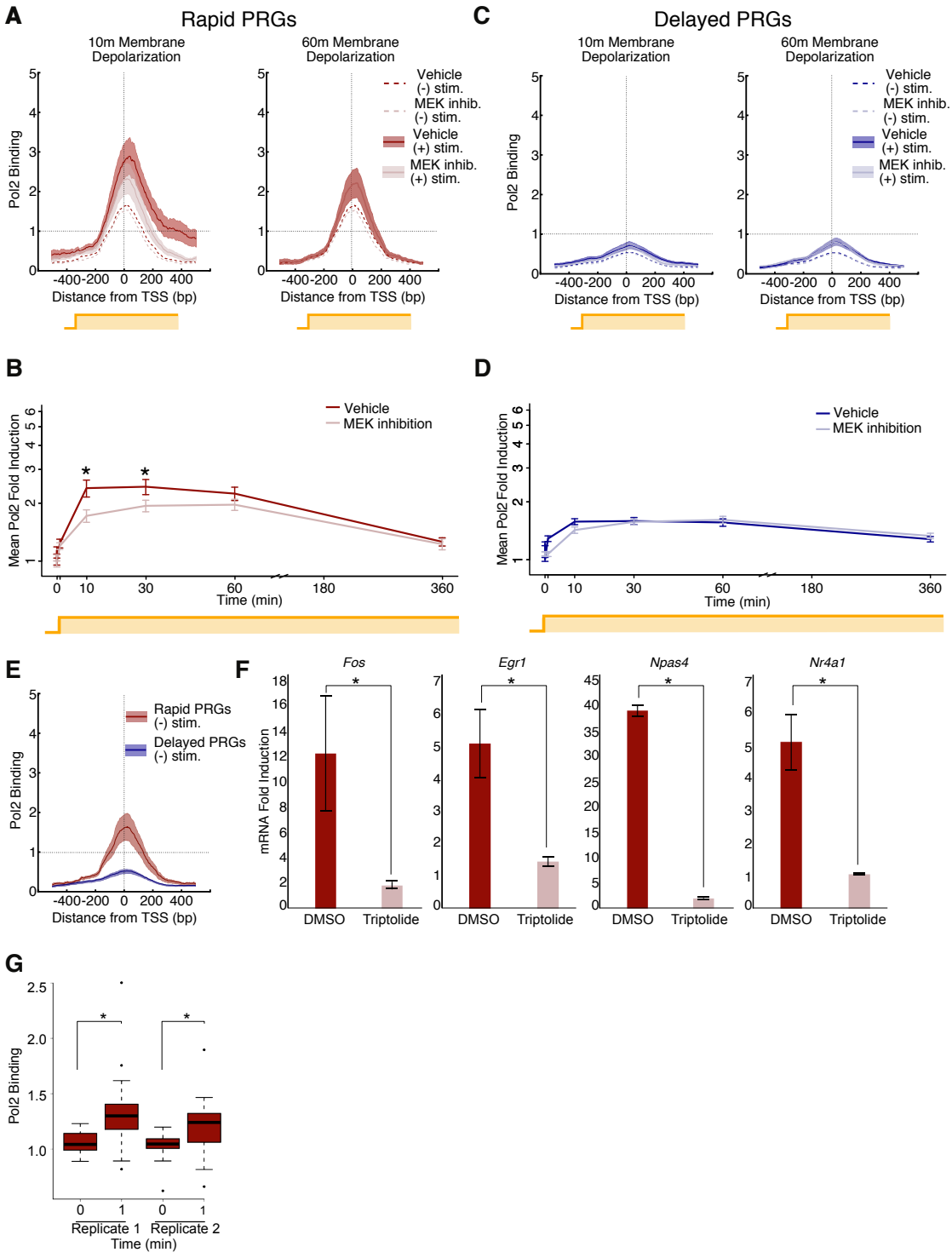

Figure 8. MAPK/ERK mediates fast recruitment of Pol2 to rapid PRG promoters.

Figure 8. (Continued) MAPK/ERK mediates fast recruitment of Pol2 to rapid PRG promoters.
(A) RNA Polymerase 2 (Pol2) binding (ChIP-seq) at the promoters of rPRGs, 10 and 60 minutes after KCl-mediated neuronal activation in the presence or absence of MEK inhibitor U0126 (10μM). Solid lines represent the mean and shading the S.E.M. across loci. Data shown are from the second of two biological replicates (see Figure 5 for the first replicate). The KCl-dependent fold-increase in mean Pol2 density (-300bp to +300bp) is significant under both vehicle and U0126 treatments (FDR<0.001 in each of two biological replicates, paired rank sum test).
(B) ChIP-seq-based time course of fold-change in Pol2 occupancy at rPRG promoters (-300bp to +300bp), with or without MEK inhibition. Shown are mean fold-change values, with +/- S.E.M error bars. *FDR <0.01 in each of two replicates (see also Figure 5B), paired rank-sum test on fold-change values with adjustment for multiple comparisons.
(C) RNA Pol2 binding (ChIP-seq) at the promoters of dPRGs, as in (A). (KCl-dependent increase, FDR <0.001 in each of two biological replicates).
(D) ChIP-seq-based time course of Pol2 occupancy at dPRG promoters. As in (B). The KCl-dependent fold-increase in mean Pol2 density (-300bp to +300bp) is significant under both vehicle and U0126 treatments (*FDR<0.001 in each of two biological replicates paired rank sum test).
(E) Promoter-binding of Pol2 in unstimulated neurons at rPRG and dPRG promoters (significantly different, p<0.001, rank sum test on area from -300 to +300).
(F) rPRG mRNA fold-change qPCR measurements following 30-minutes of depolarizing KCl, in the presence of vehicle or the transcription initiation blocker triptolide (10μM, 5-minute pre-treatment). *p<0.05 one-tail Student's t-test on log-normalized fold-change values. Error bars represent +/- S.E.M.
(G) Average unstimulated and one-minute rPRG promoter-bound Pol2 KCl fold-change values in samples treated with the vehicle, shown for two biological replicates. *FDR <0.01.

Furthermore, we found greater binding of the neuronal activity-regulated transcription factors SRF and MEF2, as well as the Mediator subunits MED23 and MED1 (Figure 7B, 6E), at rPRG promoters compared to dPRG or SRG promoters in unstimulated neurons (data from Kim et al., 2010; Telese et al., 2015). In contrast, the transcription factor CREB is pre-bound to a similar extent to rPRG and dPRG promoters but is not pre-bound to SRG promoters (Figure 7B, 6E). Interestingly, the NCoR repressor complex also binds preferentially to rPRG promoters compared to dPRG or SRG promoters (Figure 6H) and could prevent them from being transcribed despite their open state. These data suggest that in addition to an open chromatin state, pre-binding of transcriptional activators may uniquely poise rPRGs for rapid induction in unstimulated neurons.

The MAPK/ERK pathway is required for the first wave of gene induction

We next asked whether rPRGs are targeted by a rapidly-activated signaling pathway that endows them with the ability to respond quickly and to brief activity. In evaluating this possibility, we compared rPRGs and dPRGs but excluded SRGs to eliminate the confounding possibility of altered PRG induction affecting SRG induction. We first hypothesized that the CaMKIV pathway might mediate rPRG induction due to its role in rapid phosphorylation of the transcription factor, CREB (Hardingham et al., 2001; Wu et al., 2000). Using immunocytochemistry, we observed phospho-CaMKIV in the nucleus within just five minutes of membrane depolarization, indicating rapid pathway activation (Figure 9A). However, when we blocked CaMKIV phosphorylation using an inhibitor for the upstream kinase, CaMKK (Figure 9A), we found no effect on induction of rPRGs or dPRGs in response to either brief or sustained

activity, despite a small effect on ARG expression in unstimulated neurons (Fig. 9B-C, Supplemental Figure 1).

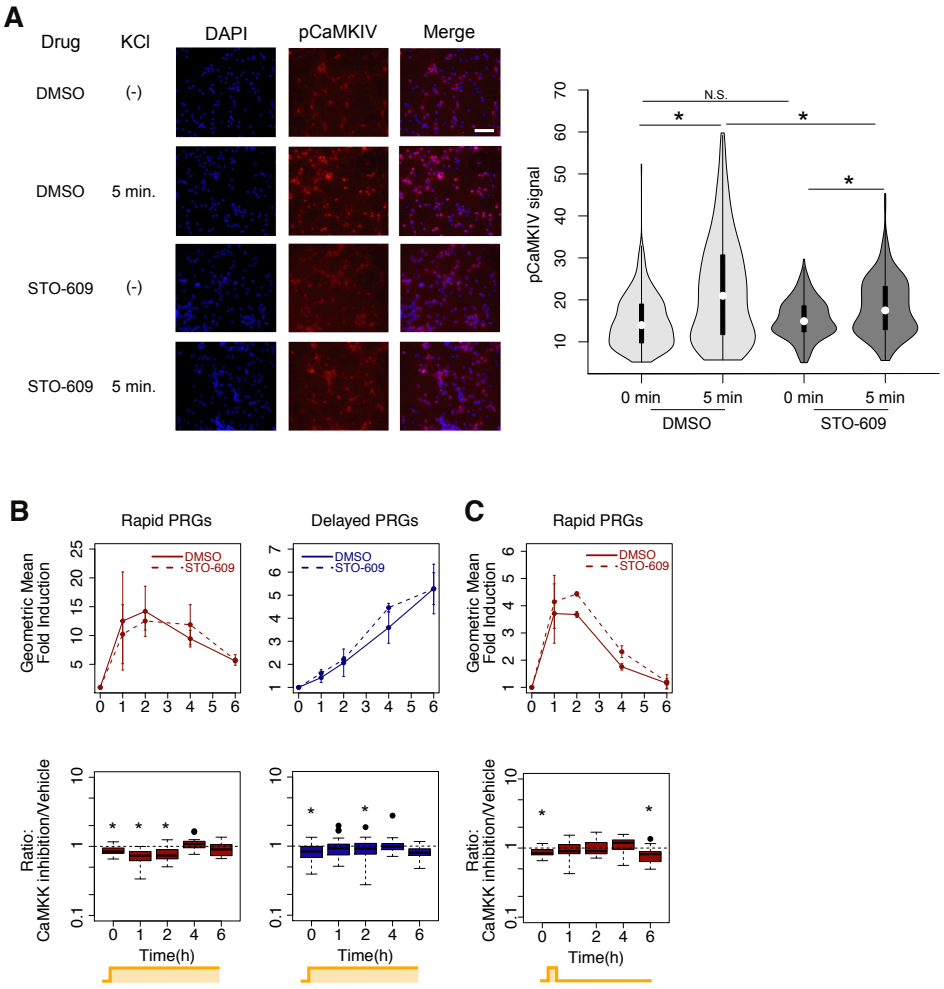

Figure 9. The CaMKK/CaMKIV pathway is not required for PRG induction.
(A) Left: immunocytochemistry for phospho-CaMKIV reveals pathway activation by 5 minutes of KCl-mediated membrane depolarization, seen by an increase in nuclear staining. 3μM of the CaMKK inhibitor STO-609 blocks nuclear accumulation of phospho-CaMKIV. Scale bar = 50μm, same for all images. Right: Quantification of nuclear phospho-CaMKIV signal (i.e., signal the overlaps with DAPI). Shown is a representative example of n=2 biological replicates. *p<0.00001, unpaired, two-tailed, t-test.
(B) High-throughput qPCR-based-based gene expression for 15 rPRGs (left) and 35 dPRGs (right) induced by sustained KCl treatment in the presence or absence of 3μM STO-609 (*significantly different from 1, p<0.05, rank-sum test). Metagene averages of fold induction (top) and boxplots showing expression of all tested genes (bottom). Error bars are +/- S.E.M. from each of n=2 biological replicates of geometric means of all genes in the category.

Figure 9. (Continued) The CaMKK/CaMKIV pathway is not required for PRG induction. (C) Same data as in (B) but for brief (1-min.) KCl stimulation. Error bars are +/- S.E.M. from each of n=2 biological replicates of geometric means of all genes in the category.

Therefore, the rapid induction and sensitivity to brief activity of rPRGs is not explained by a dependence on CaMKIV signaling.

We next asked whether another canonical neuronal signaling pathway, the MAPK/ERK pathway (Thomas and Huganir, 2004), is activated rapidly and in response to brief activity, which would be consistent with selective regulation of rPRGs. We assessed MAPK/ERK pathway activation by western blotting for the pathway's terminal kinase, phospho-ERK (pERK). In response to both brief and sustained activity, pERK levels reach the same peak magnitude by five minutes after the start of activity (Figure 7C-D,F), suggesting that the MAPK/ERK pathway is rapidly and fully activated by brief activity. Because pERK can activate transcription via phosphorylation of nuclear proteins (Thomas and Huganir, 2004), we confirmed that the MAPK/ERK target transcription factor, Elk-1, is phosphorylated rapidly and MAPK/ERK-dependently in response to sustained depolarization (Figure 10A).

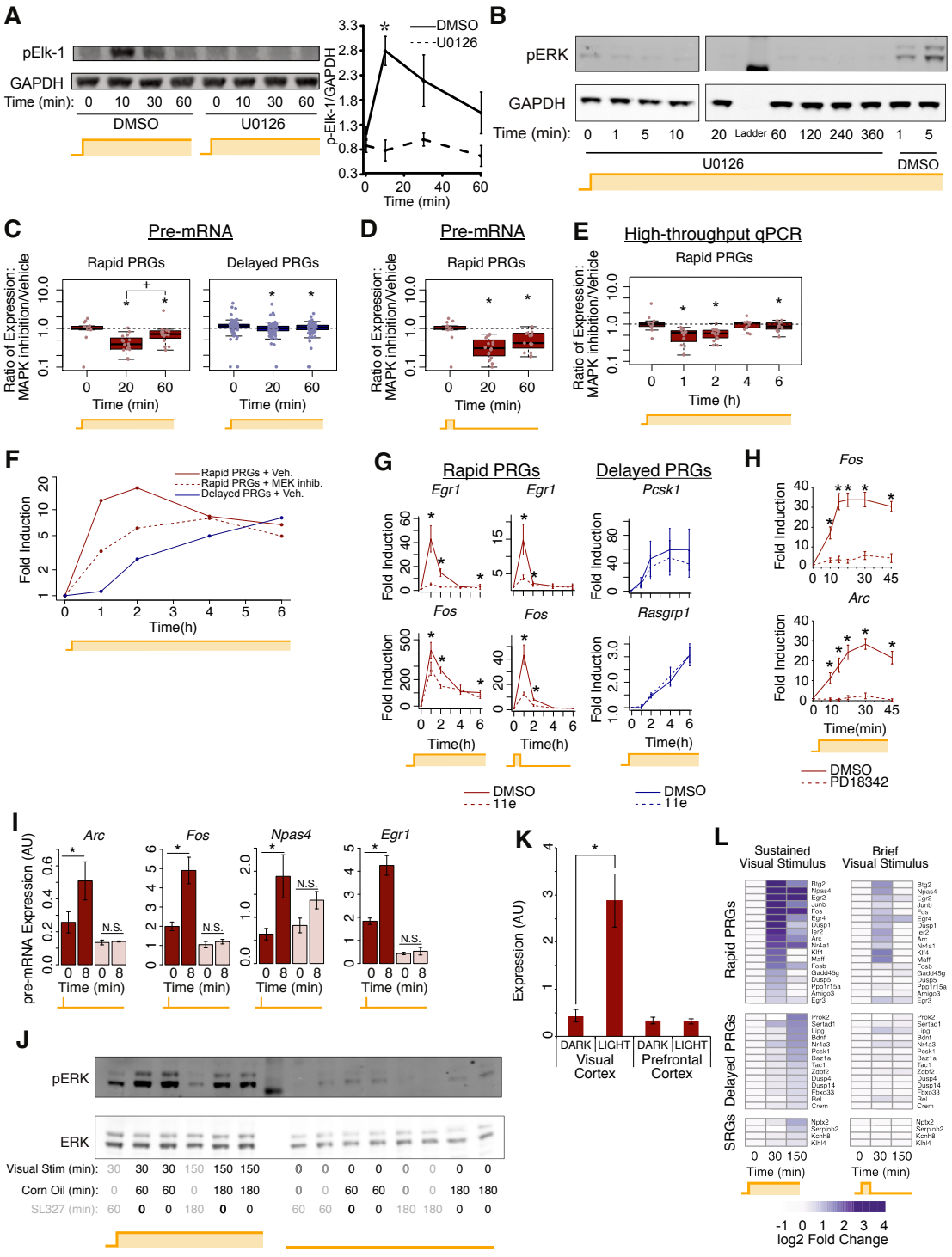

Figure 10. MAPK/ERK is required for the first (rapid PRG) but not subsequent waves of gene induction.

Figure 10. (Continued) MAPK/ERK is required for the first (rapid PRG) but not subsequent waves of gene induction.

(A) Elk-1 is phosphorylation is rapid and MAPK/ERK-dependent. Representative western blot using an antibody recognizing phosphorylated Elk-1 (pElk-1). On the right, quantification of western blotting from n=2-3 biological replicates. *pElk-1 blocked by MEK inhibition, $p<0.05$, unpaired Student's t-test. Error bars are +/- S.E.M.
(B) The U0126 inhibitor blocks MAPK/ERK pathway activation throughout a time course of neuronal stimulation via KCl-mediated depolarization. Representative western blot using an antibody recognizing phosphorylated ERK (pERK). Upper and lower bands are the phosphorylated p44 and p42 ERK paralogs (ERK1 and ERK2), respectively. Mouse cortical neurons were activated with continuous 55mM KCl-mediated depolarization for the indicated amount of time in the presence (or absence) of MEK inhibitor U0126 (10μM added 30 minutes before stimulation). Samples were run on two blots that were run, transferred, and treated with antibody together.
(C-D) Total RNA-seq intron-aligned reads to measure pre-mRNA expression for all rPRGs or dPRGs in the presence or absence of the U0126 MEK inhibitor upon KCl-depolarization. (C) Sustained activation (D) Brief activation. (*significantly different from 1, $p<0.003$, rank-sum test, $^{+}p<0.05$, rank-sum test). Expression of rPRGs is less affected by MEK inhibition than expression of dPRGs ($p = 0.003$; rank-sum test, 16 rPRGs vs. 109 dPRGs using mean for each gene from n=2 biological replicates at the time point of maximum induction).
(E) High-throughput qPCR (Fluidigm) to measure mRNA expression for all PRGs in the presence or absence of the U0126 MEK inhibitor upon neuronal activation with KCl. Expression of rPRGs is less affected by MEK inhibition than expression of dPRGs ($p = 0.003$; rank-sum test, 15 rPRGs vs. 37 dPRGs using mean for each gene from n=3-4 biological replicates at the time point with maximal induction). *significantly different from 1, $p<0.004$, rank-sum test.
(F) MEK inhibition blunts and delays the first wave (rPRGs), making it more similar to the second wave (dPRGs), based on median expression of rPRGs and dPRGs from high-throughput qPCR (Fluidigm) upon KCl-depolarization.
(G) Expression of representative rPRG and dPRG mRNA measured by qPCR in the presence or absence of the ERK inhibitor 11e (625nM) upon sustained or brief neuronal activation with KCl. *$p<0.01$, paired, two-sided, t-test. Error bars represent +/- S.E.M.
(H) Expression of representative rPRG pre-mRNA measured by qPCR in the presence or absence of the MEK inhibitor PD184352 (2μM) with sustained bicuculline/4AP treatment. *$p<0.01$, student's T-test. Error bars represent +/- S.E.M.
(I) rPRG pre-mRNA induction in response to a 10s bicuculline treatment requires MAPK/ERK signaling. MEK inhibited by 10μM U0126. Plotted is means from n=3-5 biological replicates. Error bars represent +/- S.E.M. *$p<0.05$, paired student's t-test. Vehicle-treated data same as Figure S1H.
(J) SL327 blunts MAPK/ERK pathway activation in vivo. Representative western blot of visual cortices from dark-housed mice treated with an intraperitoneal injection of corn oil or the MEK inhibitor SL327 (100mg/kg) and then exposed to visual stimulation (or left in the dark). Blotting was performed with an antibody recognizing phosphorylated ERK (pERK). Upper and lower bands are the phosphorylated p44 and p42 ERK paralogs (ERK1 and ERK2), respectively.
(K) Visual stimulation selectively induces gene expression in the visual cortex but not prefrontal cortex. qPCR of *Fos* mRNA expression in the visual and pre-frontal cortex of mice exposed to

Figure 10. (Continued) MAPK/ERK is required for the first (rapid PRG) but not subsequent waves of gene induction.
visual stimulation. Mice were dark-housed for three days and exposed to light for thirty minutes. *p<0.01, n=4 mice. Error bars represent +/- S.E.M.
(L) Profiling of gene expression in visual cortex before and after room-light visual stimulation, using ARG-seq. Only genes induced >1.4 fold in any condition in vitro were included (see methods). Data are means from n=2-4 mice. rPRG, dPRG, and SRG gene categories were defined from in vitro data as in Figure 1. Genes induced by brief visual stimulus are enriched for rPRGs (p=0.03, Fisher's exact test).

In further support that the MAPK/ERK pathway signals rapidly to the nucleus, we detected increased pERK in the nucleus by two minutes following both brief and sustained neuronal activity (Figure 7E). Interestingly, upon brief stimulation, ERK activity remains elevated for at least ten minutes after the removal of stimulus, which is more than sufficient time for activation of rPRG transcription.

We therefore hypothesized that the MAPK/ERK pathway is required for rPRG induction. To test this hypothesis, we measured ARG induction using ARG-seq in the presence of MAPK/ERK pathway inhibition (Figure 10B) using the potent and highly specific allosteric MEK inhibitor, U0126 (Favata et al., 1998). We found that MEK inhibition dramatically blunts induction of rPRGs but not dPRGs in response to sustained activity (Figure 6G-I). 95% of rPRGs but only 17% of dPRGs are sensitive to MEK inhibition (based on >40% decrease in maximum expression, Figure 6H). We also confirmed that MEK inhibition blocks induction of rPRG but not dPRG pre-mRNAs, suggesting that the MAPK/ERK pathways acts at the level of transcription (Figure 10C). This blunting of gene induction is unlikely to be due to off-target effects of U0126, since the MEK inhibitor PD184352 and the ERK inhibitor 11e have similar effects (Figure 10G-H). Most rPRGs are partially induced in the presence of MEK inhibition, but with delayed kinetics, indicating that MAPK/ERK activity is most important for the early stages of gene induction (Figure 6E-F).

We next asked whether MAPK/ERK signaling is also required for gene induction in response to brief activity. Impressively, MEK inhibition substantially decreases mRNA and pre-mRNA induction in response to brief activity (Figures 6J-L, 10D,I), blunting mRNA induction of all but

one of the induced rPRGs. Again, we observed similar results using the ERK inhibitor 11e (Figure 10G). Therefore, the MAPK/ERK pathway is required for rapid ARG induction and induction in response to brief activity, thus establishing the first wave of ARG induction in vitro.

We next investigated whether the MAPK/ERK pathway is required for rapid gene induction in vivo. We exposed dark-housed mice to brief (1-min) or sustained (up to 2.5-h) visual stimulation, consisting of turning on the room lights, in the presence or absence of MEK inhibition (Figure 10J). ARG-seq of the visual cortex revealed that MEK inhibition has a larger effect on rPRG compared to dPRG expression in cortices from mice exposed to sustained visual stimulation (Figure 11A-B), and it blocks nearly all ARG induction in mice exposed to brief visual stimulation (Figure 11C-D). Most of the ARG induction we observed appears to be due to the visual stimulation itself rather than stress from the lights or handling, as we did not observe induction of the rPRG, *Fos*, in the prefrontal cortex of mice exposed to visual stimulus (Figure 10K). We also confirmed that for the room-light visual stimulation used for this experiment, brief stimulation induces rPRGs better than dPRGs and SRGs ($p=0.03$, Fisher's exact test, Figure 10L). We therefore conclude that both in vivo and in vitro, the MAPK/ERK pathway is a fast pathway necessary rapid ARG induction and induction in response to brief activity.

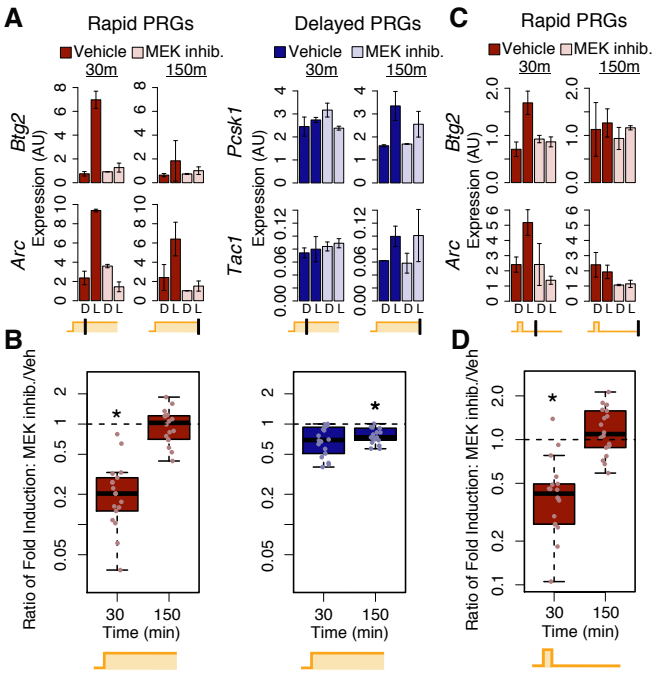

Figure 11. MAPK/ERK is required for the first wave but not subsequent waves of gene induction in vivo.
(A) Visual-stimulus-mediated gene induction of representative genes in the visual cortex upon sustained stimulation in mice injected intraperitoneally with corn oil vehicle or the MEK inhibitor SL327 (100mg/kg), based on ARG-seq. D: dark, no visual stimulation. L: light, with visual stimulation. Error bars are 95% confidence intervals across n=2-3 mice.
(B) Same experiment as (A), but showing all rPRGs or dPRGs detected by ARG-seq from n=2-3 biological replicates. *p<0.01 from rank-sum test, significant difference from 1. Induction of rPRGs is more affected by MEK inhibition than induction of dPRGs (p=0.02; rank-sum test, 16 rPRGs vs. 14 dPRGs using the mean for each gene at its most induced time point across n=2-3 biological replicates).
(C) Same as (A) but with brief visual stimulation.
(D) Same as (B) but with brief visual stimulation.

The MAPK/ERK pathway mediates fast Pol2 recruitment to rapid PRG promoters

We next sought to understand how the MAPK/ERK pathway mediates rapid induction of rPRG promoters. Because ARG induction is accompanied by Pol2 recruitment to ARG promoters within the first two hours of activity (Kim et al., 2010), we hypothesized that the rapidity of

rPRG induction could be mediated by fast, MAPK/ERK-dependent Pol2 recruitment. Indeed, using Pol2 ChIP-seq, we observed a rapid increase in Pol2 occupancy at rPRG promoters by one to ten minutes of activity (Figures 12A-B, 8A-B, Figure 8G).

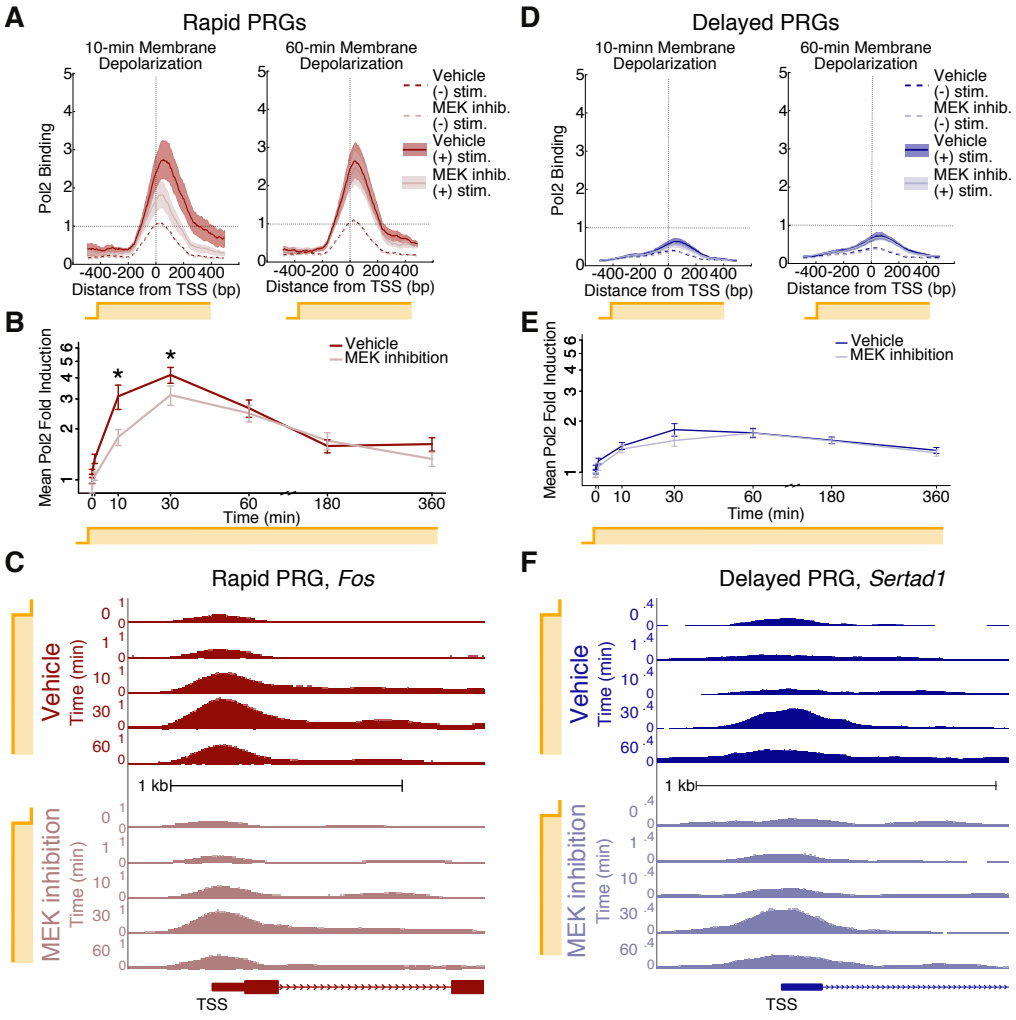

Figure 12. MAPK/ERK mediates fast recruitment of Pol2 to rapid PRG promoters.
(A) RNA Polymerase 2 (Pol2) binding (ChIP-seq) at the promoters of rPRGs. Lines represent the mean and shading the S.E.M. across loci. Data shown are from n=1 of 2 biological replicates. Pol2 binding to rPRG promoters is blunted by MEK inhibition (see (B)). The KCl-dependent fold-increase in mean Pol2 density (-300bp to +300bp) is significant under both vehicle and MEK inhibitor treatments (FDR<0.001 in each of two biological replicates, paired rank sum test). MEK inhibition does not affect Pol2 occupancy in unstimulated neurons (FDR>0.05 in each of two biological replicates, paired rank sum test).

Figure 12. (Continued) MAPK/ERK mediates fast recruitment of Pol2 to rapid PRG promoters.

(B) ChIP-seq-based time course of fold-change in Pol2 occupancy at rPRG promoters (-300bp to +300bp). Shown are mean fold-change values across genes, with +/- S.E.M error bars. *FDR <0.01 in each of two replicates, paired rank-sum test on fold-change values.
(C) Pol2 binding at the promoter of the representative rPRG *Fos* upon sustained neuronal activation. Data normalized prior to visualization.
(D) Plotting and statistics same as (A) but showing dPRG promoters.
(E) Plotting and statistics as in (B) but showing dPRG promoters.
(F) Plotting as in (C) but showing representative dPRG, *Sertad1*.

We also found that pharmacological blockade of new transcription initiation completely abolishes rPRG mRNA induction (Figure 8F), suggesting that initiation of transcription by newly recruited Pol2 is essential for rPRG induction. To ask if MAPK/ERK signaling is required for the rapid recruitment of Pol2 to rPRG promoters, we performed Pol2 ChIP-seq in a time course of neuronal stimulation in the presence and absence of MEK inhibition. MEK inhibition reduces Pol2 occupancy at rPRG promoters at ten and 30 minutes of activity (Figures 12A-C, 8A-B), indicating that MAPK/ERK signaling is required for rapid recruitment of Pol2 to these promoters. However, MEK inhibition has no effect at later time points, suggesting that other pathways mediate slower Pol2 recruitment to rPRG promoters. Because pre-bound, paused Pol2 may facilitate faster recruitment of Pol2 by maintaining an open chromatin state (Gilchrist et al., 2010), we next asked whether MAPK/ERK signaling might enable rapid Pol2 recruitment by mediating the pre-binding and pausing of Pol2 at rPRG promoters in unstimulated neurons (Saha et al., 2011). We found that MEK inhibition does not change the Pol2 occupancy at ARG promoters in unstimulated neurons (Figures 12A, 8A), indicating that MAPK/ERK signaling is required specifically for rapid, activity-dependent Pol2 recruitment.

We next assessed the effect of MAPK/ERK signaling on Pol2 recruitment to dPRG promoters. Surprisingly, despite the slow transcriptional induction of dPRGs, we observed recruitment of Pol2 to many of their promoters by ten minutes of neuronal activation (Figure 12D-E, 8C-D). However, in contrast to rPRGs, recruitment of Pol2 to dPRG promoters is not affected by MEK inhibition at early or late time points, either for the full set of dPRGs (Figure 12D-F, 8C-D) or a restricted set with greater Pol2 occupancy (FDR>0.01, rank-sum test, see methods). These results are consistent with a model in which MAPK/ERK signaling is required for rapid Pol2

recruitment to rPRG promoters, which are primed by pre-bound transcriptional machinery, but not for recruitment to dPRG promoters, which may require chromatin remodeling.

The MAPK/ERK pathway is required for eRNA transcription but not H3K27 acetylation at rapid enhancers

Pol2 could be recruited to the promoters of rPRGs in a MAPK/ERK-dependent manner via delivery from genomic enhancers (Szutorisz et al., 2005). We therefore asked whether enhancer activation might be dependent on MAPK/ERK signaling using H3K27 acetylation (H3K27ac) as a proxy for enhancer activity (Creyghton et al., 2010; Rada-Iglesias et al., 2011). We performed H3K27ac ChIP-seq throughout a time course of neuronal activation and analyzed H3K27ac levels at 940 putative ARG enhancers. We hypothesized that enhancers near rPRGs would have rapid, activity-dependent activation and require MAPK/ERK signaling whereas enhancers near dPRGs would be activated slowly and be MAPK/ERK-independent. Surprisingly, most activity-regulated enhancers rapidly gain H3K27ac within ten minutes of activity, regardless of the kinetics of their nearby promoters (Figure 13A-C). Furthermore, accumulation of H3K27ac does not require MAPK/ERK signaling, as MEK inhibition has no effect on activity-dependent H3K27ac at these enhancers, including those near MEK-dependent rPRGs (Figures 13D, S8A). Thus, H3K27ac is neither MAPK/ERK-dependent nor kinetically distinguishes enhancers near rPRGs versus dPRGs.

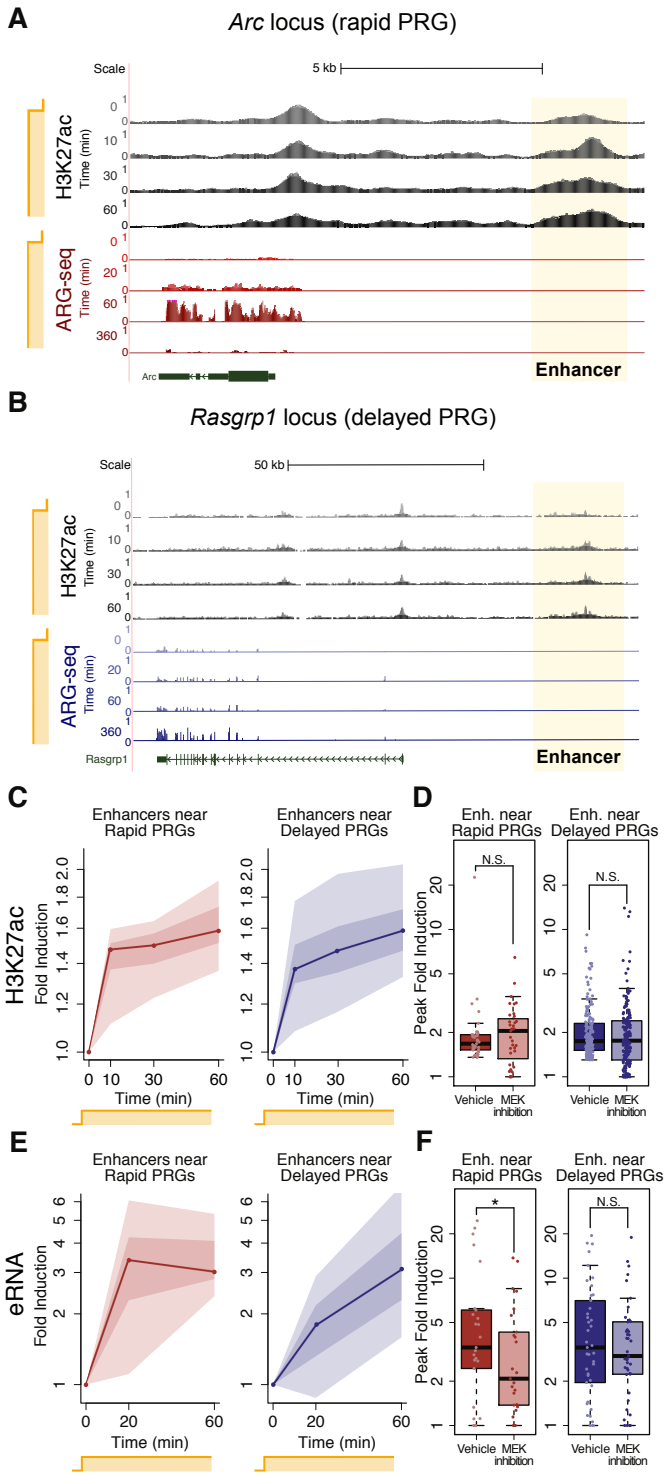

Figure 13. MAPK/ERK is required for rapid eRNA induction but not H3K27 acetylation at enhancers

Figure 13. (Continued) MAPK/ERK is required for rapid eRNA induction but not H3K27 acetylation at enhancers

(A) H3K27ac accumulation (ChIP-seq) at the rPRG *Arc* locus upon sustained KCl depolarization. The gene expression of *Arc* based on ARG-seq is shown for comparison. Data normalized by read-depth prior to visualization.
(B) Same as (A), but for the dPRG, *Rasgrp1*.
(C) H3K27ac accumulation (ChIP-seq) at enhancers upon sustained KCl depolarization. Plotted are means from n=2 biological replicates. Lines represent the median across enhancers, dark shading the two middle deciles, and light shading the upper and lower quartiles. The increase from 0 to 10 min is significant for both enhancers near rPRGs and those near dPRGs ($p<0.00001$, rank-sum test).
(D) H3K27 accumulation at enhancers near rPRGs and dPRGs is not significantly affected by MEK inhibition ($p>0.2$, rank-sum test). Data as in (C). The y-axis shows the induction at each enhancer's most-induced time point (10, 30, or 60 min) in each condition.
(E) eRNA induction (total RNA-seq) upon neuronal activation. Plotted as in (C).
(F) MEK inhibition blocks eRNA induction at enhancers near rPRGs but not dPRGs. Plotting as in (D), except showing the maximum eRNA induction at 20 or 60 min. *$p=0.01$, rank-sum test, using means for each enhancer from n=2 biological replicates; N.S., $p>0.05$.

We next assessed another proxy of enhancer activity, enhancer RNA (eRNA) transcription (Kim et al., 2010). Surprisingly, total RNA-seq revealed that eRNA is induced more rapidly at enhancers near rPRGs than at those near dPRGs, thus mirroring mRNA expression kinetics more closely than H3K27ac (Figure 13E). Furthermore, in contrast to our finding that H3K27ac is unaffected by MEK inhibition, MEK inhibition attenuates eRNA induction at enhancers near rPRGs (Figures 13F, 14A). These results indicate that rPRGs are distinguished by their proximity to rapidly activated enhancers whose eRNA induction but not H3K27ac is MAPK/ERK-dependent.

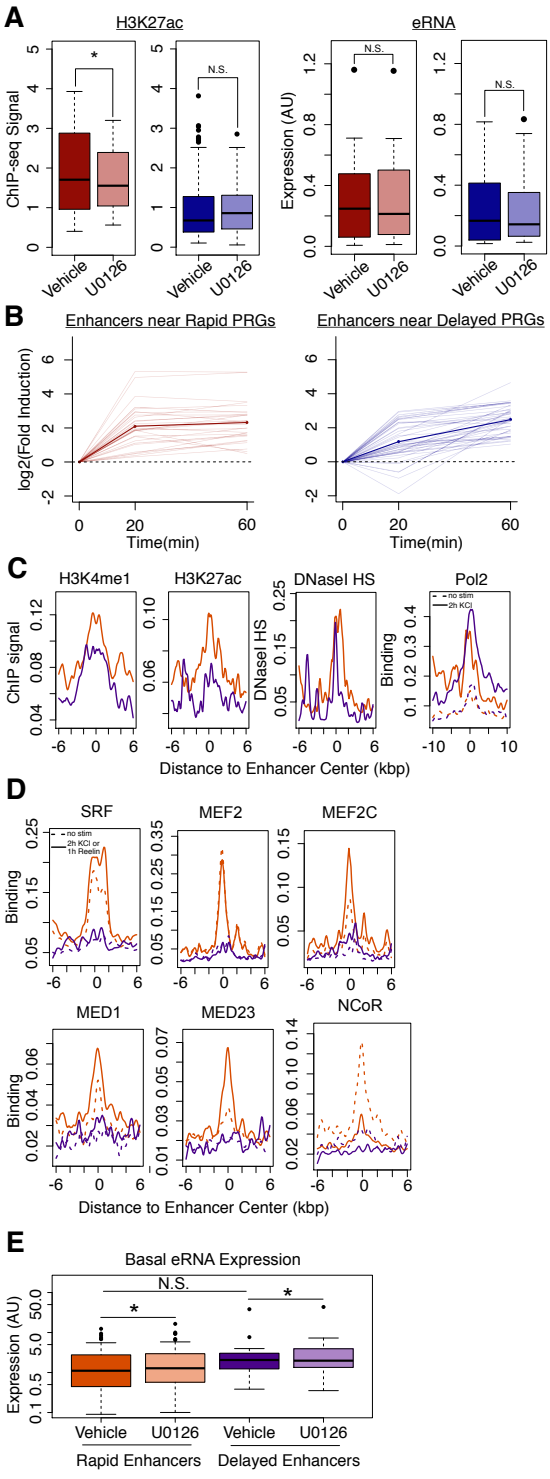

Figure 14. MAPK/ERK is required for rapid eRNA induction but not H3K27 acetylation at enhancers.

Figure 14. (Continued) MAPK/ERK is required for rapid eRNA induction but not H3K27 acetylation at enhancers.

(A) Effect of MEK inhibition on H3K27ac and eRNA expression in unstimulated neurons. There is a slight effect of MEK inhibition on H3K27ac in unstimulated neurons (*$p<0.02$, rank-sum test). H3K27ac from ChIP-seq and eRNA from total RNA-seq.
(B) Enhancers near rPRGs exhibit more rapid induction than enhancers near dPRGs, based on eRNA-seq (as done in Figure 7C with total RNA-seq data). Rapid enhancers have greater induction at 20 minutes than delayed enhancers ($p=0.01$, rank-sum test). The dark line is the geometric mean of all enhancers shown and light lines represent individual enhancers. Enhancer expression kinetics roughly mirror that of nearby promoters.
(C) DNaseI HS and H3K27ac and H3K4me1 occupancy prior to stimulation is greater at rapid than delayed enhancers (based on area under the curves, $p<0.01$, rank sum test). Pol2 binding is not significantly different between rapid and delayed enhancers ($p>0.1$). Shown as metaplots of the geometric mean of the signal all enhancers in the category. H3K4me1 and Pol2 ChIP-seq data from Kim et al., 2010. DNaseI HS data from ENCODE.
(D) Transcription regulator binding in unstimulated and stimulated mouse neurons from ChIP-seq also shown as metaplots as in (C). MEF2C and MED1 binding is greater at rapid enhancers than delayed enhancers in unstimulated neurons ($p<0.01$, rank-sum test, for significance of other transcription factors in unstimulated neurons see figure 7G). For SRF, stimulation was with 2h of KCl-mediated depolarization (Kim et al., 2010). For MEF2, MEF2C, MED1, NCoR and MED23 stimulation was with 1h of reelin (Telese et al., 2015). SRF, MEF2, MEF2C, MED1, and MED23 binding is greater at rapid enhancers than delayed enhancers in stimulated neurons ($p<0.011$, rank-sum test). NCoR binding is lost with stimulation. Stimulation shown for comparison.
(E) eRNA expression at rapid and delayed enhancers in unstimulated neurons in the presence or absence of U0126. There is no statistically significant difference between rapid and delayed enhancers under vehicle treatment ($p > 0.01$, rank-sum test). There is a very minor yet significant effect of U0126 treatment on both classes of enhancers (*$p<0.01$, rank-sum test). Data from eRNA-seq.

We next asked whether the rapidity of eRNA induction near rPRGs is inherent to the enhancers themselves or simply a by-product of activation of nearby promoters. We predicted that if enhancer activation properties are inherent to the enhancers, we should observe a subset of enhancers whose kinetics and sensitivity to brief activity differ from their nearby promoters. To test this prediction, we needed to assess enhancers individually rather than in groups based on the kinetics of nearby promoters (as above). We therefore developed (Figure 15A-B) and validated (Figure 14B) a targeted capture method, eRNA-seq, to enrich RNA-seq libraries for eRNAs by about 500-fold. We then identified and classified activity-regulated enhancers as rapid or delayed based on the kinetics of their eRNA induction (Figure 15C). While most activity-regulated enhancers near rPRG promoters are rapid enhancers, a minority (21%) are delayed enhancers (Figure 15D-E). Moreover, 50% of activity-regulated enhancers near dPRGs are rapid and 50% are delayed enhancers (Figure 15D), supporting the idea that enhancer activation kinetics are inherent to enhancers rather than nearby promoters. In further support of this idea, we found that rapid enhancers are more sensitive to brief activity than delayed enhancers (Figure 15H), even when considering only those enhancers near dPRGs ($p<10^{-4}$, rank-sum test, see methods). This dissociation between the kinetics and brief-activity sensitivity of a subset of enhancers and their nearby promoters supports the idea that enhancer activation is not merely a by-product of transcription at the promoter.

After identifying individual enhancers as inherently rapidly activated, we asked whether rapid eRNA induction at rapid enhancers might be mediated by an open chromatin state and sensitivity to MAPK/ERK signaling, similar to mRNA induction from rPRG promoters. Indeed, compared to delayed enhancers, we found that rapid enhancers have significantly elevated CpG content.

They also have more open, active chromatin in unstimulated neurons, as evidenced by higher DNAse hypersensitivity, greater binding of the transcription activators SRF, MEF2 and Mediator, and greater binding of the transcriptional repressor NCoR (Figure 15F-G, 14C-D). However, unlike rPRG promoters, rapid enhancers show little binding of Pol2 in unstimulated neurons (Figure 14C). The more active chromatin state at rapid enhancers appears to be intrinsic to the enhancers themselves rather than an indirect effect of their associated promoters, since a comparison of just those rapid and delayed enhancers near dPRGs revealed the same differences in CpG content, active chromatin marks, and transcription factor pre-binding in unstimulated neurons ($p<0.01$, rank-sum test, see methods). Using eRNA-seq in the presence of a MEK inhibitor, we also found that rapid enhancers are more sensitive to MAPK/ERK inhibition than delayed enhancers (Figure 15E,I, Figure S8E). In the case of at least one enhancer, Fos "e5" (Joo et al., 2015), MAPK/ERK-dependent enhancer activation is required for activity-dependent promoter activation, based on a luciferase reporter assay (Figure 15J). These results indicate that rapid enhancers are primed for rapid MAPK/ERK-dependent activation whether they are near first- or second-wave genes.

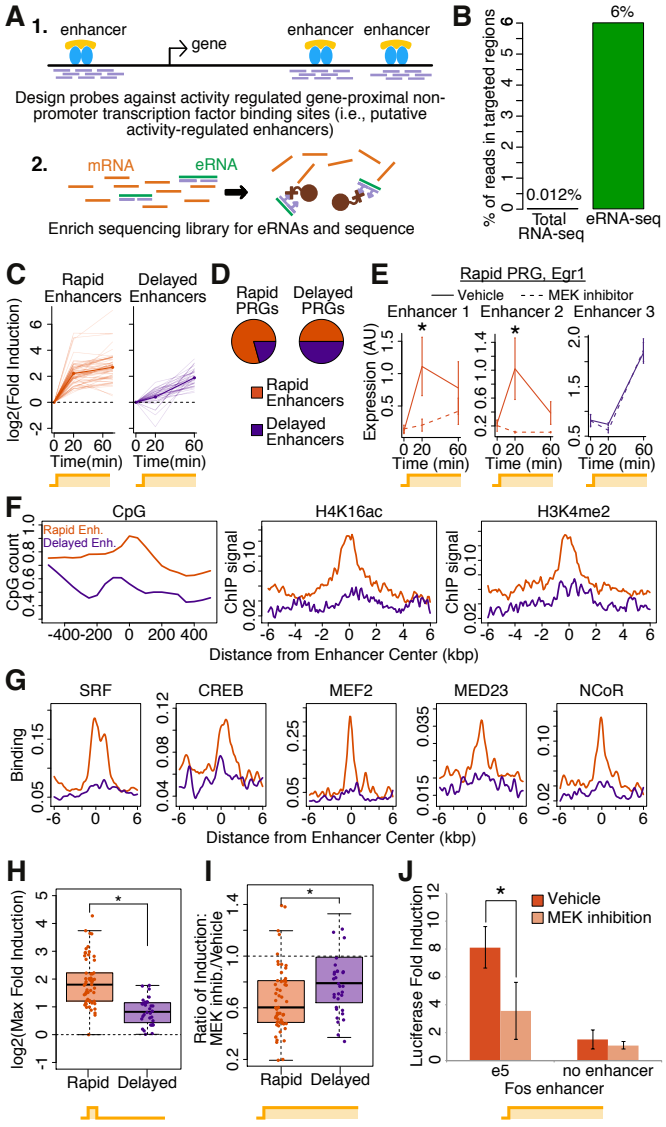

Figure 15. eRNA-seq enables eRNA quantification at individual enhancers, revealing rapid and delayed enhancers.

(A) eRNA-seq methodology.
(B) Reads in target enhancers: eRNA-seq vs. total RNA-seq.
(C) eRNA-seq-based eRNA expression at significantly induced (FDR<0.05) rapid and delayed enhancers upon sustained activation. Rapid enhancers are significantly induced by 20 minutes and delayed enhancers only by 60 minutes. Light lines are means for individual enhancers from n=4 biological replicates, and heavy lines are the geometric means for all enhancers shown.
(D) rPRGs compared to dPRGs are enriched for the presence of nearby rapid enhancers (p=0.02, Fisher's exact test), but there are also rapid enhancers near dPRGs.

Figure 15. (Continued) eRNA-seq enables eRNA quantification at individual enhancers, revealing rapid and delayed enhancers.

(E) eRNA-seq-based eRNA expression at three enhancers near the rPRG *Egr1* revealing two rapid and one delayed enhancer. *$p<0.05$, paired rank-sum test. Error bars are means +/- S.E.M.
(F) Indicators of open chromatin prior to stimulation at rapid versus delayed enhancers, with metaplots showing the geometric mean of all enhancers in each class. All are significantly different between rapid and delayed enhancers ($p<10^{-7}$, rank sum test using area under the curve). Histone mark ChIP-seq data from cultured cortical neurons, Telese et al., 2015.
(G) Binding of transcription factors, the mediator subunit MED23, and NCoR at rapid versus delayed enhancers prior to stimulation, shown as in (F). All are significantly different between rapid and delayed enhancers ($p<10^{-4}$, rank sum test on area under the curve). ChIP-seq data from cultured cortical neurons, Kim et al., 2010; Telese et al., 2015.
(H) Rapid enhancers show greater induction in response to brief activity than delayed enhancers, based on eRNA-seq ($p < 10^{-9}$, rank-sum test). The y-axis shows the mean fold induction from n=4 biological replicates for each enhancer at its most-induced time point (20 or 60 min).
(I) Rapid enhancers are more MAPK/ERK-dependent than delayed enhancers, based on eRNA-seq ($p = 0.006$, rank-sum test, using means for each enhancer from n=4 biological replicates). For each class of enhancers, the earliest time point at which that class exhibits significant eRNA induction is shown (20 min for rapid and 60 min for delayed enhancers). The y-axis shows the KCl-dependent fold induction with MEK inhibition divided by the same fold-induction with vehicle treatment only (i.e., ratio of fold-inductions).
(J) Effect of MEK inhibition on the enhancer function of the Fos enhancer e5, using a luciferase reporter assay in which the enhancer drives transcription from a minimal Fos promoter. *$p<0.03$ from t-test based on n=3 biological replicates.

2.4 Discussion

Using genome-scale technology, we demonstrate that a neuron's activity pattern is encoded in its gene expression profile. Furthermore, we uncover a principle underlying the coupling map that links activity pattern to gene expression: the duration of neuronal activity has a logical relationship to three temporally and mechanistically distinct waves of gene induction. These three waves of gene induction include rPRGs, dPRGs, and SRGs, which are all induced by sustained neuronal activity. In contrast, brief activity induces only the first of these waves, rPRGs, which are uniquely dependent on MAPK/ERK signaling for their induction (Figure 16).

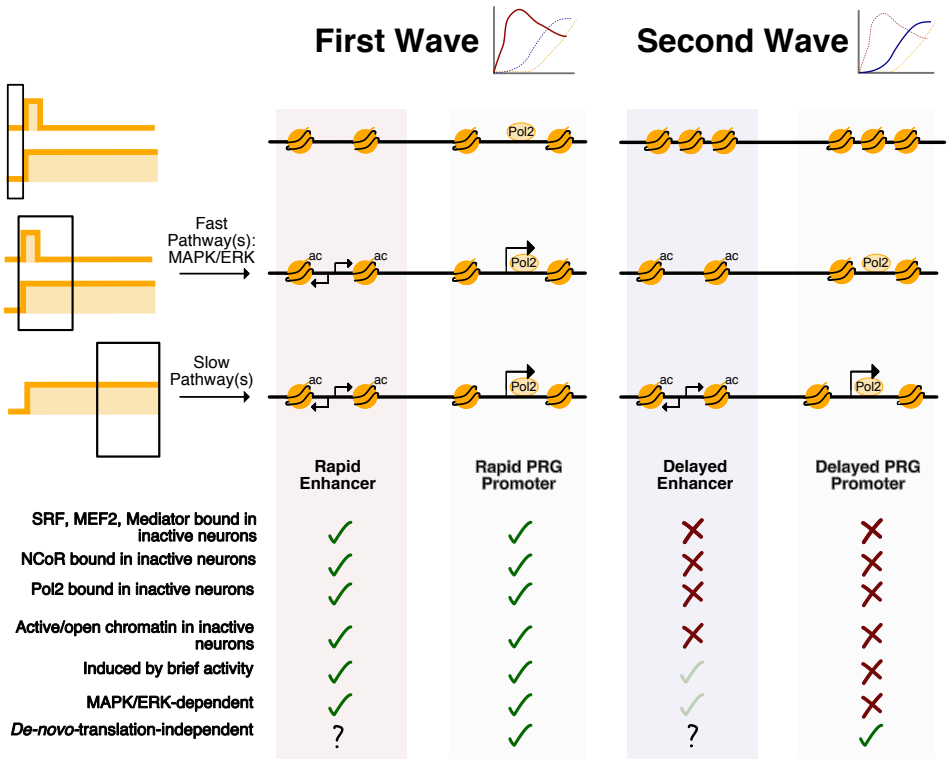

Figure 16. Distinguishing features of first wave genes (rapid PRGs) and second wave genes (delayed PRGs).
rPRGs are distinguished by dependence on MAPK/ERK signaling, proximity to rapid enhancers, and an open chromatin state. Light green check marks indicate partial effects.

Abolishing MAPK/ERK signaling not only alters the multi-wave structure of the ARG response by blunting and delaying rPRG induction, but it also abolishes rPRG induction in response to brief activity. In this way, MAPK/ERK both establishes the multi-wave structure of ARG transcription and enables activity-duration-specific gene induction. This shared mechanism suggests that a biological advantage of the multi-wave structure of ARG induction is to enable different activity patterns to induce different subsets of genes.

MAPK/ERK establishes the first wave of gene induction

We identify the MAPK/ERK pathway as a key determinant of the first wave of neuronal ARG induction, enabling first-wave genes to respond rapidly and to brief activity. However, our results suggest that other pathways must establish later waves of ARG induction. In contrast to this idea that multiple different pathways each regulate their own subset of genes, in PC12 cells the MAPK/ERK pathway itself mediates two different cellular outcomes depending on the duration of MAPK/ERK activation (Gotoh et al., 1990; Marshall, 1995; Santos et al., 2007). Our finding that MAPK/ERK pathway is a fast pathway for activating ARG induction also differs from previous studies that suggest it could be a relatively slow regulator of transcription, including those showing it is slow to phosphorylate the transcription factor CREB (Hardingham et al., 2001; Murphy et al., 1994; Toettcher et al., 2013; Wu et al., 2000). Slow MAPK/ERK-dependent phosphorylation of CREB could be important for regulating SRGs, especially given the persistence of phospho-ERK in response to sustained stimulation. Despite its slow phosphorylation of CREB, others have found that the MAPK/ERK pathway can be rapidly activated in the nucleus in response to brief stimulation (Dudek and Fields, 2001; Zhai et al.,

2013) and is required for induction of several genes that we can now classify as rPRGs (Davis et al., 2000; Eriksson et al., 2006; Zheng et al., 2009).

There are at least two ways that MAPK/ERK could specify which genes are included in the first wave. In a passive model, rPRG promoters could be uniquely sensitive to MAPK/ERK signaling solely due to their open chromatin state in inactive neurons. This open chromatin state could prime rPRG promoters to be activated by MAPK/ERK within the first few minutes following neuronal activation, when MAPK/ERK is most active. Our study and previous work (Saha et al., 2011) suggest that this open chromatin state may be maintained in inactive neurons by the paused Pol2 found at rPRG promoters prior to neuronal activation. This function for Pol2 is consistent with the current view of the function of paused Pol2 generally (Gilchrist et al., 2010), as well as our finding that the paused Pol2 is insufficient for appreciable gene induction in the absence of new Pol2 recruitment and initiation. In an active model of how MAPK/ERK specifies first-wave genes, MAPK/ERK signaling could activate rPRGs due to specific binding of MAPK/ERK-dependent transcriptional activators, including SRF (Treisman, 1996). SRF is required in vivo for the transcription of rPRGs (Ramanan et al., 2005) and often acts in concert with Elk-1, which is directly phosphorylated by MAPK/ERK (Figure S6A, Marais et al., 1993; Sgambato et al., 1998; Xia et al., 1996). Elk-1 facilitates Pol2 recruitment via interactions with the Mediator subunit MED23 (Allen and Taatjes, 2015; Wang et al., 2005). We present correlative evidence that rPRGs may be regulated by SRF, Elk-1, MEF2, and MED23 and by activation of nearby rapid enhancers, but further work is required to causally link these mechanisms to rPRG induction.

Separable mechanisms of enhancer activation revealed by MAPK/ERK

Surprisingly, we find that the MAPK/ERK pathway regulates eRNA induction but not H3K27ac accumulation at rapid enhancers, suggesting that enhancer activation occurs in multiple mechanistically separable steps. H3K27ac is a commonly used mark for enhancer activity (Creyghton et al., 2010; Rada-Iglesias et al., 2011), but we find H3K27ac accumulates at enhancers even in the presence of MAPK/ERK inhibition, which blocks eRNA (and mRNA) induction. In other contexts histone acetylation has been shown to accumulate despite blocking eRNA transcription, Pol2 recruitment, or initiation of transcription (Hah et al., 2013; Kaikkonen et al., 2013; Wang et al., 2005). These and other experiments (Zhu et al., 2013) suggest that eRNA transcription may be a better marker for enhancer activation than H3K27ac, more accurately reflecting the extent to which an enhancer is activating transcription at a nearby promoter. Given these findings, our eRNA-seq method may be a particularly useful technique for reliably assaying enhancer activation genome wide.

Role of rapid PRG protein products

The protein products of rPRGs may be required for the cell biological changes that occur following a single occurrence of brief neuronal activity. For example, brief single behavioral trials are sufficient both for *Arc* induction in hippocampal region CA3 (Miyashita et al., 2009) and for CA3-dependent spatial learning (Nakazawa et al., 2003), suggesting that *Arc* may be required for this learning. In another example, just seven minutes of bicuculline treatment (similar to our five-minute treatment) is sufficient to induce transcription- and MAPK/ERK-dependent long-lasting synchronous bursting of primary neurons (Arnold et al., 2005). We

hypothesize that the ARG-dependent cell biological effect of brief activity is due in large part to the effect of just a few rPRGs that are not transcription factors (e.g., *Arc*, *Amigo3)*. In contrast, physiological responses to prolonged activity, including homeostatic responses like synaptic scaling and firing rate homeostasis (Hengen et al., 2016; Ibata et al., 2008; Turrigiano, 2011), may be mediated by the protein products of dozens to hundreds of dPRGs and SRGs. Our identification of the MAPK/ERK pathway as structural determinant of the first wave of ARG induction now makes it possible to test the specific function of these first wave genes in transcription-dependent plasticity. In other words, by defining the contribution of MAPK/ERK to the coupling map, our work should enable manipulation of the coupling map to investigate its functional significance.

Chapter 3

Allosteric inhibitors of p97/VCP inhibit neuronal activity-dependent transcription

3.1 Introduction

Neuronal activity initiates cascades of gene expression that coordinate long-lasting neuronal plasticity. The earliest wave of activity-dependent transcription comprises a small set of immediate-early genes (IEGs) which predominately encode for transcription factors that specify the expression of downstream effector genes. A key feature of IEG transcription is its ability to be both rapidly and transiently activated in response to neuronal activity, waning even in the continued presence of elevated neuronal activity or calcium signaling. While several candidate mechanisms have been proposed for the negative regulation of specific IEGs, such as the actions of HDACs or transcriptional repressors, their contribution globally to IEG downregulation remains untested.

The DNA damage response (DDR) has been linked to stimulus-dependent transcription (Calderwood, 2016; Ju & Rosenfeld, 2006) including AP-1-dependent transcription and neuronal activity-dependent transcription (Madabhushi et al., 2015), though the precise relationship remains poorly understood. Recent observations in primary neurons have raised the hypothesis that the repair of DNA double-stranded breaks (DSBs) might underlie the negative regulation of IEG transcription, as inhibition of the repair kinase DNA-PK was shown to produce elevated IEG mRNA levels hours after NMDA stimulation—time points in which levels of some immediate early genes had returned to baseline (Madabhushi et al., 2015). Moreover, shRNA-knockdown of Tdp2, an enzyme essential for the repair of DNA lesions caused by TOP2B, was reported to enhance the magnitude of mRNA induction of these same genes (Madabhushi et al., 2015). Other work focusing on nuclear hormone activation has shown that single-stranded DNA lesioning by topoisomerase-I is essential for the activation of ligand-dependent transcription,

through a mechanism that involves enhancer activation (Puc et al., 2015). This nuclease activity activates a DNA-damage response, leading to the recruitment of DDR proteins to these stimulus-dependent enhancers and promoters (Puc et al., 2015). Notably, the recruitment of essential DNA-repair enzymes, Ku80 and DNA ligase, occurs at late time-points relative to stimulus onset and transcription activation (Puc et al., 2015). The delayed kinetics of repair-enzyme recruitment are supportive of a model in which repair of single-stranded or double-stranded DNA lesions acts to then downregulate stimulus-dependent transcription. In fact, some of these repair enzymes, such as Ku70 and Ku80 (which are p97/VCP substrates) have been shown to inhibit transcription (Sucharov et al., 2004).

Therefore, I decided to test the contribution of the DDR to neuronal activity-dependent transcription by treating cultured primary neurons with pharmacological inhibitors of DDR proteins and DNA-repair mechanisms and then measuring transcriptional responses to depolarizing KCl treatment. These experiments produced an unexpected result. One inhibitor, NMS-873, acted to completely suppress activity-dependent transcription. NMS-873 is an allosteric inhibitor of p97/VCP (Magnaghi et al., 2013), an AAA ATPase which functions as a molecular "segregase" to disassemble protein complexes. p97/VCP most commonly processes poly-ubiquitinated substrates, many of which are then targeted to the proteasome for degradation. p97/VCP has also recently been identified as being essential for the repair of double-stranded breaks (DSBs) (Meerang et al., 2011; van den Boom et al., 2016). These results concerning NMS-873 raise the possibility that p97/VCP might have an unknown function in the series of molecular events underpinning the activation of IEGs, in a manner which might involve DNA damage.

p97/VCP is best known for its essential activity in the Endoplasmic Reticulum Associated Degradation (ERAD) protein quality control process (Ye, Meyer, & Rapoport, 2001). The discovery of chromatin-based functions of p97/VCP represent relatively recent advances in the study of p97/VCP. While it is unknown whether p97/VCP regulates stimulus-dependent transcription and whether it may do so by acting directly upon chromatin, some published work has implicated p97/VCP in transcriptional regulation. p97/VCP has been shown to be required for the activation of cytoplasmic-localized transcriptional activators (Franz, Ackermann, & Hoppe, 2016), the extraction of promoter-bound transcriptional repressors (Wilcox & Laney, 2009), the reduction in promoter occupancy of yeast and mammalian transcription activators (Ndoja, Cohen, & Yao, 2014), the regulation of gene-body histone H2B mono-ubiquitination (H2B-Ub) and inducible transcription in yeast (Bonizec et al., 2014), the extraction of stalled mammalian and yeast RNA polymerase (RNAPII) from sites of UV-induced DNA damage (Verma, Oania, Fang, Smith, & Deshaies, 2011), the inhibition of neuronal transcription and histone acetylation under prolonged proteostatic stress (Koike et al., 2010) and to have a direct role in the activation of unfolded-protein-response (UPR)-dependent transcription in C. elegans.(Caruso et al., 2008; Marza et al., 2015). Most recently, work conducted in mammalian cells has shown p97/VCP to be required for the degradation of IKAROS transcription factors in response to Lenalidomide treatment (Nguyen et al., 2017) and for Wnt-dependent transcription via the degradation of a transcriptional repressor at Wnt/TGFbeta-responsive enhancers (Flack, Mieszczanek, Novcic, & Bienz, 2017). The yeast ortholog, Cdc48, also shows enrichment upon immune-precipitation of initiating RNAPII complexes (Harlen, et al., 2016).

p97/VCP could function to extract a transcriptional repressor from activity-regulated promoters, in some necessary step for transcriptional activation. There are several transcriptional

repressive molecules that are regulated by the ubiquitin proteasome system and/or p97/VCP. For example, the total protein levels and activity of the transcriptional repressor complex, NCoR1, on chromatin are tightly regulated by ubiquitination and degradation (Mottis, Mouchiroud, & Auwerx, 2013). At active, CREB-dependent genes, NCoR1 is constitutively turned over in a proteasome-dependent manner at active sites of transcription bound by the transcription factor (Catic et al., 2013). NCoR1, is also pre-bound to neuronal activity-dependent genes in the absence of stimuli and then may be evicted with activity (Ebert et al., 2013; Telese et al., 2015). The essential NHEJ response heterodimer Ku70/80, which is recruited to TOP2B lesions, is a known substrate of p97/VCP (van den Boom et al., 2016). Ku70/80 binding to DNA has been associated with transcriptional repression (Sucharov et al., 2004) and its extraction from DNA requires p97/VCP(van den Boom et al., 2016).

One of the original proposed mechanisms to explain stimulus-dependent transcriptional activation by TOP2B-dependent DSBs was the eviction of repressive histone variant histone H1 and the recruitment of activating variant HMGB1 (Ju et al., 2006). Histone H1 has also been shown to be evicted at neuronal immediate early genes by a mechanism that involves the DNA response protein PARP (Azad et al., 2018). Histone H1 has been shown to be poly-ubiquitinated at DSBs (Mandemaker et al., 2017), raising the possibility that it could be a substrate of p97/VCP. Alternatively, p97/VCP could act in concert with a chromatin remodeler to facilitate the histone variant exchange. This is the mechanism by which p97/VCP extracts poly-ubiquitinated RNAPII from sites of damaged DNA. Through a mechanism that is conserved from yeast to mammals, p97/VCP binding is required for the recruitment of the INO80 chromatin remodeling complex, which then acts along with the p97/VCP to evict RNAPII (Lafon et al., 2015). It is possible that a similar process occurs at TOP2B-occupied promoters. The

chromatin remodeling complex INO80, is known to act at sites of DNA-damage (Morrison & Shen, 2009), where it processes histone substrates such as H2A.Z and gamma-H2AX, both of which have been linked to the regulation of neuronal immediate early gene transcription (Madabhushi et al., 2015; Yang et al., 2016). INO80 complex proteins have also been linked to stimulus-dependent transcription in *C. elegans,* in which an INO80 complex protein J requires p97/VCP-dependent degradation for unfolded protein response (UPR) transcription (Marza et al., 2015). H2A.Z is a repressive histone variant which is linked to DNA-damage, is dynamically regulated by neuronal activity, and has been linked to the repression of activity-dependent transcription. Deposition of H2A.Z at neuronal IEG promoters has been linked to their repression immediately following cessations in activity, through the actions of the NuRD complex chromatin remodeling complex (Yang et al., 2016). Moreover, H2A.Z has been shown to be evicted in a stimulus-dependent manner from ligand-bound enhancers by INO80 (Segala, Bennesch, Pandey, Hulo, & Picard, 2016). It is possible that p97/VCP is required for some of the regulation of H2A.Z.

Bonizec et al. 2014 show that the yeast ortholog of p97, Cdc48, is dynamically recruited to actively transcribed gene bodies, including galactose-inducible genes, and suggest that Cdc48 is required for maintaining gene-body histone mono-ubiquitination (H2Bub1) (Bonizec et al., 2014). This work also shows that acute disruption of mammalian Cdc48/97/VCP in myoblasts produces elevated levels of nuclear H2Bub1, suggesting that p97/VCP may regulate mammalian histone mono-ubiquitination. This work suggests that inhibition of p97/VCP could repress activity-dependent transcription through a mechanism that involves gene-body or promoter levels of H2Bub. Regulation of H2Bub1 at neuronal activity-regulated genes has not been studied. Depletions of gene-body H2Bub1act to negatively regulate RNAPII elongation and

reduce transcription. Androgen-dependent enhancers, which are a classic model of stimulus-dependent transcription, have been shown to possess depleted levels of H2Bub1, through the actions of an unknown deubiquitinase (Segala, Bennesch, Pandey, Hulo, & Picard, 2016). Stabilization of H2Bub1 at these stimulus-dependent enhancers was shown to stabilize H2A.Z through a mechanism which inhibits recruitment of INO80. Elevated levels of H2Bub1 and H2A.Z at these enhancers was associated with reduced RNAPII initiation and reduced transcription. Therefore, were p97/VCP inhibition to elevate levels of H2Bub1 at stimulus-dependent promoters, this effect would be expected to inhibit transcriptional induction.

The effects of NMS-873 could also be linked to DNA damage, which orchestrates chromatin-remodeling that requires the poly-ubiquitination of histone and other protein substrates (Dantuma & van Attikum, 2016; Mandemaker et al., 2017; Shi et al., 2007) and the p97/VCP-dependent extraction of chromatin-bound substrates (Acs et al., 2011; Dantuma, Acs, & Luijsterburg, 2014). For example, TOP2B-dependent activation of stimulus-dependent transcription has been hypothesized to require the eviction of repressive histone H1 (Ju et al., 2006), which is also known to be poly-ubiquitinated and degraded at DSBs. It is possible that p97/VCP acts to extract histone H1 from activity-dependent promoters, in a process that licenses their activation.

Independently of a DNA damage response, though, p97/VCP could also directly regulate RNAPII initiation or elongation through a mechanism that requires poly-ubiquitination (Horwitz, Affar el, Heine, Shi, & Parvin, 2007; Mitsui & Sharp, 1999) Alternatively, p97/VCP could process transcription activators, such as CBP (Wei et al., 2017) or labile repressor complexes, including NCOR (Catic et al., 2013) which are positioned at IEG promoters and enhancers. In fact, proteasome-dependent degradation of repressor complexes has been shown to occur at

active androgen-receptor target genes (Gaughan, Logan, Neal, & Robson, 2005) and at genome-wide CREB sites (Catic et al., 2013). p97/VCP may also orchestrate other chromatin-remodeling events that have been loosely associated with neuronal IEG activation. These include neuronal proteasome-dependent histone extraction and turnover (Maze et al., 2015) and the deposition of the repressive histone variant H2A.Z to IEG promoters or enhancers (Yang et al., 2016). H2A.Z deposition at ligand-activated enhancers is regulated by histone ubiquitination and by the INO80 chromatin remodeling complex (Segala et al., 2016)—components of which have previously been identified as p97/VCP substrates or as direct p97-interacting proteins (Caruso et al., 2008; Lafon et al., 2015; Marza et al., 2015).

This chapter focuses on determining whether NMS-873 suppresses activity-dependent transcription through an on-target mechanism, on identifying the specific aspect of transcription or mRNA-processing that might be regulated by p97/VCP, and on identifying specific p97/VCP complexes that coordinate its transcription activity. On-target activity of NMS-873 would suggest either a novel function of p97/VCP on transcription or that p97/VCP-dependent cell stress signaling acts acutely to inhibit activity-dependent transcription by some unappreciated mechanism.

3.2 Results

NMS-873 acts acutely to inhibit neuronal activity-dependent transcription.

An initial goal was to determine whether NMS-873 treatment acts rapidly to suppress activity-dependent transcription. We found that applying the p97 inhibitor to primary neurons at the onset of depolarization blocked immediate early gene induction (Figure 17, Supplemental Fig. 2). In fact, treating neurons with the inhibitor as late as five minutes after the onset of a depolarizing

stimulus was sufficient to block transcription. Inhibition occurred at concentrations consistent with reported IC50 values for various *in vivo* assays such as effects on viability and activation of the unfolded protein response (UPR) (Figure 18) (Her et al., 2016; Magnaghi et al., 2013). NMS-873 is considered to be one of the most specific inhibitors in use today and is in widespread use in studies of p97/VCP (Magnaghi et al., 2013). The combination of low dose and acute onset of action suggest that NMS-873 acts through an on-target mechanism to regulate activity-dependent transcription. This data potentially reveals a new function for the disease-associated gene p97/VCP.

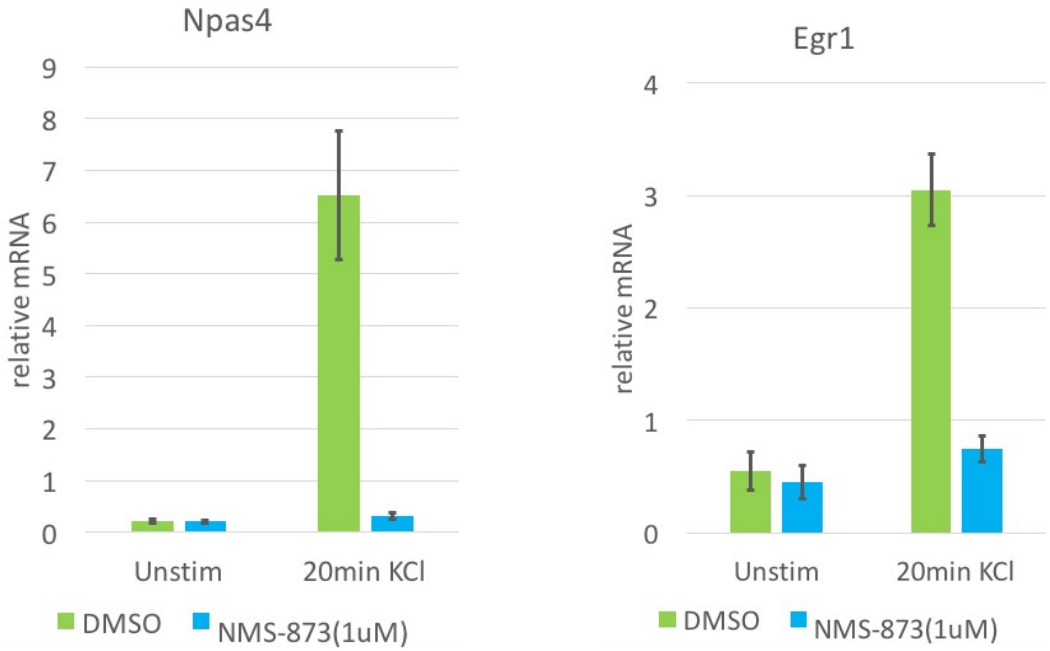

Figure 17. NMS-873 acts rapidly to inhibit neuronal activity-dependent transcription.

qPCR quantification of Npas4 (left) and Egr1 (right) mRNAs from primary cortical neuron culture. NMS-873 (1uM) or DMSO vehicle was applied concurrently to KCl stimulus. (n=3, error bars are SEM).

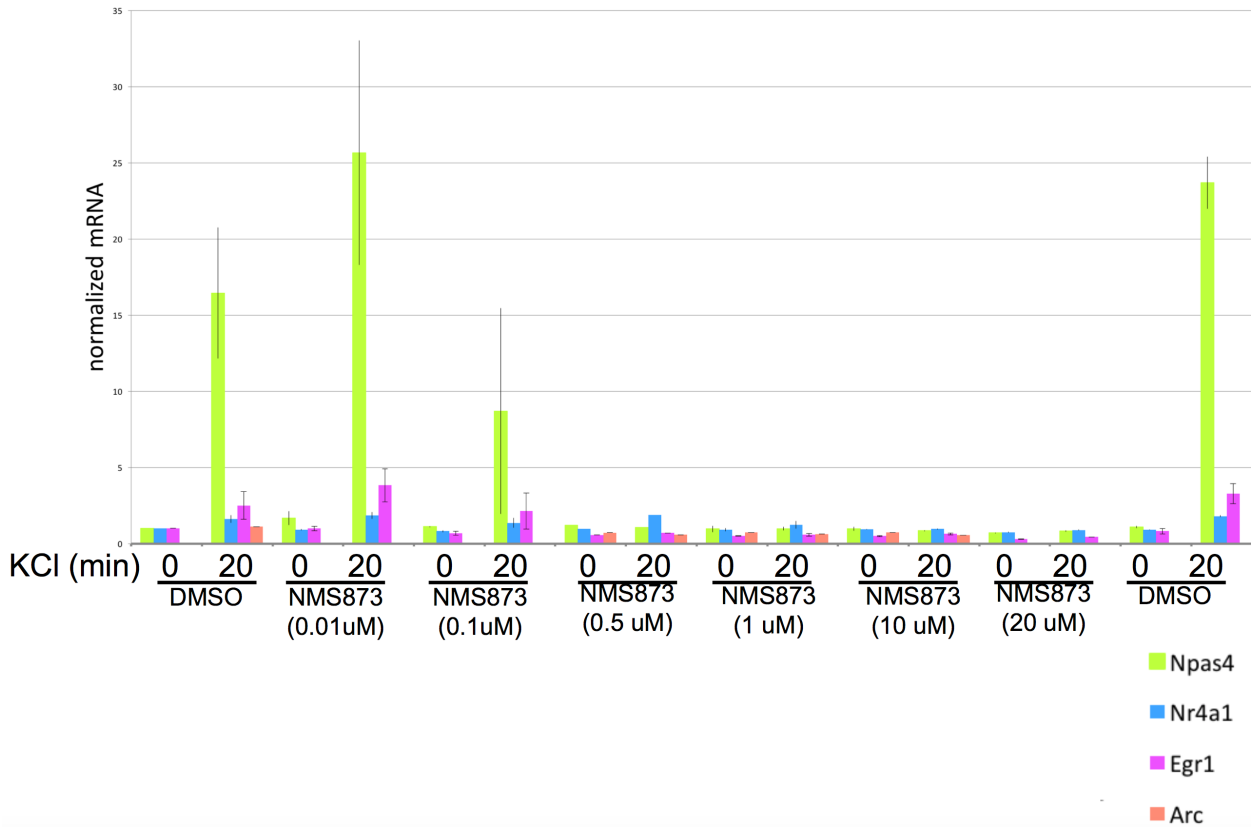

Figure 18. Dose-response relationship NMS-873 and inducible transcription.

qPCR measurements of IEGs following 20-minutes depolarizing KCl. Neurons were pre-treated for 5-minutes with either vehicle or NMS-873 at the indicated concentrations. (n=2-3). Error bars are SEM.

Transcription of inhibition by NMS-873 appears to be specific to activity-regulated genes.

While there are several plausible mechanisms by which p97/VCP could regulate stimulus-dependent transcription, there are fewer which might explain how p97/VCP could regulate transcription globally. Therefore, it was necessary to determine whether NMS-873 disrupts the expression of constitutively active genes or whether its actions are specific to activity-regulated genes. Genome-wide analysis using RNA-seq shows that constitutive transcription is unaffected by up to three hours of NMS-873 treatment in primary neuronal culture (Figure 19). Thus, the

inhibition of neuronal transcription by NMS-873 on neurons is likely specific to activity-regulated genes.

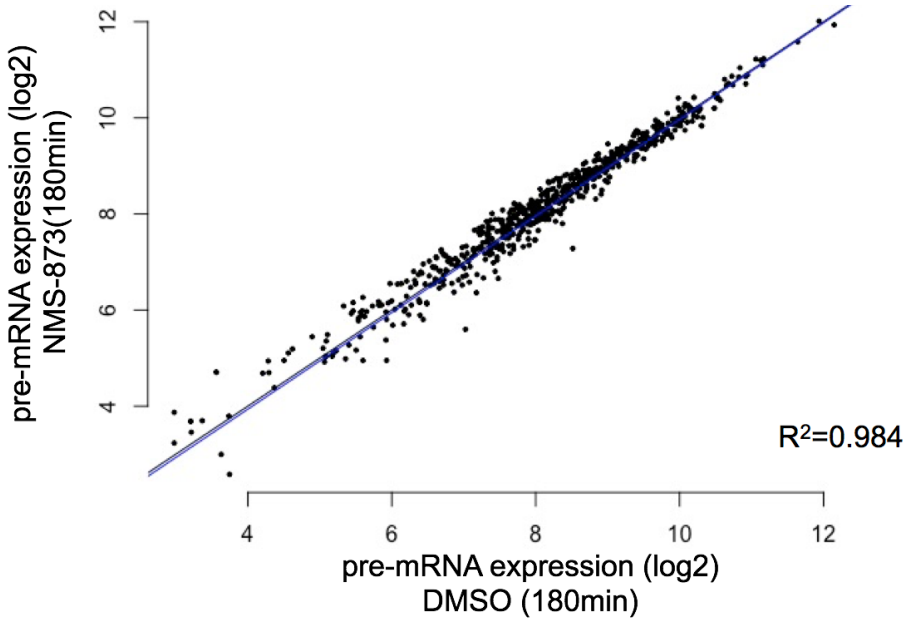

Figure 19. Effects of alternate p97/VCP inhibitors on constitutively expressed pre-mRNAs.

RNA-seq quantification and comparison of constitutively expressed and non-activity-regulated pre-mRNAs following three-hour treatment of either vehicle or NMS-873 (1uM). Shown is x=y line in black and the linear best fit in blue (R2=0.984). Data from one replicate each treatment condition.

NMS-873 blocks inducible transcription in response to diverse stimuli of multiple cell types.

Stimulus-dependent induction of immediate-early and delayed response genes occurs in many cell types, through both common and unique regulatory mechanisms. Therefore, we next sought to determine whether inhibition of p97/VCP by NMS-873 disrupts other types of stimulus-dependent transcription. These experiments showed that NMS-873 acts to inhibit inducible transcription in response to a variety of stimuli and in different cell types. Specifically, NMS-873

inhibits serum-dependent transcription in mouse embryonic fibroblasts (MEFs) (Figure 20). NMS-873 also inhibits forskolin-dependent transcription of Nr4a2 in HEK293T (Figure 21, Supplemental Figure 4). Forskolin activates PKA and elevates cellular levels of cAMP, initiating transcription in HEK293T cells that is thought to be CREB-dependent (Zhang et al., 2005). CREB is similarly responsible for much of the neuronal activity-dependent transcription.

Additionally, we found that preliminarily, serum-stimulation of HeLa and HCT-116 cells is likely not inhibited acutely by NMS-873, even at highest soluble concentrations (Supplementary Figure 8-9). Serum stimulated transcription was similarly unaffected by NMS-873 treatment even when cellular division had been arrested by thymidine treatment. The basis for this stimulus specificity is unclear. It may reflect different inhibitor efficacies across cell types. But it also may reveal specificity of NMS-873 or p97/VCP to particular signaling pathways or transcription factors. Arresting cellular division by inhibiting DNA-synthesis with thymidine treatment did rescue serum-dependent transcription inhibition by NMS-873.

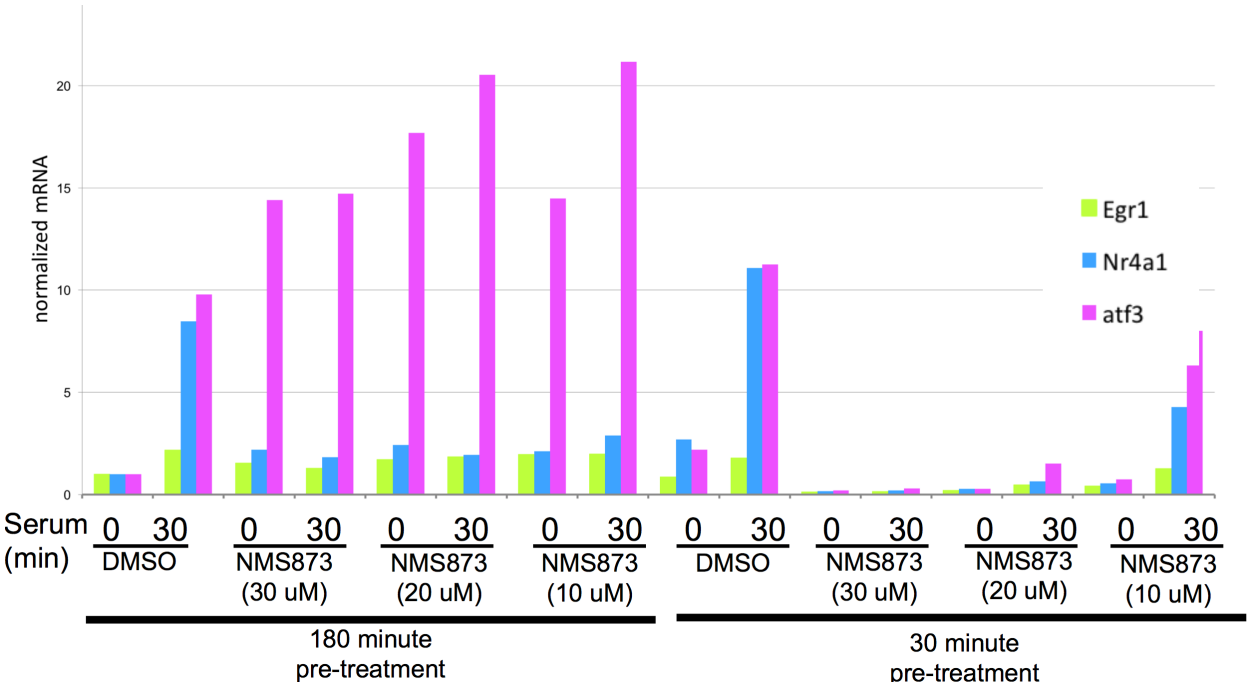

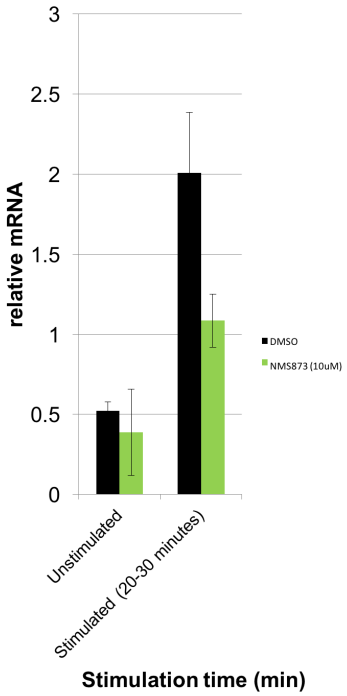

Figure 20. NMS-873 inhibits serum-stimulated transcription in primary mouse embryonic fibroblasts.

Top, qPCR measurements of serum-inducible mRNAs. Mouse embryonic fibroblasts (MEFs) were stimulated with serum for 30 minutes (n=1). Prior to stimulation, cells were treated with vehicle or NMS-873 at the indicated concentrations for either 180- or 30- minutes, as indicated.

Figure 20. (Continued) NMS-873 inhibits serum-stimulated transcription in primary mouse embryonic fibroblasts *Bottom,* As in *Top* panel, but shown is quantification for Nr4a1 over multiple replicates +/- 10uM NMS-873 (n=2 replicates, error bars are SEM). (p=0.07, stimulated levels of Nr4a1 DMSO vs. NMS-873).

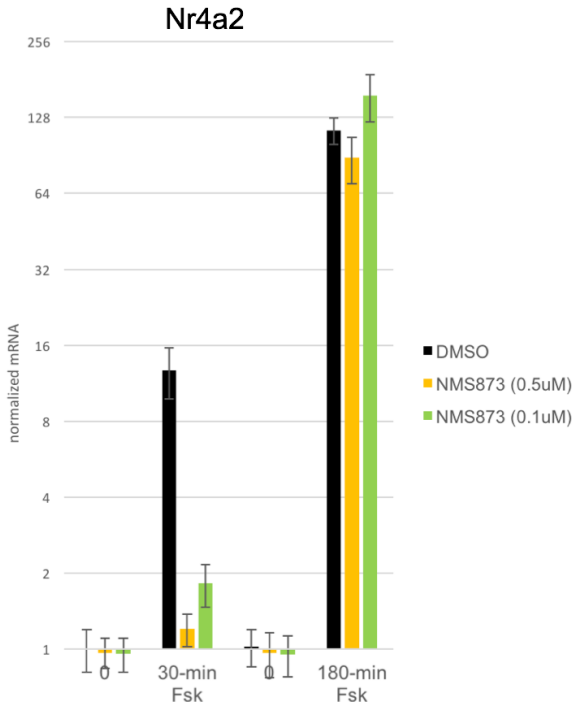

Figure 21. NMS-873 inhibits Forskolin-induced Nr4a2 transcription in HEK293T cells.

qPCR measurements of Nr4a2. Serum-deprived HEK293T cells were stimulated with 10uM forskolin for 30- or 180- minutes. Cells were treated with vehicle (black), 0.1uM NMS-873 (green), or 0.5uM NMS-873 (orange). Inhibitor was applied simultaneously to Forskolin stimulation. Values are normalized to beta-2-microglobulin control mRNA values. Shown are mean values of n=3 replicates. Error bars are SEM.

Neuronal activity-dependent signaling and transcription factor activation appear intact following NMS-873 treatment

One possibility for the effects of NMS-873 on activity-regulated transcription is that p97-inhibition disrupts the integrity of the signaling pathway and transcription factor network that is essential for transducing depolarization into a transcriptional response. However, we find that depolarization-dependent activation of CREB and ERK persists under NMS-873 treatment (Figure 22) . These results suggest that activity-dependent signaling is overall unaffected by brief

application of NMS-873. Specifically, 30-minute pre-treatment of neuronal cells with NMS-873 does not inhibit KCl-dependent CREB phosphorylation at S133, which is a proxy for CREB activation. Nor does it inhibit ERK activation (Figure 22). However, high dose NMS-873 treatment may lower total cellular levels of CREB phosphorylation in the un-stimulated condition. Perhaps NMS-873 reduces total CREB protein levels or CREB occupancy at ARG promoters. Neither total CREB levels nor chromatin-occupied pS133-CREB have been measured in these experiments.

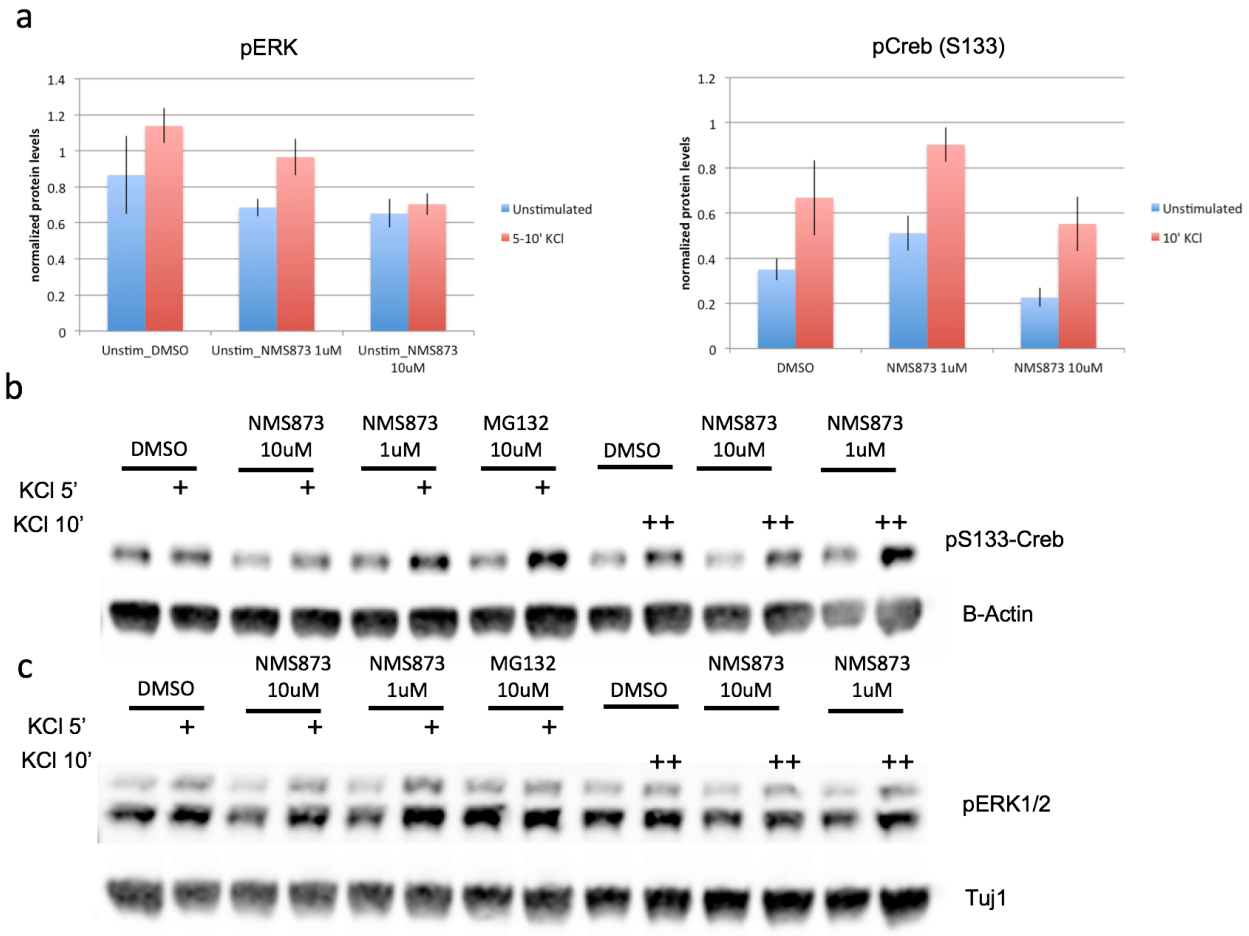

Figure 22. Summary quantification of phospho-Creb and phospho-ERK pre- and post-depolarization under NMS873 treatment.

(a) Average normalized blotting density of pErk *(left)* and pCreb *(right)* in un-stimulated and

Figure 22. (Continued) Summary quantification of phospho-Creb and phospho-ERK pre- and post- depolarization under NMS873 treatment. depolarized (5-10') primary neurons (n=3 independent reps, data presented as mean +/- SEM, normalized to loading control). *(b-c)* Representative blotting for pCreb *(b)* and pERK1/2 *(c)*

The inhibition of activity-dependent transcription is likely not attributable to indirect consequences of p97/VCP inhibition such as activation of the unfolded-protein-response or apoptosis.

p97/VCP exerts a number of diverse cellular functions, and its inhibition would be expected to initiate many cellular consequences. However, transcription inhibition is not a known consequence of p97/VCP inhibition. In fact, p97/VCP inhibition has been shown to activate a number of cell stress signaling and transcription responses—including activation of UPR-dependent transcription (Her et al., 2016; Magnaghi et al., 2013). It remains possible though that p97/VCP inhibition impacts transcription as a previously unappreciated consequence of effects on apoptotic signaling or activation of the UPR. Here, as expected given observations in other cell types, we find that NMS-873 treatment activates the UPR, as shown by elevated phosphorylation of the eukaryotic initiation factor, p-eIF2alpha. We did not detect activation of either of the other two arms (by ATF6 proteolysis or Xbp1 splicing—neither of which is thought to require p97/VCP). In primary neurons, increases in p-eIF2alpha occur only at higher doses and after prolonged treatment, whereas lower doses that continue to inhibit activity dependent transcription appear not to elevate p-eIF2alpha over brief time-courses (Figure 23). Additionally, treatment of neurons with drugs that activate the UPR (Oslowski & Urano, 2011) do not replicate the effects of NMS-873 on activity-dependent transcription, as they do not suppress transcription—although treatment with the reducing reagent DTT diminishes Npas4 induction by depolarizing KCl (Figure 24).

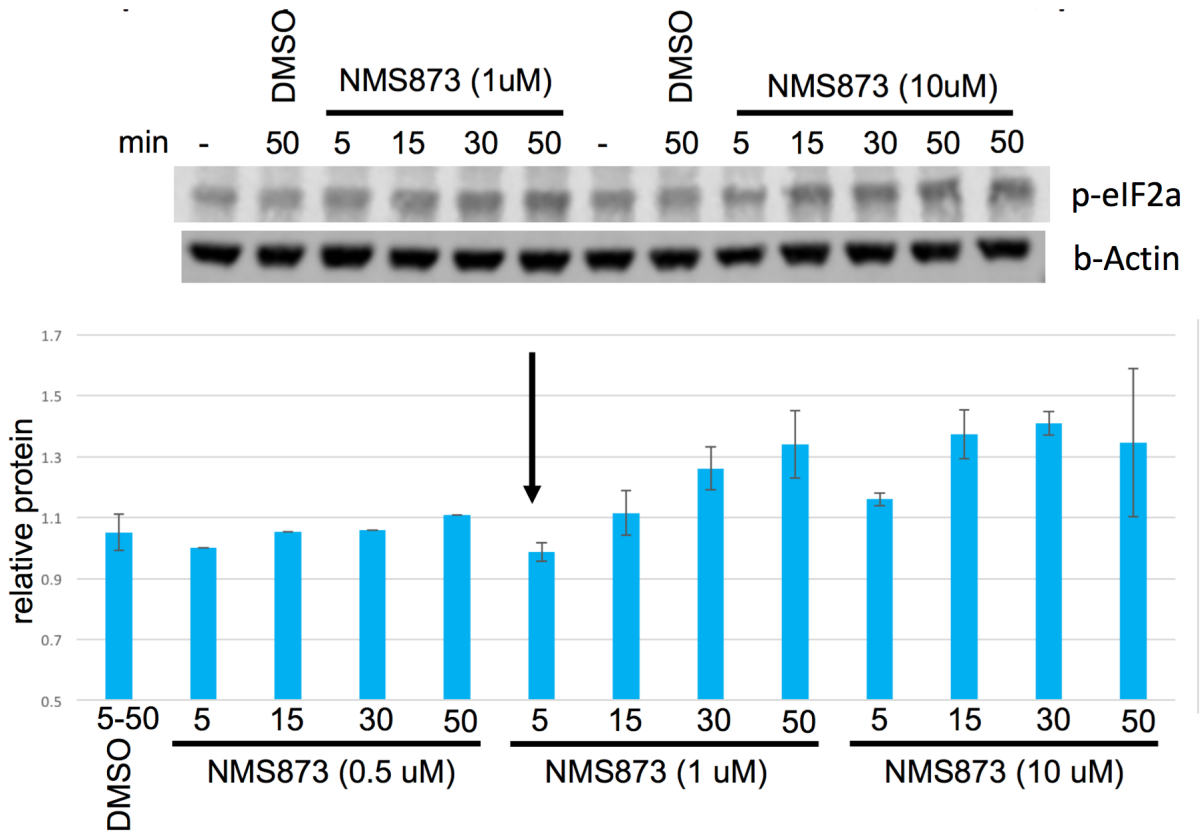

Figure 23. Measurements of p-eIF2alpha following acute treatments NMS-873

Primary neuronal cultures were treated with vehicle or NMS-873 (0.5uM, 1uM, or 10uM) for the indicated number of minutes (5-50-minutes). Top, representative Western blot. Bottom, average values p-eIF2alpha, normalized to beta-Actin loading control (n=2 for 1uM and 10uM treatments +/- SEM; n=1 for 0.5uM, no error plotted). "DMSO 5-50" time point is the average of two replicates, where DMSO treated for 5-minutes and for 60-minutes. T-test comparisons made to DMSO condition for 1uM and 10uM treatments (n=2 reps). $p>0.05$ each comparison. $p<0.10$ for NMS-873 (10uM) 15- and 30- minute treatments.

Surprisingly, we also find that despite activating one arm of the UPR (p-eIF2alpha), NMS-873 also does not induce the expression of a number of UPR genes (Figure 25). This is an unexpected dissociation of UPR signaling and its transcription. However, the *C. elegans* p97/VCP ortholog has been shown to be required for UPR-driven transcription, raising the possibility that mammalian p97/VCP is required for UPR-dependent transcription in primary neurons as well. Overall, these results suggest that the actions of NMS-873 may not be through indirect consequences of ER-stress or UPR signaling.

Treatment with NMS-873 could activate apoptotic pathways, and this could inhibit activity-dependent transcription. This is of particular concern given the strong UPR activation (p- eIF2alpha) but blocked UPR-transcription, which ordinarily functions to maintain proteostasis under cellular stress. However, we find that NMS-873 does not initiate the cleavage and activation of PARP (Figure 26), as has been reported following prolonged NMS-873 treatment or p97 disruption in proliferating, cancer cell lines (Chapman, Maksim, de la Cruz, & La Clair, 2015). Furthermore, the rapid onset of inhibitory effects on activity-dependent transcription suggests that these effects are less likely to be attributable to cell stress or apoptosis.

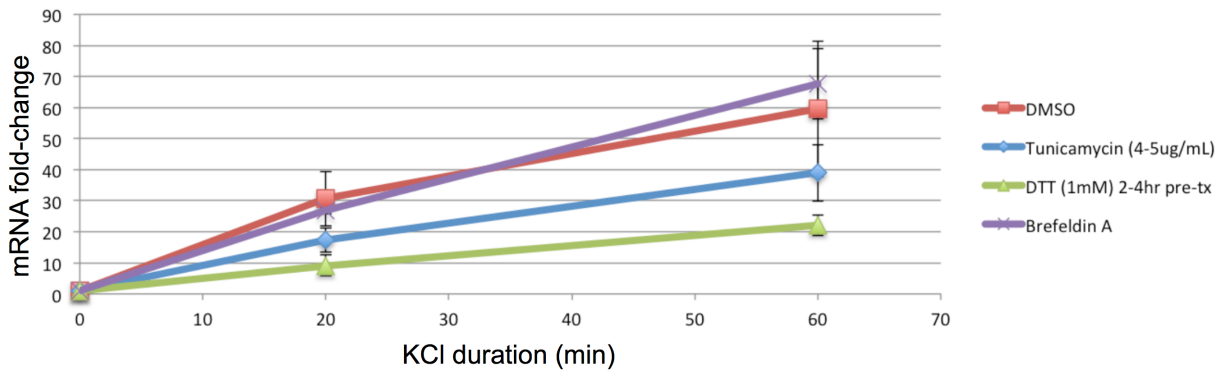

Figure 24. UPR activation by pharmacologic treatment of primary neurons can reduce activity-regulated IEG transcription. qPCR measurements of fold-change Npas4 mRNA levels over time-courses of depolarizing KCl (0, 20', 60') under pre-treatment with ER-stress drugs and vehicle. Tunicamycin (4-5ug/mL, 360 min. pre-treatment), DTT (1mM, 120-240 min. pre-treatment, Brefeldin A (10uM, 360 min. pre-treatment). Npas4, n=2-3 biological replicates per time-point and drug (Error bars are SEM).

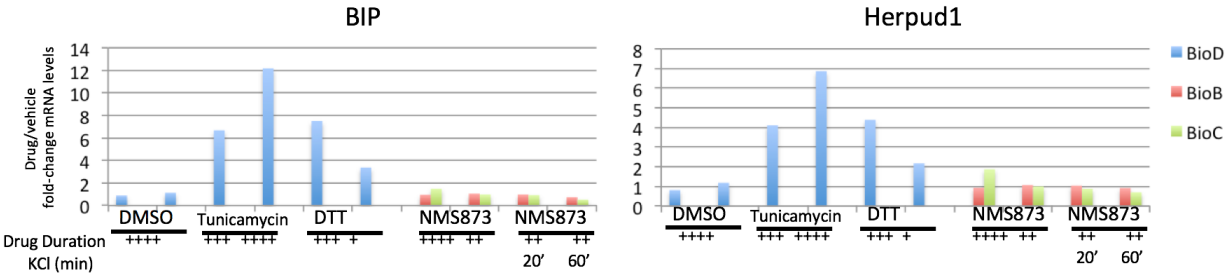

Figure 25. NMS-873 fails to induce the expression of UPR proxy genes. Fold-change measurements of BIP and Herpud1 mRNA expression under ER-stress (Tunicamycin 5ug/mL, DTT 1mM, single replicate each) and NMS-873 (10uM) for various durations. Measurements were also made under depolarizing KCl (20',60') in the presence of NMS-873. ++++ 360min, +++ 240min, ++ 180min, + 120min. Values from independent biological replicates are plotted separately (in blue, red, green).

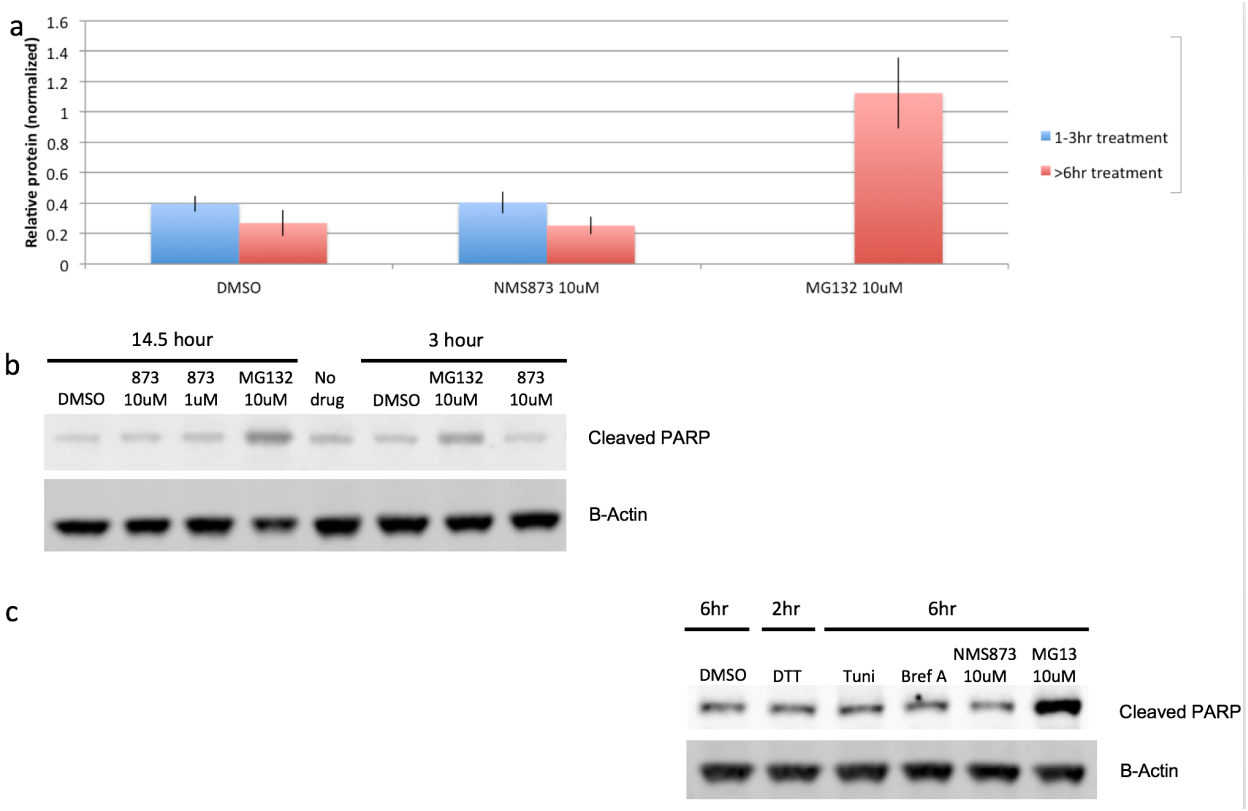

Figure 26. NMS-873 treatment does not elevate cleaved PARP. (a) Summary western blotting density (normalized to B-Actin loading control) presented as mean +/- SEM (n=3 biological replicates). Drug treatments are as indicated, colored by time (1-3 hours, blue ; 6-14.5 hours, red). (b-c) Representative western blotting, where "873" refers to NMS-873.

Total RNA-seq and RNAPII ChIP-seq reveal that NMS-873 represses neuronal depolarization-dependent transcription via a mechanism that is consistent with RNAPII initiation defects

In order to characterize the mechanism of transcription repression by NMS-873, we applied strand-specific total RNA-sequencing methods. Our lab has previously used strand-specific total RNA-sequencing to delineate the discrete stages of transcription and mRNA synthesis that are modulated by small molecule regulators of transcription and RNA splicing (Magnaghi et al., 2013). Our data showing intact MAPK activation and CREB phosphorylation in response to

neuronal depolarization under NMS-873 suggests that this inhibitor acts downstream of transcription factor activation. *Bonizec et al. (2014)* proposes a model based on observations obtained from yeast cdc48/p97 ortholog in which p97 is recruited co-transcriptionally to active gene-bodies to regulate histone mono-ubiquitination (H2Bub1), which promotes RNAPII elongation (Bonizec et al., 2014). This work therefore raises the expectation that disruption of p97/VCP may produce a transcription elongation defect by reducing gene-body histone ubiquitination. However, *Bonizec et al. (2014)* also finds that inhibition of mammalian p97/VCP unexpectedly elevates total H2Bub1 levels—observations which contrast their results in yeast and perhaps too with other published work demonstrating reduced H2Bub1 in response to proteasome inhibition (Catic et al., 2013). This and other published work showing that H2Bub1 represses transcription initiation at ligand-activated enhancers and promoters (Segala et al., 2016) suggests that p97/VCP inhibition could disrupt RNAPII initiation if p97/VCP inhibition stabilizes H2Bub1. Alternatively, if p97/VCP responds to either DSBs or DNA damage-induced signaling occurring at IEG promoters, then this too might suggest a function for p97/VCP in transcription initiation at activity-regulated genes.

Overall, the RNA-seq results reveal that NMS-873 acutely inhibits transcription of several IEGs in response to 20-minutes of depolarization and represses nearly all delayed-response genes activated over three-hours of depolarization (Figures 27-28). However, RNA-seq revealed that many of the immediate early genes that are induced by twenty minutes of depolarization continued to show slight induction under NMS-873 treatment. It is possible that co-treatment of the inhibitor and depolarizing KCl allowed for a delay in the actions of the inhibitor, reducing the ability to detect significant differences in the induced mRNA levels for

many IEGs—most of which have smaller fold-changes after only twenty-minutes of depolarization. Overall, this data shows that the mechanism of inhibition for genes like Npas4 and for delayed response genes (dPRGs) appears consistent with a mechanism that occurs upstream of transcription initiation. Inhibition of activity-dependent transcription by NMS-873 does not appear to be attributable to effects on transcription elongation. This is supported by preliminary RNAPII ChIP-qPCR data, which shows reduced RNAPII recruitment to activity-regulated promoters in response to depolarization under NMS-873 treatment (Supplemental Figure 3). Expression of constitutively active genes remains unaffected over three hours of drug treatment, indicating that this inhibition is likely specific to activity-dependent transcription (Figure 19).

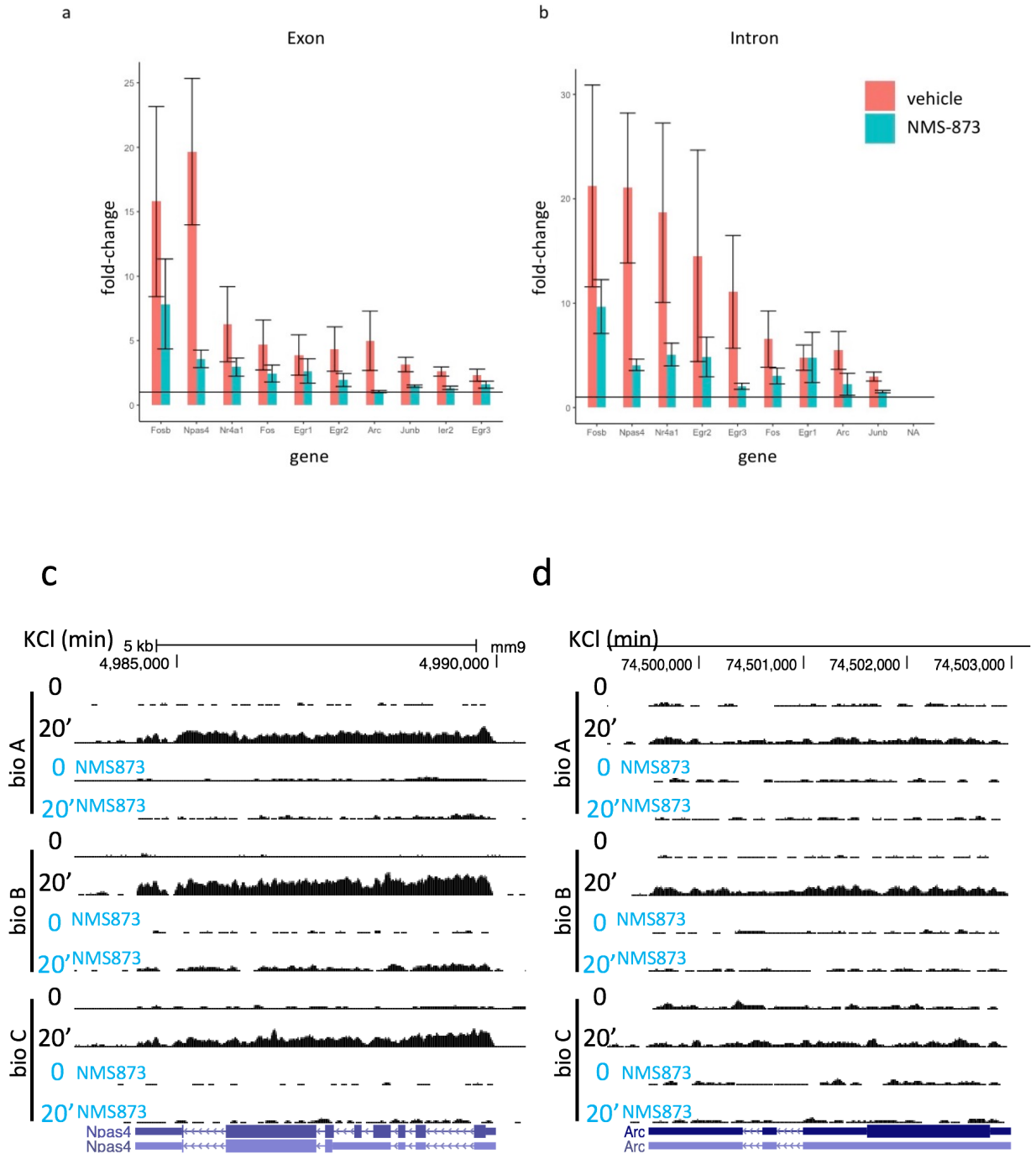

Figure 27. NMS-873 inhibits neuronal activity-regulated gene transcription

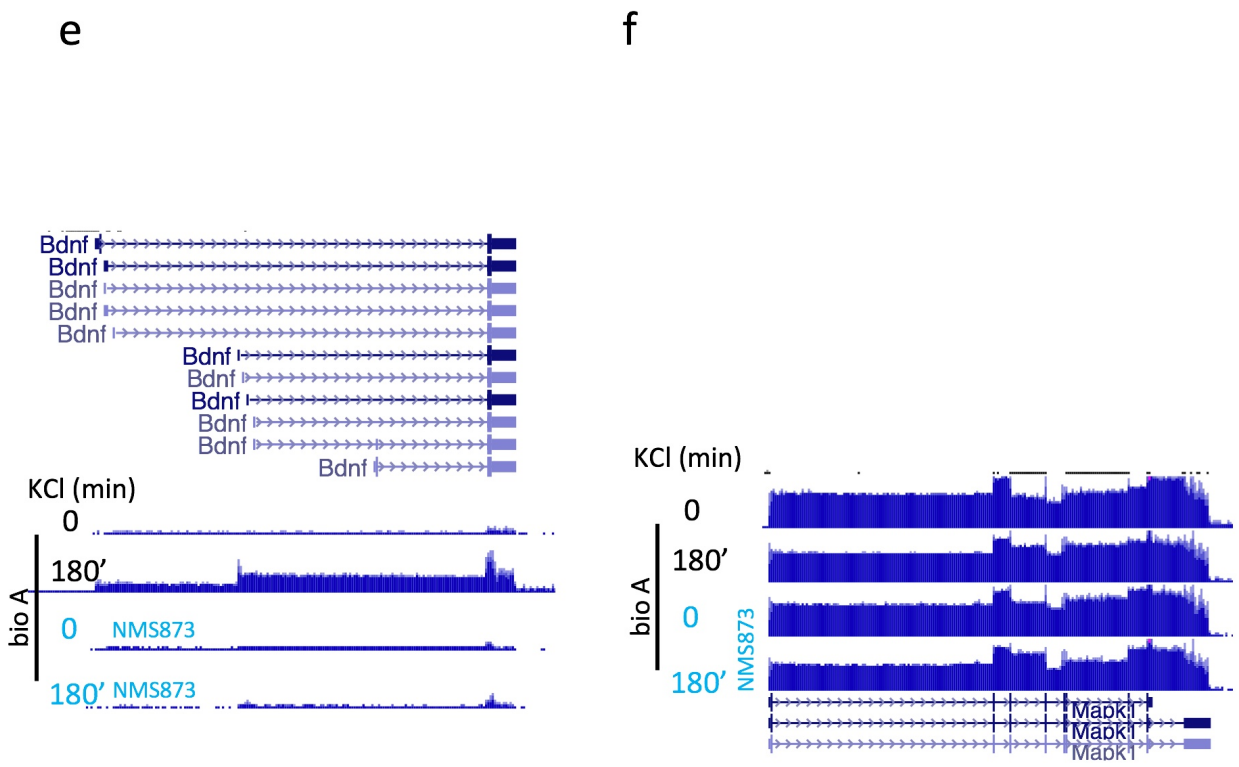

Figure 27. NMS-873 inhibits neuronal activity-regulated gene transcription.

(a-b) Fold-change measurements of reads mapping to (a) exon and (b) intron regions of immediate early genes found to be induced in response to 20-minutes depolarization. NMS-873 (1uM) and depolarizing KCl are applied simultaneously. Values are mean +/- SEM (n=3). c-f, UCSC alignment of RNA-seq data for representative genes. (c=Npas4 (IEG), d=Arc (IEG), e=Bdnf (dPRG), f=Mapk1 (control)).

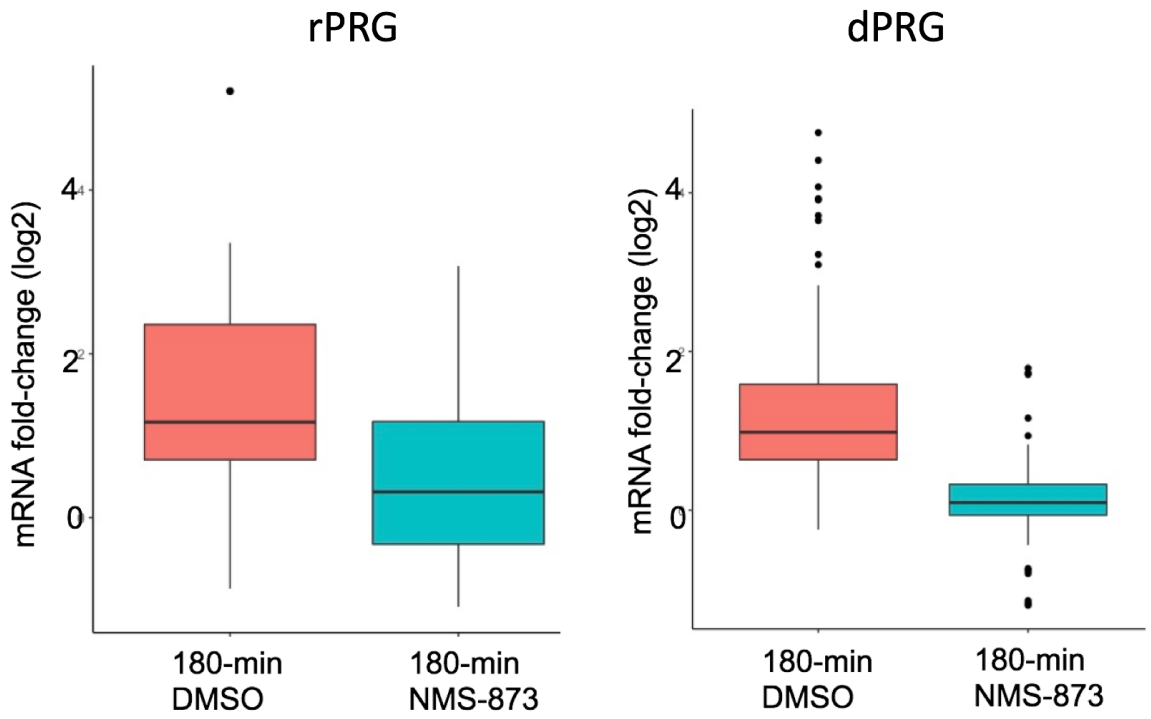

Figure 28. NMS-873 represses rPRG and dPRG transcription in response to depolarizing KCl.

Comparisons of depolarization-dependent fold-change values for rPRG (n=19 genes) (left) and dPRGs (n=154 genes) (right) under three-hours of vehicle or NMS-873 (one replicate each condition). Shown are distributions of per-gene KCl-dependent fold-change values under each treatment condition.

Allosteric, but not competitive, inhibitors of p97/VCP block activity-dependent transcription

Next, we sought to determine whether NMS-873 acts through an on-target mechanism to block transcription, through some novel function of p97/VCP. As an initial approach, we applied alternate inhibitors of p97/VCP to determine if they too exerted effects on activity-dependent

transcription. Prior to the development of NMS-873, several alternate small molecule inhibitors of p97/VCP were in widespread use, and all of them were competitive ATPase inhibitors of varying specificity (Chapman et al., 2015). The covalent modifier, NMS-859, was created by Genetech as part of the work that produced the allosteric inhibitor NMS-873 (Magnaghi et al., 2013). NMS-859 acts to inhibit p97/VCP by covalently modifying an essential active site cysteine. Most recently, two new drugs have been developed. One is a second allosteric inhibitor, UPCDC30245, that is structurally unrelated to NMS-873 but appears to bind to similar, but not completely overlapping, sites within the same binding pocket within the D2 domain (Alverez et al., 2016; Banerjee et al., 2016; Burnett et al., 2017; Segura-Cabrera et al., 2017). Both drugs potently arrest ATPase cycling. It has been used in cryo-EM studies of p97/VCP but has not been studied in *in vivo.* The second inhibitor, CB5083, arose from optimization of the competitive inhibitor DBeQ, and it is in use in clinical trials for myeloma (Anderson et al., 2015). CB5083 acts competitively to inhibit ATPase activity. We found that treatment of primary neuronal cultures with UPCDC30245 abolished activity-dependent transcription, replicating the effects of NMS-873 (Figure 29, Supplemental Figure 7). However, none of the other alternate inhibitors inhibited Npas4 induction by depolarizing KCl (Figure 30). The other four drugs act on p97/VCP via one of two alternate mechanisms which are distinct from that of the allosteric inhibitor NMS873. DbeQ, MLN, and CB5083 are competitive inhibitors, while NMS859 is a covalent modifier of the p97/VCP ATPase active site. There is some indication that these alternate inhibitors either caused cell death (i.e. ML240, DBeQ) or did not activate the UPR as strongly as NMS-873 (NMS-859).

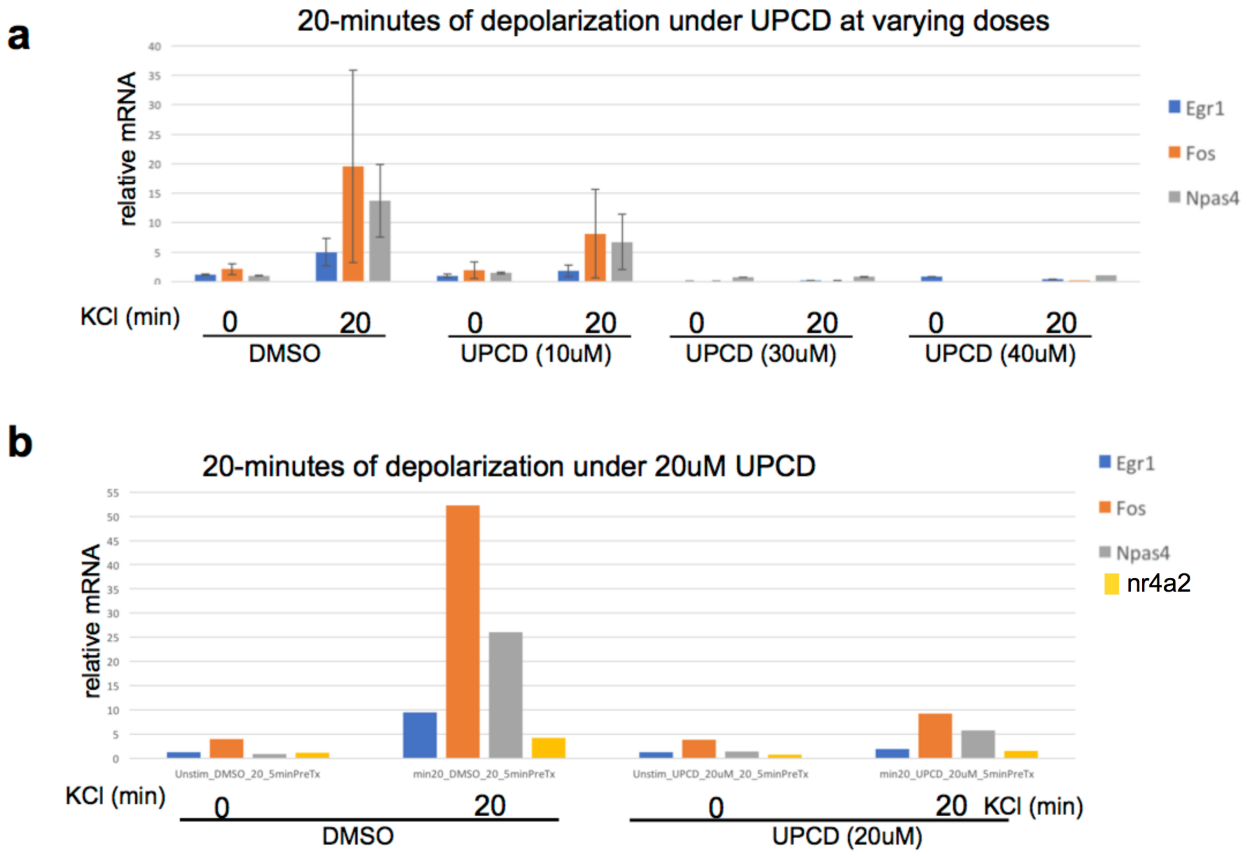

Figure 29. Allosteric P97 inhibitor UPCD30245 inhibits neuronal activity-dependent transcription of immediate early genes.

a) Average mRNA levels under un-stimulated and 20-minutes depolarizing KCl following 5-30 minutes pre-treatment with either vehicle or UPCDC30245 ("UPCD") at increasing doses (n=3 biological replicates, error bars +/-SEM). b) as in (a) but following 5-minutes pre-treatment with 20uM UPCD (n=1 replicate).

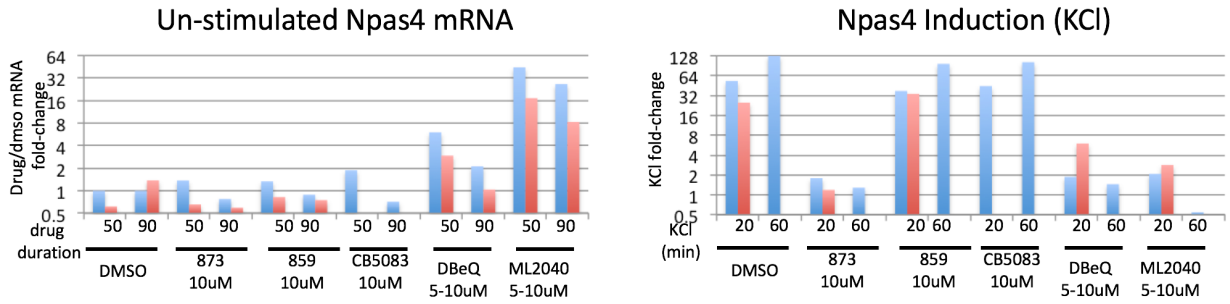

Figure 30. Effect of alternate p97/VCP inhibitors on constitutive pre-mRNA and Npas4 mRNA levels. (b-c) qPCR measurements of Un-stimulated (b) and KCl-induced (c) Npas4 mRNA levels under p97 inhibition at indicated drug and concentrations. Independent replicates shown in blue and red.

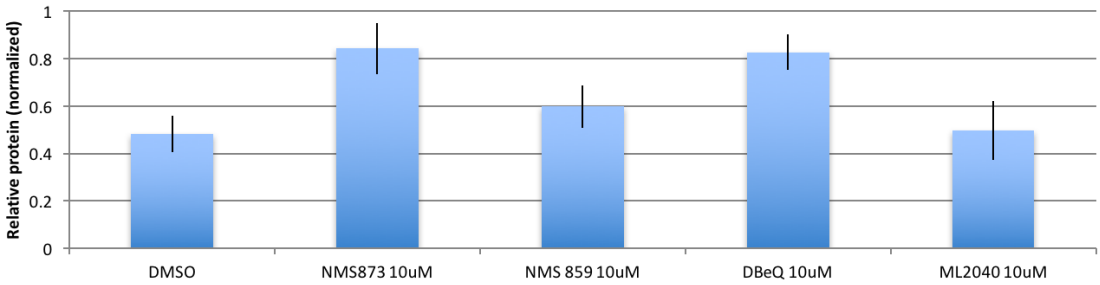

Figure 31. Effect of p97/VCP inhibitors on p-eIF2alpha.

Western blotting for p-eIF2lpha in primary neurons following 90-minute treatment with vehicle (DMSO) or the indicated inhibitor at the indicated concentration (10uM). Neurons were stimulated for 60-minutes with depolarizing KCl. Values are normalized to beta-Actin loading control and presented as mean +/- SEM (n=3).

It is possible that these drugs did not inhibit p97/VCP as effectively as the allosteric inhibitors or that they initiated cell stress signaling that complicates the study of depolarization-dependent transcription. These results could also suggest that that NMS-873 inhibits activity dependent transcription through an off-target mechanism of action. Alternatively, this data could suggest that only those inhibitors which most strongly inhibit ATPase cycling act to inhibit transcription. It is possible that NMS-873 and UPCDC30245 most effectively inhibit cycling of all six hexamers of the p97/VCP complexes, making them more effective inhibitors than the

competitive inhibitors. Two of these inhibitors (MLN and DBeQ) caused cell death and activated baseline IEG transcription, even at low concentrations.

The inhibition of activity-dependent transcription by a second inhibitor, UPCD, is encouraging, and in general allosteric inhibitors are likely to be more specific than competitive inhibitors. The lack of effects on transcription by the competitive inhibitors and by NMS-859 suggest that the allosteric inhibitors may act independently of p97/VCP, via an off-target mechanism of action. However, these inhibitors also differentially activate the UPR, suggesting that the magnitude of p97/VCP inhibition varies between inhibitors. This could also explain the different effects on transcription between cell types. Overall, these results do not rule out the possibility that NMS-873 acts via off-target effects. Given the level of confidence in NMS-873 versus the known competitive inhibitors, we decided to proceed with a direct test of on-target specificity.

Homozygous p97/VCP mutant HEK293T cell lines exhibit resistance to NMS-873 and suggest that NMS-873 inhibits stimulus-dependent transcription through an off-target mechanism of action

To determine whether NMS-873 inhibits transcription through an on-target mechanism, I initially attempted to make use of NMS-873-resistant, HCT-116 colon carcinoma cell-lines that had been generated using CRISPR-HDR (Her et al., 2016). However, I found that preliminarily serum- stimulated transcription was not blocked by NMS-873 in this cell type (Supplemental Figure 8). Therefore, I generated drug resistant HEK293T cell lines—selecting HEK293T cells for their ease of use and for the strong inhibition of Forskolin-dependent transcription by NMS873 treatment. Using CRISPR-mediated homology-directed repair (HDR), we introduced one of three different point mutations to HEK293T cell lines to produce three different homozygous mutant cell lines and two additional control cell lines. The control lines carry the

same silent mutations that were introduced to aid in the homologous recombination and screening, but they do not possess the functional point-mutations that are expected to confer *in vivo* resistance to NMS-873. These functional mutations (N616F, K615V, and A530T) were each anticipated to confer drug resistance while preserving p97/VCP activity. Specifically, each of the two amino acid substitutions N616F and K615V are positioned at the allosteric binding pocket and have been shown to disrupt inhibitor binding in *in vitro* experiments (Magnaghi et al., 2013). Whereas K615V shows only ~10-fold reduction in IC50, N616F shows no evidence of inhibitor binding. In addition to these two mutations, A530T has recently been shown to confer *in vitro* and *in vivo* resistance to NMS-873 in the colon carcinoma cell line HCT116. (Her et al., 2016) This occurs through an intrinsic mechanism that may exist too in alternate cell types, such as HEK293T. Specifically, A530T mutants exhibit enhanced *in vitro* ATPase activity compared to wild-type and preserved inhibitor binding. Inhibitor binding, though, is ultimately rendered ineffective at inhibiting p97/VCP ATPase activity, as shown through *in vitro* ATPase measurements and *in vivo* measurements of cell viability and UPR activation. We ultimately obtained ~5 individual clones per genotype (K615V, N616F, and A530T mutants, and two control lines K615CNTL and A530CNTL).

These mutants did not show significant differences in cellular levels of p97/VCP protein compared to wild-type cell lines that had been grown alongside the mutants through the CRISPR-HDR process—though the mutants did appear to trend toward lower total cellular levels of p97/VCP (Figure 32). Characterization of these cell lines for resistance to NMS-873 showed resistance to the effects of NMS-873 on viability when compared to HDR control and wild-type lines (Figure 33). Reduced cell viability over multi-day inhibitor treatments has previously been shown to occur through on-target effects of NMS-873, validating this assay for use in

determining whether these novel cell lines are in fact resistant to NMS-873*(Her et al., 2016)*. However, these mutant cell lines showed resistance to NMS-873 at higher inhibitor concentrations but not at lower concentrations, which were still effective at reducing cell viability. Despite their resistance to NMS-873 treatment, these resistant cell lines continue to exhibit Forskolin-dependent transcription inhibition when treated with NMS-873, with effects that do not differ between wild type and control lines (Figure 34). These results suggest that NMS-873 inhibits stimulus-dependent transcription in HEK293T cells through an off-target mechanism of action. This raises the possibility that similar off-target mechanism operates in neurons treated with NMS-873.

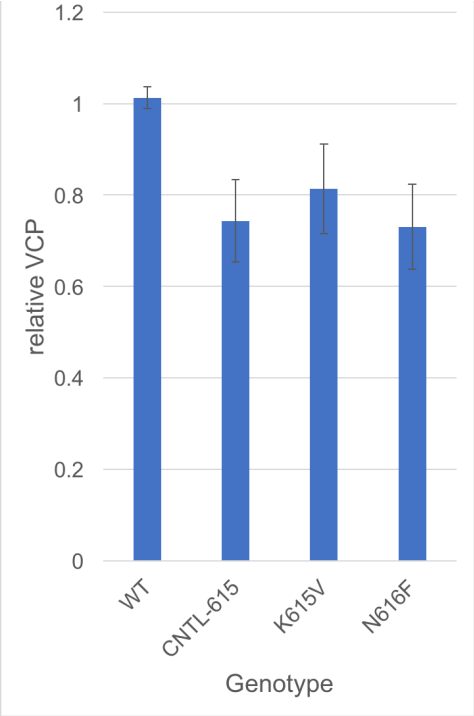

Figure 32. Comparison of cellular p97/VCP levels across wild-type and mutant HEK293T cell lines.

Figure 32. (Continued) Comparison of cellular p97/VCP levels across wild-type and mutant HEK293T cell lines. VCP levels were quantified by Western Blotting and normalized to beta-Actin loading control. "WT"=wild-type clones, "CNTL-615"=control line carrying silent mutations only. Shown are average values per genotype (obtained from n=3-4 clones per genotype. Mean values per clone obtained from 2-3 replicates). Error bars are SEM. $p>0.05$ each comparison to wild-type (2-tail t-test).

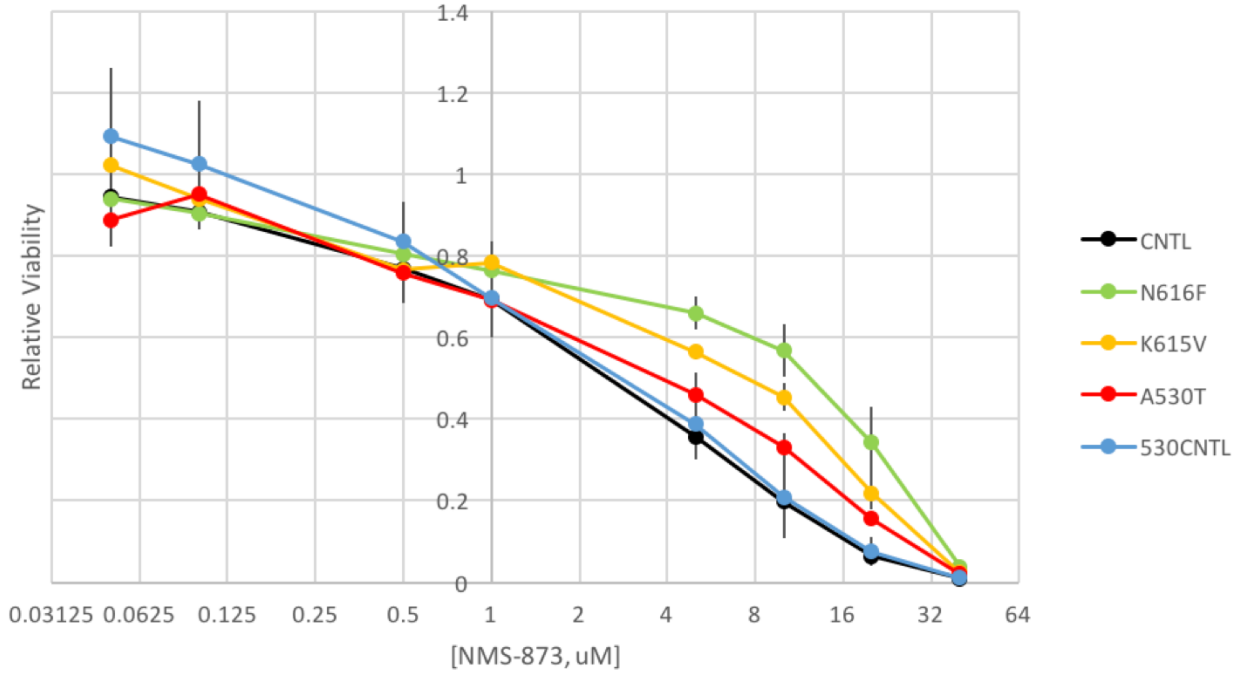

Figure 33. Mutant HEK293T cell lines show resistance to NMS-873.

HEK293T cells were passaged and grown for 36-hours with NMS-873 before being lysed and measured for [ATP] as a proxy for cellular viability, using the Promega CellTiterGlo Viability Assay. "CNTL" is "CNTL615" and is the control clone possessing the same silent mutations as K615V and N616F but without the amino-acid mutations. Shown are average values (n= 3-8 independent replicates per genotype; n=2-4 independent clones per genotype). Control cell lines are shown in black and blue ("CNTL" and "530CNTL"). Mutants shown as indicated in legend to right.

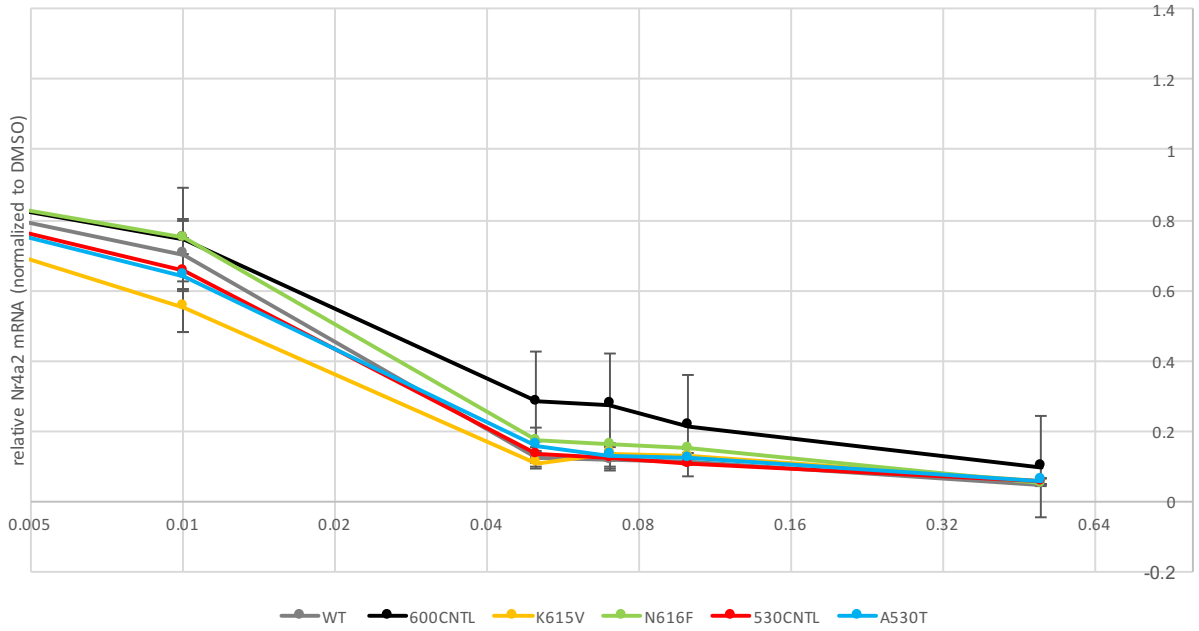

Figure 34. NMS-873 continues to inhibit activity-dependent transcription in NMS-873-resistant HEK293T cells.

Dose-response curves for Nr4a2 mRNA induction following treatment with NMS-873 for each genotype. Relative mRNA levels stimulated by 60-min Forskolin treatment are presented as NMS-873/DMSO, at the indicated doses. (N616F n=1 clone, All others n=2-3 independent clonal cell lines. Error bars are SEM. WT=wild type. 600CNTL=aa615/616 control cell line, 530CNTL=A530 control cell line).

Identifying the p97/VCP complexes that regulate stimulus-dependent transcription

In parallel to the work that went into generating mutant HEK293T cell lines, we had attempted to knockdown required p97/VCP co-factors and adapter proteins (Kloppsteck, Ewens, Forster, Zhang, & Freemont, 2012) in order to specify p97/VCP complex or complexes that may coordinate activity-dependent transcriptional regulation, were the inhibitor to represent an on-target effect of p97/VCP inhibition. The majority of studied p97/VCP complexes contain one of two sets of mutually exclusive cofactors (Buchberger, Schindelin, & Hanzelmann, 2015)—the

UFD1/NPL4 heterodimer and p47—and one of multiple additional adapter proteins, and these proteins specify unique cellular functions for p97/VCP (Stach & Freemont, 2017). p97/VCP adapter proteins have been shown to have overlapping and non-overlapping functions, suggesting that depletion experiments might identify a specific p97/VCP complex that functions to regulate IEG transcription. For example, deletion in yeast of either the adapter protein Ubx3 (which has no known mammalian ortholog) or NPL4 has been shown to phenocopy the transcription and histone mono-ubiquitination effects of cdc48/p97 disruption (Bonizec et al., 2014). And UFD1/NPL4, together with UBXD7, are required for many of the chromatin-based actions of p97/VCP, including the extraction of stalled RNAPII complexes at sites of DNA damage (Lafon et al., 2015). Therefore, we used lentiviral shRNA delivery to knockdown down UFD1L, p47/NSFL1C, and UBXD7 (Supplemental Figure 5) to determine whether any is necessary for IEG transcription in response to neuronal depolarization in primary neuronal culture. These results show that depletion of UFD1 and p47 affect Npas4 induction (Figure 35). These effects could be attributable to indirect cellular effects of prolonged depletion or they may suggest a role for p97/VCP in regulating the expression of this gene in neuronal cells.

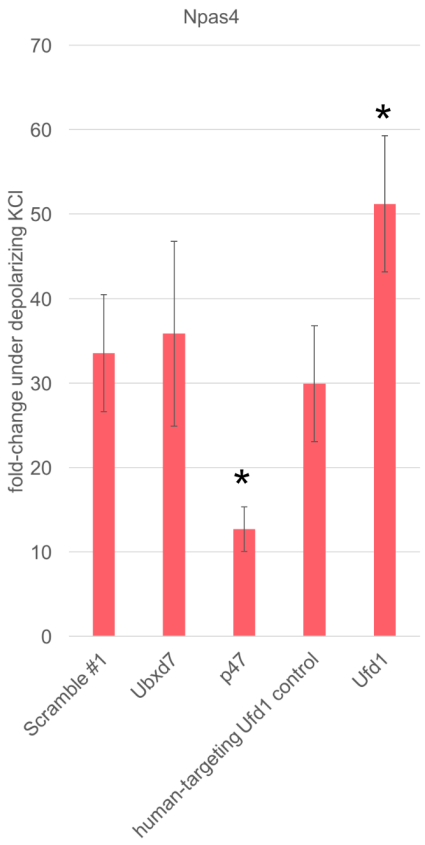

Figure 35. Induction of Npas4 mRNA following knockdown of p97/VCP co-factor and adapter proteins.

Mean fold-change qPCR measurements of Npas4 mRNAs in response to 20-30 minutes of depolarizing KCl treatment. Neurons were transduced with single lentiviral shRNA for the indicated mRNA targets. "Scramble #1" and "human-targeting Ufd1 control" are non-targeting controls. mRNA knockdown efficacies summarized in Supplementary Figure 5. mRNA values normalized to Tubb3 control mRNA. (n=4 biological replicates, error bars are SEM, *$p<0.01$ in comparisons to both control shRNAs, paired t-test on log-normalized fold-change measurements.

3.3 Discussion

We have shown that two allosteric inhibitors of p97/VCP act to inhibit neuronal activity-dependent transcription. In neurons and in other cell types, low concentrations of one allosteric inhibitor, NMS-873, are sufficient to block stimulus-dependent transcription when applied

acutely to cell cultures—acting within minutes to block transcription. This transcription inhibition appears specific to neuronal activity-regulated genes. This inhibition extends to multiple forms of stimulus-dependent transcription, including forskolin-treatment of HEK293T cells and serum stimulation of serum-starved primary fibroblasts. The combination of this rapidity of onset, allosteric mechanism of action, and measured specificity of action in other cell types suggested that NMS-873 may act to disrupt transcription through its inhibition of p97/VCP. This is perhaps supported too by the observation that low concentrations which are effective at inhibiting stimulus-dependent transcription do not appear to activate the unfolded-protein response (by p-eIF2alpha phosphorylation or transcriptional induction) over the short time-courses of interest. However, alternate inhibitors, acting by competitive and covalent inhibitory mechanisms, failed to replicate the effects of the allosteric inhibitors on neuronal activity-regulated. DBeQ appeared to potently activate stress-related signaling and eventually led to apoptosis after several hours of treatment. This made difficult interpreting the effects of activity-dependent transcription. NMS-859 did not appear to cause as strong activation of the UPR (p-eIF2alpha) compared to higher doses of NMS-873, suggesting that perhaps these drugs are less effective at inhibiting p97/VCP in neurons.

We elected to assume that NMS-873 acts via an on-target mechanism of action and pursued several experiments in parallel. First we aimed to characterize the mechanism by which NMS-873 inhibits transcription or mRNA processing by using stranded, total RNA-seq. Second, we aimed to generate mutant cell lines possessing p97/VCP point mutations that are anticipated to be resistant to NMS-873, to validate this resistance, and to then test whether transcription inhibition by NMS-873 proceeds through an on-target mechanism of action using mutant cell lines. Third, we aimed to specify the p97/VCP complex or complexes that regulate neuronal-

activity-dependent transcription by using shRNAs to knockdown various UBX adapter proteins and the mutually exclusive co-factors Ufd1/Npl4 and p47. Results from this work showed that NMS-873 appears to act upstream of transcription initiation, which are consistent with preliminary RNAPII ChIP-seq data showing that NMS-873 blocked depolarization-induced increases in RNAPII occupancy at activity-regulated promoters. The mutant HEK293T cell lines appeared to have similar VCP protein levels compared to one another, but possibly reduced p97/VCP compared to wild-type cells. These cells showed resistance to NMS-873, exhibiting enhanced viability over 36-hour treatments—effects which had previously been shown to be dependent on inhibitor actions on p97/VCP. However, inhibition of forskolin-activated transcription of the genes Nr4a1 and Fos showed no resistance to NMS-873 in the mutant cell lines, suggesting that NMS-873 acts independently of p97/VCP to inhibit transcription.

A role for p97/VCP co-factors UFD1 and p47 in transcription?

Interestingly, knockdown of two p97/VCP co-factors, p47 and UFD1, each had effects on depolarization-induced expression of Npas4 in neuronal cells. Knockdown exerted effects in opposite directions, as p47 depletion reduced Npas4 induction whereas UFD1 enhanced induction. These opposing effects may suggest that one or more of them is attributable to indirect effects of prolonged depletion, though p47 has been suggested to inhibit activity of UFD1/NPL4 containing p97 complexes. p47 is abundantly expressed in the nucleus, but has no known function on chromatin. p47 has been shown to negatively regulate TNFa or interleukin-dependent transcription through effects on NFKB signaling (Shibata et al., 2012). Its primary function is related to heterotypic membrane fusion(Kondo et al., 1997; Meyer, Kondo, & Warren, 1998) though it is also required for nuclear envelope assembly(Hetzer et al., 2001).

Disruption of p47 is therefore expected to have a number of different cellular effects, particularly those related to cellular division.

Any enhancement of inducible transcription following knockdown of UFD1 could conceivably be due to disruption of DSB repair, were DSBs to regulate activity-regulated transcription. UFD1 knockdown has been shown to disrupt p97/VCP recruitment to sites of irradiation-induced DNA damage, including DSBs (Acs et al., 2011; Meerang et al., 2011). Furthermore, UFD1 depletion prolongs y-H2AX histone modifications at damaged DNA and, in some cases, UFD1 and p97/VCP depletion have been shown to prolong DSBs. Under a model in which lesioned DNA at IEG operates to enhance transcription and repair of these breaks, through recruitment of repair enzymes such as Tdp2, reduced p97/VCP recruitment might be expected to prolong the DNA damage enhance transcription. IEG transcription might then be expected to remain elevated at late time points. Perhaps these knockdown results warrant follow-up experiments in neurons, such as using ChIP-qPCR to determine if p97/VCP is recruited to activity-regulated gene promoters or gene-bodies upon their activation or whether acute depletion (using heterologously expressed C-terminal inducible-degron tagged mutants) of p97/VCP disrupts neuronal activity-dependent transcription.

Chapter 4: Discussion

This work demonstrates that neurons couple activity patterns to specific programs of gene expression, and we have uncovered mechanisms enabling neurons to specify these activity-regulated gene programs. By modeling activity-pattern differences in primary neuronal culture using different durations of *in vitro* and *in vivo* neuronal activation, we identified a subset of genes that is uniquely sensitive to changes to neuronal activity and that can activate in response to brief depolarization. Activation of this fast activating gene program was shown to require MAPK signaling in response to both in vitro and *in vivo* physiologic neuronal stimuli. This necessity of MAPK for rapidly-activated transcription is unanticipated given prior work in neurons and in other cell types that implicated MAPK as a signaling pathway that acts late to promote delayed transcription (R. H. Chen, Juo, Curran, & Blenis, 1996; Hardingham, Arnold, & Bading, 2001; Murphy et al., 1994; Roux & Blenis, 2004). In contrast, CaMKK/CaMKIV, has previously been understood to act as a key fast-acting pathway, based on its ability to rapidly activate CREB (Hardingham et al., 2001; G. Y. Wu et al., 2001). We show here though through that CaMKIV activity is not required for rapid activity-dependent transcription. Our work raises new questions about the mechanisms by which transient stimulation selectively activates rapid genes but not others. Analysis of previously-published ChIP-seq data for key neuronal activity-dependent transcription factors implicates SRF in specifying rapid-gene activation, as its genomic localization at baseline and with depolarization is enriched proximal to rapidly-activating promoters and enhancers, compared to delayed promoters and enhancers. In support of this model, we have shown that SRF/ELK-1 heterodimer is responsive to MAPK even under brief stimulation and requires MAPK for its rapid activation by brief stimulation. Future work in which SRF is acutely depleted can be used to test the contribution SRF to rapid enhancer and

promoter activation and to study the mechanistic basis for these actions. Our results also demonstrate that depolarization-dependent increases in enhancer and promoter acetylation—which occur even in the absence of MAPK signaling—is insufficient for activating transcription—though it likely plays a contributory role in activity-dependent gene activation (L. F. Chen et al., 2019). In contrast, activity-dependent eRNA transcription is shown to be MAPK-dependent. The physical association of inducible enhancers with target promoters—which is known to be enhanced in neurons following depolarization (Schaukowitch et al., 2014)—may be required for eRNA synthesis (Y. W. Kim, Lee, Yun, & Kim, 2015; Li et al., 2015) but is not required for enhancers to carry activating histone modifications, including histone acetylation (Rao et al., 2017). Therefore, we hypothesize that rapid enhancers might exhibit rapid interaction with target promoters and that, as for eRNA synthesis, this rapid strengthening in the engagement of enhancers and promoters may be dependent on MAPK-signaling. MAPK may act on a subset of enhancers proximal to rapidly activating promoters, raising questions about how MAPK specifies certain enhancers. We also hypothesize that despite undergoing rapid increases in histone acetylation, enhancers proximal to delayed genes are likely to be differentiated from rapid-gene enhancers by exhibiting slower, non-MAPK dependent interaction with target promoters, as might be anticipated for genes which require chromatin remodeling at promoters for their activation (Ramirez-Carrozzi et al., 2006). Chromosome conformation capture techniques can be used to study the function of MAPK signaling or SRF activation on activity-regulated enhancer activation. This should also enable validation of candidate delayed response gene enhancers. Identification of the enhancers which specify delayed response genes and knowledge of their mechanisms of action will enable future manipulation of delayed response gene programs.

The mechanisms coupling continuous, prolonged stimulation to the activation of these delayed, continuously expressed genes is unknown. Neuronal secondary-response gene transcription has been shown to require rapidly-activating gene products, such as AP1, and chromatin remodeling complexes, including SWI/SNF proteins (Vierbuchen et al., 2017). Prior work studying delayed primary gene transcription in other cell types has shown that this process, similarly to secondary-response gene activation, proceeds in response to chromatin-remodeling activities at gene promoters (Tullai et al., 2007). The delayed synthesis of enhancer RNAs at delayed primary response genes suggests that enhancer-promoter engagement may require such chromatin remodeling. However, specific signaling mechanisms and chromatin remodeling complexes that induce neuronal delayed primary genes remain unidentified. We have shown that this transcription does not require MAPK or CaMKIV signaling. Recent work has shown that delayed response genes, but not rapidly-activating genes, require the activity bromodomain-containing transcription elongation factors (Sullivan et al., 2015), suggesting that the regulation of rapidly- and delayed- activating genes involve distinct mechanisms of transcription activation and differentially require mechanisms that influence promoter proximal pause-release and elongation. Another possibility is that these delayed genes require DNA cleavage activity of topoisomerases. Work in other systems has demonstrated the necessity of topoisomerase I in the transcription of secondary-response genes (Rialdi et al., 2016), and topoisomerase I has been implicated in the transcription of long neuronal genes (King et al., 2013; Mabb et al., 2016).

Studying the regulatory mechanisms controlling the activation of rapid and of delayed genes will provide critical knowledge that can explain cell-type specific mechanisms of expression and which can enable the selective manipulation of gene programs that are activated in response to physiologic stimuli. This is an essential capability for experiments that seek to test

the contribution of activity-dependent transcription to *in vivo* neuronal circuit plasticity both in development and in the adult brain. Therefore, future work should evaluate candidate signaling pathways and transcription factors for specifying rapid- and delayed- genes.

The work presented in Chapter 3 tests the hypothesis that an essential DNA-damage response protein, p97/VCP, regulates neuronal activity-dependent transcription. This is based on prior work demonstrating the necessity of DNA-damage, including double-stranded breaks (DSBs), for stimulus-dependent transcription. Topoisomerase IIB (TOP2B) which relieves torsional stress from DNA during transcription, has been shown to be required for induction of neuronal activity regulated early response genes (Madabhushi et al., 2015). These results suggest that double-stranded DNA breaks are required for activity dependent transcription. Classically, TOP2B acts to produce transient DNA-cleavage that is self-resolved without detection by DNA-damage surveillance mechanisms or the initiation of a DNA-damage response (DDR) (Nitiss, 2009). An unresolved question is whether TOP2B acts at early gene promoters to produce bona fide double-stranded breaks and to activate DDR at neuronal activity-regulated genes. It remains possible that while TOP2B binding to these genes is widespread, only a small fraction of these promoters undergo DSB formation. This is a critical unresolved question. The strongest evidence for neuronal activity-regulated DSB formation in neurons is work by *Madabhushi et al. 2015,* which demonstrates substantial increases in gamma-H2AX (y-H2AX)—an early signature of DNA damage (DSB)—occurring at immediate early gene promoters in response to neuronal activation (Madabhushi et al., 2015). It remains possible, though, that ATM (which activated gamma-H2AZ) and y-H2AX are activated independently of DNA-damage in response to activity (Blackford & Jackson, 2017). Notably, though, the magnitude increase in y-H2AX shown in neurons activated by glutamatergic stimulation is similar to that measured following etoposide

treatment, which acts to stall TOP2B-DNA complexes and produce DSBs and a DDR. This suggests that the number of immediate early loci undergoing DSB formation is similar between the two treatments, raising that possibility that DSB formation is a widespread feature of neuronal immediate early gene activation. This is suggested, too, by work in other cell types. For example, transient depletion of TDP2, an essential repair enzyme which acts upon DSBs generated by abortive TOP22B activity, limits the induction of androgen-induced gene expression, suggesting that TOP2 abortive activity and DSB formation is required for stimulus-dependent transcription (Gomez-Herreros et al., 2014). Multiple additional studies have shown that neuronal activity stimulates the DDR, including physiologic stimuli *in vivo*. For example, exposure of wild type mice to novel environments activates DNA-damage signaling in specific brain regions and produces increased levels of DSBs as measured by DNA comet assay (Suberbielle et al., 2013).

TOP2B has been shown to be pre-bound to many genomic sites, including activity-regulated gene promoters, and biochemical experiments show that TOP2B in unstimulated neurons is catalytically active despite the absence of detectable DDR signaling at these promoters (Madabhushi et al., 2015). Thus, in the absence of stimulation, TOP2B does not initiate DSB formation and DRR to activate gene expression. This suggests that neuronal depolarization acts upon TOP2B by an unknown mechanism to cause DSB formation and initiate DDR signaling. One possibility is that neuronal stimulation leads to activity-dependent post-translational modifications of TOP2B to modulate its catalytic activity and favor abortive TOP2B-DNA complexes that lead to DSB formation and DDR activation. Post-translational modifications, including phosphorylation, are known to modulate top2B catalytic activity

(Ackerman, Glover, & Osheroff, 1985; DeVore, Corbett, & Osheroff, 1992), though the biological significance of such modifications is unknown.

It remains to be determined the degree to which DSBs occur at activity regulated promoters, whether TOP2B is modulated by neuronal activity to predispose DSB formation at activity-regulated genes, and whether the mechanism of activation requires DDR-dependent chromatin remodeling events. The earliest work demonstrating the necessity of TOP2B-dependent DSBs in stimulus-dependent transcription used DNA-end labeling techniques to directly measure DSB formation at estradiol-responsive promoters (Ju et al., 2006). What is needed, however, are experiments that detect and quantify individual free DNA-ends to profile DSBs globally and quantify the degree to which activity-dependent loci undergo DSB formation (Bouwman & Crosetto, 2018). In situ hybridization methods, which allow for the detection of active immediate early gene alleles (L. F. Chen et al., 2019), could be combined with staining for DDR components to estimate the proportion of total number of early gene loci that undergo gamma-H2AX deposition or NHEJ-based repair methods in response to depolarization (B. Ma & Tanese, 2013). This information would advance understanding of the causal relationship between DSB formation and activity-dependent transcription.

The mechanism by which TOP2B and DSBs activate transcription is not yet understood. One hypothesis is that the DSB itself relieves torsional strain to enhance RNAPII initiation and elongation and to permit conformational changes to the 3D-structure of the genome that strengthen enhancer-promoter interactions that are required for activity-dependent transcription (Madabhushi, 2018). DNA-lesioning by the single-stranded topoisomerase I are known to be required for strengthening enhancer-promoter interactions in response to androgen-stimulated transcription (Puc et al., 2015). Supportive of this hypothesis for TOP2B in neurons are the

results of *Madabushi et al., 2015,* which demonstrate that recruitment of active Cas9, which acts to produce DSBs, to activity-regulated gene promoters, is sufficient to activate transcription (Madabhushi et al., 2015). Alternatively, TOP2B-dependent DSBs may also activate transcription by initiating chromatin remodeling that lead to the evictions of repressive histone variants and transcriptional repressor complexes, and the recruitment of histone variants which are more permissive of transcription (Calderwood, 2016; Ju et al., 2006).

The work presented in Chapter 3 tests the hypothesis that the required DNA-damage response protein, p97/VCP, regulates neuronal activity-dependent transcription. Experiments using pharmacologic inhibitors of DNA-damage repair pathways revealed that allosteric inhibitors of the AAA-ATPase p97/VCP acted acutely to suppress activity dependent transcription while preserving constitutive transcription. This raised the intriguing possibility that p97/VCP acts to regulate stimulus-dependent transcription, by a mechanism that may involve the DDR. p97/VCP is essential for the repair of DSBs, and inhibition of p97/VCP or depletion of required protein co-factors has been shown to inhibit repair and resolution of DSBs (Meerang et al., 2011). Known p97/VCP substrates, such as the NHEJ repair protein Ku70/80 (van den Boom et al., 2016), have been shown to be recruited to stimulus-dependent gene promoters (Puc et al., 2015) in other cell types and to be required for stimulus-dependent transcription (Trotter, King, & Archer, 2015). Ku70/80 has also been shown to repress gene transcription (Sucharov et al., 2004). Neuronal activity has been shown to lead to nuclear accumulation of the DSB-repair protein 53BP1, which is known to require p97/VCP for its recruitment to sites of double-stranded breaks (Acs et al., 2011). To test the hypothesis that p97/VCP regulates stimulus-dependent transcription, we generated homozygous cell lines containing DNA mutations that produce amino-acid substitutions in the mammalian p97/VCP protein. These point mutations

render p97/VCP insensitive to allosteric inhibitors. Three independent point mutations were introduced, two of which (N616F, K615V) act at allosteric binding site to disrupt inhibitor-binding (Magnaghi et al., 2013) and one of which (A530T) is positioned at an alternate site of the D2 ATPase domain, where it acts via an allosteric mechanism to render p97/VCP complexes insensitive to allosteric inhibition by NMS-873 (Her et al., 2016). Appropriate control cell lines were produced containing silent nucleotide mutations that aided selection of homozygous clones. Our work finds that these cell lines are resistant to the effects of NMS-873 on cell viability, which has previously been validated as an on-target activity of NMS-873 (Her et al., 2016). However, these experiments also show that the allosteric inhibitor NMS-873 continued to inhibit stimulus-dependent transcription with a Forskolin stimulus. Therefore, these results suggest that allosteric inhibitors of p97/VCP act via off-target mechanisms to inhibit activity-dependent transcription in HEK293T cells. It is difficult to identify candidate off-target mechanism of actions that explain the ability of NMS-873 to suppress stimulus-dependent transcription, particularly with such acuity and potency. NMS-873 has been well-validated *in vivo* and it thought to be one of the most potent and specific inhibitors. NMS-873 shows negligible inhibition of other AAA ATPase complexes, including RuvBL1, which has been implicated in transcription and found at active enhancers (Local et al., 2018). Future work can make use of affinity-based experiments combined with mass spectrometry to identify candidate off-target proteins that enable NMS-873 to inhibit transcription (McFedries, Schwaid, & Saghatelian, 2013).

Chapter 5: Methods

mRNA knockdown

Lentivirus was prepared in HEK293T cells transfected using PEI reagent, with pVSVg, psPAX2, and lentiviral genome plasmids carrying shRNA hairpins. shRNAs were ordered as bacterial glycerol stocks from Simga Mission shRNA library, which uses the plk0 backbone, as follows: Ubxd7 mouse (TRCN0000339996), Ufd1 mouse (TRCN0000092226), p47 mouse (TRCN0000030465), Ufd1 human (TRCN0000279806). Virus was prepared by transfecting HEK293T cells in 10% FBS/DMEM containing media, exchanging media for 2% heat-inactivated serum/DMEM 12 hours later, and preparing viral supernatants over the next 24-48 hours. Supernatants were then collected, filtered with 0.45uM PES filters, and stored at 4C or -80C prior to use. Primary neurons were transduced with viral supernatants at a 1:1 neuronal media to viral supernatant ratio at 1DIV or 3DIV and grown to 6-8DIV before silenced (APV/NBQX) and depolarized according to primary neuronal protocol indicated above.

Culturing

Cortical neurons were dissected from embryonic day 16 (E16) CD1 embryos of mixed sex. They were dissociated with papain (Worthington, (L)(S)003126) and plated on plates coated for at least one hour with poly-ornithine (30mg/mL, Sigma) in water and then washed three times with water. They were maintained at 37C at 5% CO_2 in neurobasal media (ThermoFisher) supplemented with B27 (ThermoFisher), Glutamax (ThermoFisher), and penicillin/streptomycin (ThermoFisher).

Stimulation

At 6 or 7 days in vitro (DIV), neurons were silenced with APV (100uM, Tocris) and NBQX (10uM, Tocris) to block NMDA and AMPA receptors. 14-16 hours later neurons were stimulated with a final concentration of 55mM potassium chloride using KCl depolarization solution (170mM KCl, 10mM Hepes pH 7.4, 1mM $MgCl_2$, 2mM $CaCl_2$). For sustained stimulation, KCl was left on neurons for up to 6 hours, whereas for brief stimulation, it was added for one minute, and then removed and replaced with conditioned neurobasal supplemented with APV and NBQX until RNA collection. While sustained KCl-mediated depolarization elevates intraceullular calcium for a minimum of 20 minutes and likely indefinitely (Dolmetsch et al., 2001; Evans et al., 2013), brief KCl-mediated depolarization elevates intracellular calcium only during the period of elevated KCl (Kingsbury et al., 2007). 10μM U0126 (Tocris), 625nM 11e (Tocris), 3μM STO-609 (Tocris), 30μM cycloheximide (Cell Signaling) or DMSO (equal volume) were added 30 minutes before stimulation and left on the neurons throughout the experiment. 10μg/mL ActinomycinD (Sigma) was added 15 minutes before stimulation. 10μM triptolide (Tocris) was added 5 minutes before stimulation.

Rat primary neuronal culture

Culture

Cultures of cortical neurons were prepared from embryonic day 18 Sprague Dawley rats of mixed sex (NIEHS Animal Study Proposal #01-21). Dissociated cortical neurons were plated in Neurobasal medium (Invitrogen) supplemented with 25 mM glutamate (Sigma-Aldrich) and 0.5 mM L-glutamine (Sigma-Aldrich) and either B27 (Invitrogen) or NS21 and maintained in a

similar medium without the glutamate. NS21 was prepared in the laboratory (Chen et al., 2008). Cultures were grown at 37C with 5% CO_2.

Stimulation

Neurons were used routinely between 10–14DIV. To induce synaptic stimulation, we triggered neuronal activity by co-treating neurons with 50μM Bicuculline (Sigma-Aldrich) and 75μM 4-Aminopyridine (Acros Organics) (or a DMSO control). To induce brief activity, activity was ceased at the desired time point (5 min or 10s) using 2μM TTX. Neurons were collected at various time points. 2μM PD184352 (Tocris) was added with bicuculline. 10μM U0126 was added 30 min before treatment with bicuculline.

Mice

Animal Care

All animal care and experimental procedures were approved by the Institutional Animal Care and Use Committees at each institution. Animals were housed with standard mouse chow and water provided *ad libitum*. Male C57BL/6J adult male mice (6-14 weeks old) were used for in vivo experiments in this study.

Visual Stimulation

For the flashing-light visual stimulation used in experiments with qPCR-based gene expression analysis and photometry, adult mice were housed in the dark for three days (for gene expression) or 12 h (for photometry). Bright lights (two GE White 18” Fluorescent Light Fixtures, part #

UCF18P and F15T8, 15W/60Hz) were placed on either side of the mouse home cage. Mice were housed with 3 mice per cage (for gene expression) or single-housed (for photometry). Sustained stimulation was achieved by repeated 60s of illumination followed by 20s of darkness for up to 4 hours. For intermediate (7 min) and brief (1 min) stimulation, the cage was illuminated using the same program, but stopping after 7 or 1 minute(s), respectively, followed by waiting for up to 4 hours in the dark before tissue collection. This illumination schedule was achieved using a Raspberry Pi B (Model #756-8308) and relay (Adafruit Controllable Four Outlet Power Relay Module ID#: 2935). For gene expression experiments, at several time points following the start of stimulation, mice were sacrificed using carbon dioxide, eyes were enucleated, both visual cortices were separately dissected and homogenized in Trizol (Invitrogen) for subsequent qPCR.

For in vivo experiments testing the effects of MEK inhibition, mice were singly dark-housed for 3 days. The stimulus consisted of turning on the room lights either continuously or briefly (for one minute). On the day of the experiment, mice were intraperitoneally injected with 100mg/kg of SL327 (Tocris), a blood-brain-barrier-crossing analog of U0126 (Atkins et al., 1998), in corn oil or with a corn oil vehicle. Injections started 30 minutes before visual stimulus and continued once per hour for the duration of the experiment to maintain the effects of the drug. SL327 was solubilized first in 100% ethanol. Then this ethanol mixture was added to corn oil and vortexed for 30 minutes. The ethanol was then removed from the mixture using a speed vac. The vehicle was prepared in the same way using just ethanol and corn oil without any drug. Mice were sacrificed before the stimulus or either 30 min or 2.5 h after turning on the lights using carbon dioxide. After enucleating the eyes, their visual cortices were immediately dissected. One hemisphere from each mouse was homogenized in Trizol (Invitrogen) for subsequent ARG-seq,

and the other was homogenized in cold lysis buffer (see Western Blotting) for western blotting to confirm ERK activation.

METHOD DETAILS

RNA extraction and qPCR

Mouse neurons/cortex

Samples were collected in Trizol (Invitrogen), and total RNA was extracted using the RNeasy mini kit (Qiagen) with in-column DNase treatment (Qiagen) according to the instructions of the manufacturer. The RNA was then either used for RNA sequencing (see below) or converted to cDNA using the High Capacity cDNA Reverse Transcription kit (Applied Biosystems). For standard qPCR experiments, we used SsoFast Evagreen supermix (BioRad) with primers in Table S6. For high-throughput qPCR, we used Taq-man qPCR probes (designed by Invitrogen) using the Fluidigm microfluidics system (see Table S3). High-throughput qPCR was performed by the BCH IDDRC, 1U54HD090255 according to the manufacturer's protocol.

Rat neurons

Total RNA was isolated from dissociated neurons using the RNeasy Mini Kit (Qiagen) with in-column DNase (Qiagen) digestion or the illustra RNAspin Mini kit (GE Healthcare) with on-column DNase (GE Healthcare) digestion. cDNA was synthesized using MuLV reverse transcriptase (Promega), random primers (Promega), oligo dT primers (Promega), and RNase inhibitors (Thermo Scientific). qPCR was performed using iTaq Universal Sybr Green Supermix

(BioRad) and the BIO-RAD CFX Connect realtime PCR Detection System or the PerfeCTa SYBR Green FastMix (Quantabio). To measure pre-mRNA, primers that target intron-exon borders served for cDNA synthesis and subsequent amplification (14 cycles) using the manufacturer's protocol in the One-Step RT-PCR kit (Qiagen). The amplified product level was quantified by qPCR using the same primers. Pre-mRNA primers are in Table S6 (Saha et al., 2011).

NanoString

NanoString probes were designed for indicated pre-mRNAs (Table S4) by NanoString technologies and assays were performed following the manufacturer's protocol.

RNA sequencing

General protocol

Before library preparation, for capture experiments, ERCC spike-in RNA (Ambion) was added to RNA samples according to the instruction of the manufacturer. Libraries were prepared using the High Throughput Total RNA TruSeq kit (Illumina), following the instructions of the manufacturer but scaling down all volumes to 1/3 of the recommended volumes. Libraries were sequenced on a NextSeq 500 (Ilumina) to a depth of at least 30 million reads per library for total RNA-seq, 20 million reads per library for eRNA-seq and 3 million reads per library for ARG-seq. We aligned reads to the mm9 genome using the STAR aligner (Dobin et al., 2013), and then made the resulting SAM files into BED files using SAMtools and BEDtools (Li et al., 2009; Quinlan and Hall, 2010). We used UCSC-tools (Kuhn et al., 2013) to make bigWig files for

viewing on the genome browser. We used bedtools map to count reads in both exons and introns. We then analyzed the raw count data using R, including edgeR (Robinson et al., 2009).

ARG-seq probe design synthesis

For ARG-seq, capture probes were designed as oligonucleotides tiling activity-regulated exons and control exons. Genes to be captured were 251 ARGs that showed a reproducible 3.5 fold increase in transcription at either 1 or 6 hours of KCl treatment in two replicates of published RNA-seq data (Kim et al., 2010) and 47 genes that showed no change with KCl but spanned a range of expression values (controls). Synthesized probes were 100 base pairs in length, with each probe overlapping the previous probe by 76 base pairs (Table S1). Probes had PCR primer binding sites and IVT promoters added. These oligonucleotides were ordered from Custom Array, PCR-amplified, and transcribed in vitro into biotinylated RNA baits using the Megascript SP6 In Vitro Transcription kit (ThermoFisher).

eRNA-seq probe design and synthesis

For eRNA-seq, capture probes were designed as oligonucleotides tiling putative activity-regulated enhancers, which were identified based on their location relative to ARGs and their transcription factor binding. To identify these putative enhancers, we started with all CREB, SRF, CBP, Npas4 or Pol2 binding sites from a previous study (Kim et al., 2010). We then took only those sites that were within 100kb of a transcription start site of one of the ARGs used in our ARG-seq experiment. We chose this threshold because 80% of enhancers regulate transcription start sites (TSSs) within 100kb (Chepelev et al., 2012). We eliminated intragenic enhancers and those located within 1kb from the transcription end site or 500bp from the

transcription start site of a gene. We designed probes to span the entire TF-bound putative enhancer, plus 500 bp on each side. Synthesized probes were 99 base pairs in length, with each probe overlapping the previous probe by 73 base pairs (Table S1). This oligonucleotide library was ordered from Twist Biosciences. We amplified and in vitro transcribed the RNA baits as described above for the ARG-seq baits. We also designed probes to tile the ERCC spike ins (Ambion) that were designed and ordered with our eRNA capture oligonucleotides. ERCC spike in oligonucleotides were made with different PCR adaptors so that they can be amplified and in-vitro-transcribed separately.

Capture

For ARG-seq and eRNA-seq, samples were treated in the same manner as with total RNA-seq, except that after library preparation, 250ng of pooled libraries were heated to 95C to denature DNA and then incubated with 250ng ARG-seq or eRNA-seq RNA baits (plus ERCC baits in a volume to allow for equal molar ratios of all probes) overnight at 65C in hybridization buffer (2.5ug Cot1 DNA (ThermoFisher), 2.5ug Salmon Sperm DNA (ThermoFisher), 15mM p5 blocking primers, 15mM p7 blocking primers, 5X SSPE (ThermoFisher), 5X Denhardt's Solution (ThermoFisher), 0.133% SDS). Blocking primers are: p5-AATGATACGGCGACCACCGAGATCTACAC, ACACTCTTTCCCTACACGACGCTCTTCCGATC/3InvdT/ p7-CAAGCAGAAGACGGCATACGAGAT, GTGACTGGAGTTCAGACGTGT GCTCTTCCGATC/3InvdT/ Primers for amplification are: p5-AATGATACGGCGACCACCGAGA, p7-CAAGCAGAAGACGGCATACGAG.

Hybridized samples were incubated with MyOne Streptavadin T1 Dynabeads (Invitrogen) in binding buffer (1M NaCl, 10mM Tris-HCl pH 7.5, 1mM EDTA). Beads were washed once in 1x SCC, 0.1% SDS at room temperature and three times in 0.1x SCC 0.1% SDS at 65C. Captured libraries were eluted with 0.1M NaOH and neutralized with 1M Tris-HCl pH 7.5. Libraries were then purified using the Qiagen MinElute PCR cleanup kit and re-amplified using Herculase II Fusion polymerase (Agilent).

Capture-seq processing and normalization

Data was normalized by the geometric mean of the reads from control genes or enhancers. Control regions were identified as regions that do not change with KCl in published RNA-seq data (Kim et al., 2010). ERCC spike-ins confirmed that capture occurred with similar efficiency across initial RNA concentrations.

Fiber Photometry

Viral injection and optic fiber placement

To monitor bulk activity of neurons in mouse primary visual cortex (V1), mice were anesthetized with isoflurane in 100% O_2 (induction, 3%–5%; maintenance, 1%–2%), and placed on a heating pad (CWE) in a stereotaxic apparatus (KOPF). Ophthalmic ointment (Puralube) was applied to the eyes. We expressed a genetically-encoded calcium indicator via viral injection (0.2 μL per hemisphere of AAV1.Syn.GCaMP6s.WPRE.SV40, Penn Vector Core) bilaterally into V1 (coordinates relative to Bregma: AP: -3.6 mm; ML: +/- 2.9 mm; DV: 250 μm and 500 μm below the pial surface, via a burrhole).

Two weeks after viral injection, mice were again anesthetized with isoflurane in 100% O_2 (induction, 3%–5%; maintenance, 1%–2%), and optic fibers (400 μm diameter, NA 0.48) were implanted bilaterally at the injection sites (150 μm below pial surface). Mice were allowed to recover for at least 10 days prior to recording.

Fiber photometry recordings of bulk calcium activity from V1

For photometry recordings, we delivered blue light via an LED (Plexon LED Driver PLexBright LD-1, 20 μW output, calibrated prior to each recording session) and patch cable (Doric). Recordings demonstrated very similar visual responses from each hemisphere, so a data from a single hemisphere was used per mouse.

Experimental paradigm during GCaMP6 recordings

We used the following visual stimulation paradigm during recordings. Singly-housed mice at the end of their 12-hr dark cycle (~7 am) were fitted with a patch cable for photometry recordings and moved, together with their home cage, to a light- and sound-isolated cabinet. The cabinet was initially fully dark, other than IR illumination (light source: HTX-F5-48-23), used for concurrent collection of videography to track mouse locomotion using a IR-sensitive camera (Flea3 1.3 MP Mono USB3 Vision camera, FL3-U3-13Y3M-C; Lens: H2Z0414C-MP).

Recordings were collected in darkness for one hour prior to bright light illumination of the homecage (two GE White 18” Fluorescent Light Fixtures, part # UCF18P and F15T8, 15W/60Hz) placed on either side of the mouse home cage. For the subsequent 3 hours, the cage was illuminated with the visual stimulation paradigm described above. Black heat-shrink tubing

was used to prevent room light from affecting photometry signals. We confirmed that contamination of photometry signals by illumination of the cage was negligible, by recording photometry signals in the absence of delivery of blue light via the patch cable at the end of each recording session.

All photometry signals and timestamps from stimulus delivery and videography were acquired on a standard PC and data acquisition board (National Instruments).

Histology

In a subset of experiments (4/8), fiber localization was confirmed histologically to be in area V1 and among strongly GCaMP6-expressing cell bodies. Mice were given an overdose of tribromoethanol, perfused with 10% formalin, and brains were cut in 40-μm coronal sections and stained with 4'-6-diamidino-2-phenylindole (DAPI) to visualize nuclei. Sections were then imaged on a digital slide scanner (Olympus VS120).

Western blotting

Mouse cortical neurons

To detect protein expression in mouse cortical neurons, neurons were collected in cold lysis buffer (for pERK and ARC western blots - 1% Triton X-100, 50 mM HEPES, pH 7.4, 150 mM NaCl, 1.5 mM $MgCl_2$, 1 mM EGTA, 10% glycerol, and freshly added protease and phosphatase inhibitors from Roche Applied Science Cat. # 05056489001 and 04906837001, for pElk-1 western blots – RIPA buffer (10mM tris pH 7.4, 1% NP-40,150mM NaCl, 0.1%SDS, 1mM

EDTA, 1mM Na(3)VO(4), 0.1% Sodium Deoxycholate) with protease and phosphatase inhibitors). Lysed neurons were treated with 4X sample buffer (40% glycerol, 8% SDS, 0.25M Tris-HCL, pH 6.8, 10% 2-mercaptoethanol) and boiled for 5 minutes. Samples were centrifuged at full speed for 3 minutes before loading on NuPage 4-12% Bis-Tris Gels (Invitrogen). Gels were run at 140V for 55 minutes. We transferred onto nitrocellulose membranes using the BioRad transfer system at 114V for 1h and 7min. Membranes were blocked in 5% milk-TBST for 1 hour. They were treated with primary antibody in 5% milk-TBST for at least one hour at room temperature or overnight at 4C. To visualize protein, blots were incubated with secondary antibody in TBST in the dark for 45 minutes. Blots were imaged using a LiCor Odyessy and quantified using ImageJ. Primary antibodies used were: rabbit anti-phosphoERK1/2 (Cell Signaling Technology 4370, 1:1000), mouse anti-GAPDH (Pierce, GA1R, 1:10000), rabbit anti-ARC (Synaptic Systems, 156-003, 1:1000), mouse anti-pElk-1 (Santa Cruz, sc-8406X, clone B4, 1:1000), rabbit anti-GAPDH (Cell Signaling D16H11, 1:1000). Secondary antibodies used were: IDR dye 680 goat anti-rabbit (LiCor, 1:10000), IDR dye 800 goat anti-mouse (LiCor, 1:10000).

Rat cortical neurons

To detect protein expression in rat cortical neurons, neurons were disrupted by brief sonication (three cycles of 30 sec in low setting in Bioruptor at 4C) and then cleared of debris by high-speed centrifugation (14500 RPM for 1 minute). The supernatant was collected in separate tubes and resolved by gel electrophoresis on 4-20% pre-cast gels (Life technology) and transferred to a nitrocellulose membrane using the iBlot gel transfer apparatus (Life technology). Immunoblots were incubated with primary antibody overnight. Blots were visualized with a LiCor Odyssey infrared scanner after immunolabeling primary antibodies with Goat anti-Mouse IgG (H+L)

Cross-Adsorbed Secondary Antibody, Alexa Fluor 680 (ThermoFisher). Images were processed using the Odyssey 2.1 software. Primary antibodies used were: rabbit anti-phosphoERK1/2 (Cell Signaling Technology 4370), H4 (Cell Signaling Technology 2935), Actin (Millipore, AM4302).

Nuclear Isolation

Nuclear lysate was prepared from treated neurons by first liberating the nuclei in a non-ionic detergent buffer (10mM HEPES (pH 7.9), 10mM KCl, 2mM $MgCl_2$, 0.5mM dithiothretol, 0.1% NP-40) for precisely 30 seconds and subsequently lysing them in NETN buffer (0.5% NP-40, 1mM EDTA, 50mM Tris, 120mM NaCl, pH 7.5) freshly supplemented with 0.5% protease inhibitor cocktail (Sigma) and phosphatase inhibitor cocktails (Sigma). Nuclear liberation was confirmed under the microscope before the released nuclei was scraped and dissolved in the NETN buffer.

Immunocytochemistry

To detect nuclear phospho-CaMKIV levels, after stimulation, neurons were fixed in 4% PFA for 15 minutes. Neurons were then washed twice in PBS and blocked and permeablized for 30 minutes using 1% BSA in PBS + 0.25% Triton-X100 (BSA-PBST). Neurons were then incubated overnight at 4C in BSA-PBST and phospho-CaMKIV antibody (1:500, Santa Cruz sc-28443-R). They were then washed 3 times with PBS and incubated for 1 hour at room temperature in secondary antibody (1:1000 ThermoFisher, R37117). They were then washed once with PBS, incubated for 10 min with DAPI (Roche, 10236276001) in PBS, and washed again with PBS. Neurons were imaged with a Leica inverted microscope. Images were taken with LAS software and quantified using ImageJ.

CRISPR Homology-Directed Repair

Homozygous mutant HEK293T cell lines were generated using CRISPR-HDR methods with single-stranded DNA oligonucleotide templates (ssODN) synthesized by IDT. ssODNs were designed to flank guide-RNA DNA-cleavage sites with approximately 70 bases of homology to genomic DNA sequence on either side of the cleavage site. The point mutants were generated by mutating codons as indicated: K615V AAA->GTG, N616F AAT->TTC, A530T GCC->ACC. Three additional silent mutations were used to introduce a restriction enzyme site to aid in the screening for edited clones and to prevent recurrent cas9 cleavage, including destruction of PAM (K615/N616 SfoI, A530 NheI). DNA targeting sequence for the K615V, N616F, and CNTL615 gRNA cloning: TCATCATTGGCGCTACCAAC. DNA targeting sequence for A530T and CNTL530 gRNA cloning: gcattcattagcaatggctt. gRNAs were cloned into plasmid pSpCas9 (PX330, Addgene 42230) (Cong et al., 2013). gRNA/Cas9 plasmid and ssODNs were transfected into HEK293T with Lipofectamine 3000 reagent. Cultures were then re-suspended and individual clones were then seeded by flow cytometry into 96-well plates for screening. Colonies were screened using PCR amplification and restriction digest to identify putative homozygous clones, and the amplified DNA was then sequenced by Sanger methods to confirm homozygosity.

Cell Viability Assay

Assay was conducted according to the manufacturer protocol for Promega CellTiter-GLO luminescent reagent. Specifically, HEK293T cells were plated at density of 8,000 cells in total 50 uL per well on a 96-well plate (Corning 96-well half-area clear bottom sterile white plates),

with either DMSO vehicle or NMS-873 inhibitor present at time of plating. Cells were grown for approximately 36 hours, prior to confluence, before then being lysed in equal volume Promega CellTiter GLO reagent and quantified for luminescence on SpectraMax M5 microplate reader (VWR International).

Chromatin immunoprecipitation (ChIP)

Media on the neurons was removed and neurons were fixed in crosslinking buffer (10 mM HEPES pH 7.5, 100 mM NaCl, 1 mM EDTA, 1 mM EGTA, 1% formaldehyde) for ten minutes at room temperature, and this reaction was quenched using 125mM glycine for 5 minutes. For H3K27ac ChIP, 250,000 neurons were used per ChIP sample. For Pol2 ChIP, 2 million neurons were used per sample. Neurons were then washed with cold PBS and then collected in PBS with 0.25% BSA and pelleted by centrifuging at 700 x g for 15 minutes. Cell pellets were stored at -80C. Neurons were sonicated using a Covaris E3 sonicator in lysis buffer (10 mM Tris pH 8.0, 1mM EDTA, 1 mM EGTA, 1X Roche complete EDTA-free protease inhibitors, 0.15% SDS). Sonication was done for 8 minutes per samples with 200 cycles/burst, a 2% duty cycle at power level 3. This reliably produced fragments between 100 and 700bp in length. Samples were then supplemented with ChIP Buffer to make SDS-ChIP buffer (10 mM Tris pH 8.0, 0.1% SDS,1% Triton X-100, 150 mM NaCl, 1 mM EDTA, 0.3 mM EGTA, 1X Roche complete EDTA-free protease inhibitors). For H3K27ac ChIP, Protein A beads (Dynabeads) were washed with 1% BSA/TBST and added to the fragmented DNA for a pre-clear and rotated at 4C for one hour. A different set of protein A beads was pre-treated with 0.48ug of antibody (Abcam, ab4729)/sample for H3K27ac ChIP. The same procedure was followed for Pol2 ChIP, but with Protein G Dynabeads and 4ug antibody (Abcam, ab817) per crosslinked input. Following the

pre-clear, pre-clear beads were removed, an aliquot of fragmented DNA was set aside as the input, and antibody-treated beads were incubated with the fragmented DNA overnight at 4C. were washed twice with cold low salt wash buffer (0.1% SDS, 20 mM Tris pH 8.0, 1% Triton X-100, 150 mM NaCl, 2 mM EDTA), twice with cold high salt wash buffer (0.1% SDS, 20 mM Tris pH 8.0, 1% Triton X-100, 500 mM NaCl, 2 mM EDTA), twice with cold LiCl wash buffer (1% NaDOC, 10 mM Tris pH 8.0, 1% NP40, 250 mM LiCl, 1 mM EDTA), and once with room temperature TE. Crosslinks were reversed by incubating samples in TE+1%SDS at 65C overnight. Samples were then treated with RNAse A (Ambion) and Proteinase K (New England Biolabs), and DNA was eluted using MinElute Columns (Qiagen) according to the instructions of the manufacturer.

Chromatin immunoprecipitation sequencing (ChIP-seq)

H3K27ac ChIP-seq

For H3K27ac ChIP-seq, libraries were prepared using 5ug of immunoprecipitated DNA or input DNA with the NuGen Ultralow V2 1-96 library prep kit. Libraries were sequenced on an Illumina NextSeq500 to a depth of at least 30 million reads per library. Reads were aligned to mouse genome mm9 using bowtie2 (Langmead and Salzberg, 2012). The resulting SAM files were made into BED files using SAMtools and BEDtools, with reads extended to 300 base pairs (Li et al., 2009; Quinlan and Hall, 2010) and then into bigWig files using UCSC-tools (Kuhn et al., 2013). Reads were assigned to individual enhancers or promoters using bedtools map and data was analyzed using R.

For downstream analysis, H3K27ac ChIP-seq data was input-normalized and then normalized by dividing by the geometric mean of control enhancers identified based on their location near the same control genes used for ARG-seq (control enhancer selection described in Capture RNA sequencing section). The data used for plotting (Table S7) included the mean input-normalized and control-normalized signal from the same regions targeted by eRNA-seq of each enhancer for two biological replicates, averaging each enhancer across replicates prior to plotting, and including only enhancers captured in eRNA-seq. Plots in figures S4 and S8 were made as describe in the "Published ChIP-seq data" section (see below).

Pol2 ChIP-seq

For Pol2 ChIP-seq, reads were aligned to mouse genome mm9 using the STAR aligner (Dobin et al., 2013). The resulting SAM files were made into read-extended (200 bases per fragment) BED files using SAMtools and BEDtools (Li et al., 2009; Quinlan and Hall, 2010) and then into bigWig files using UCSC-tools (Kuhn et al., 2013). For analysis, the metaseq (Dale et al., 2014), numpy (Van Der Walt et al., 2011), and matplotlib (Hunter, 2007) python packages were used to process aligned bam files, extend reads to 200 bases, and to produce read-depth- and input-normalized data. TSS positions were obtained from UCSC gene annotations and refseq gene databases (see table S8). For two genes (*Amigo3*, *Dusp5*), we used Refseq TSSs that are now deprecated. The mean Pol2 density at each TSS was measured using 600bp windows centered (-300bp to +300bp) on the TSS. ARG gene lists were filtered for a single TSS per gene, using the TSS with greatest average Pol2 density of all samples within single biological replicate. Additional analysis was performed in R. Given across-sample variability in read-depth- and input-normalized data, the samples were further normalized to Pol2 ChIP-seq density measured

at constitutively active, non-activity-regulated control gene promoters—similar to the across-sample ChIP-seq normalization methods adopted by others for quantitative analysis of peaks (Shao et al., 2012). Specifically, data from each sample was normalized to the median value of a distribution of Pol2 density values occurring at ~800 constitutively active TSSs (-300 to +300bp) with unchanging mRNA levels under KCl as measured by RNAseq (Kim, et al. 2011).

Published ChIP-seq Data

For analysis of published data, data from Kim et al. 2010 was used as aligned and processed by the authors and downloaded from GEO as bigwig files. Data from Telese et al. 2014 was downloaded from GEO as fastq files, re-aligned to mm9 using bowtie2, and processed like the H3K27ac data in this study. Data from ENCODE was downloaded as processed by the authors. Signal was binned across TSSs and enhancers and input-normalized using the Python package metaseq (Dale et al., 2014). Plots were made using R, smoothing with the lowess function.

Luciferase assays

The sequences for enhancer e5 was amplified using PCR from genomic DNA extracted from wildtype (C57BL/6J) mice, utilizing primers that included flanking KpnI and XhoI sites (ATACGGTACCCGAGACTACGTCA, ATGTCTCGAGATTAAAAAGGCCC). These amplified sequences were cloned into pTAN02, an ITR-containing AAV screening vector containing minimal human pFos upstream of the Firefly luciferase gene (Nguyen at al., 2016) with the KpnI and XhoI sites. Additionally, pTAN02 without an enhancer insert was included as a "no enhancer" control. Primary cortical neuron cultures (see above) were transfected using PEI (4:1 PEI:DNA mass ratio) on DIV5. These cultures were co-transfected with an internal

control Renilla luciferase construct, pTK-RN, at a fixed mass ratio of 9:1, Firefly construct:Renilla construct. Each experiment was run in triplicate. 30 minutes prior to depolarization, 10uM U0126 in DMSO or a DMSO vehicle was added to the culture media. Cultures were depolarized for 12 hours. A non-depolarized control received a media change with no additional KCl. Cultures were collected on the night of DIV7 and prepared using the Dual-Luciferase Reporter Assay System (Promega) according to the manufacturer's protocol. The lysate was assayed over a 10 second period using the GloMax 20/20 Single Tube Luminometer (Promega), and the luciferase activity was calculated as a ratio of the Firefly to Renilla output values.

QUANTIFICATION AND STATISTICAL ANALYSIS

We have included most statistical details in our Figure legends, including p-values, statistical tests used, 'n's for each experiment, and a description of to what 'n' refers. Biological replicates refer to biological material from different mice (all experiments), with biological replicate samples also collected on a different day (in vitro experiments only).

Gene Classification

In vitro

In experiments in mouse cortical neurons, our gene lists consisted of genes that showed significant induction (FDR<0.05) of at least 1.5 fold at any time point in ARG-seq experiments, as determined by edgeR (173/251 captured ARGs). We classified genes as PRGs if they showed

less than a 2-fold reduction in expression in 6h-KCl-treated neurons in the presence of cycloheximide. SRGs showed a greater than 2-fold reduction in the presence of cycloheximide (FDR<0.05 by edgeR). We classified PRGs as rapid if they had higher induction at 1h compared to 6h and delayed if they had higher induction at 6h compared to 1h. All rapid PRGs showed >2-fold pre-mRNA induction by 20min of stimulation. We eliminated four PRGs from our analysis due to ambiguity in our classification scheme, which exclusively relied upon kinetics of induction to distinguish rapid from delayed PRGs. We eliminated two genes (*Vgf* and *Homer1*) because their expression peaked at 6 hours of KCl stimulus, but they showed robust and significant pre-mRNA induction at 20 minutes. We also eliminated two genes (*Gadd45b* and *Nfkbid*) because while their mRNA induction peaked at 1h, they did not show a trend towards pre-mRNA or mRNA induction at 20 minutes of KCl. For significance testing in the classification, we used edgeR's glmFit and glmTreat functions (Robinson et al., 2009). PCA was performed using the prcomp function in R using normalized mRNA expression values. Specifically, to better assess expression kinetics, each gene was normalized such that its lowest expression value was set at 1 and its highest at 10.

In vivo

For in vivo data in Figure 9, gene classification was based on in vitro mouse data. However, we eliminated delayed PRGs with higher induction at 30 minutes compared to 150 minutes of visual stimulus.

Functional Annotation

Functional annotation was performed using PANTHER version 13.1 (Mi et al., 2017) (Table S5). Text of the table reflects output from the program with duplicate entries deleted. Colors in table represent manual classification. Genes were identified as directly regulating transcription if they were annotated as transcription factors/cofactors or as binding to DNA. Genes were identified as indirectly regulating transcription if they were annotated as part of a signaling pathway likely to regulate transcription. Genes were also identified as indirectly regulating transcription if they are not channels, receptors, or secreted proteins that were annotated as regulating transcription but not as transcription factors or binding to DNA.

Nearest-neighbor classifier

Our first classifier for post-hoc determination of in vitro activity pattern based on in vitro gene expression used the maximum expression at any time point for each gene, such that the kinetics of gene induction did not contribute to the classifier. It compared each replicate in a testing set to all replicates in a training set using Euclidean distance and classified based on the minimum distance. It was run with both separate testing and training sets (6 biological replicates each, randomly sorted) and leave-one-out cross validation. This classifier was run using all genes targeted by ARG-seq, only induced ARGs, and only control (non-induced) genes.

Our second classifier tested in vivo activity pattern and was trained using in vitro gene expression. We used 60-minute time points for both training and testing sets to enable detection of both rPRGs and dPRGs. The 11 ARGs used were *Egr1, Fos, Bdnf, Npas4, Cdkn1a, Crem, Grasp, Maml3, Scg2, Pcsk1,* and *Egr2*. To compare expression without influence of the absolute magnitude of expression, which differs between in vivo and in vitro experiments, data for each

experiment (i.e., in vitro or in vivo), was quantile normalized between genes. The classifier then compared each replicate in the in vivo testing set to all replicates in the in vitro training set using Euclidean distance and classified based on the minimum distance.

scRNA-seq analysis

Data

We used raw scRNA-seq (inDrops method) expression values from neurons in the visual cortex that had been exposed to 0, 1 or 4 hours of sustained visual stimulation (Hrvatin et al., 2017). We limited our analysis to only neurons classified with high confidence as excitatory neurons by Hrvatin et al. Our analysis was done on data from n=4 individual visual cortices for each time point pooled together.

Activity History Inference

Briefly, to infer activity history, each gene in each neuron at 1h was first called as ON or OFF based on the distribution of expression of that gene in excitatory neurons from the unstimulated visual cortex. Next, the numbers of rPRGs and dPRGs that were ON or OFF in each cell were summed. The number of genes ON in each gene class was used to determine whether that class as a whole was ON or OFF, based on thresholds set using data from unstimulated neurons (see below). The rPRG and dPRG states were then used to infer activity history as inactive (or unchanged from unstimulated), BRIEF, or SUSTAINED in response to visual stimulation.

A detailed description: For this analysis we used read-depth normalized data. We started by determining whether each rPRG or dPRG was induced in each neuron. A gene was defined as induced in a neuron from the stimulated cortex if its expression in that neuron was greater than a threshold set based on the expression of that gene in neurons from unstimulated cortex. This threshold was set at the 95th percentile of expression values for that gene in all the excitatory neurons in unstimulated cortex.

We then used these classifications of individual genes to determine whether neurons induced our gene classes (i.e., rPRGs or dPRGs) as a whole. We counted the number of rPRGs and dPRGs induced in each neuron. We set a threshold for the number of genes in each class that needed to be induced for that class to be considered ON in the neuron. We determined this threshold separately for rPRGs and dPRGs. To determine this threshold, we compared distributions of rPRG or dPRG metagenes between the stimulated and unstimulated samples. rPRG and dPRG metagenes were summed expression of all rPRGs or dPRGs, respectively, in each cell. We specifically compared metagene distributions between stimulated OFF neurons (i.e., neurons in the stimulated cortex for which the class is OFF) and unstimulated neurons (i.e. neurons from the unstimulated cortex), as our goal was for the stimulated OFF neurons to be similar to the unstimulated neurons to ensure that the class is actually OFF in stimulated OFF neurons. The threshold was therefore set as the maximum number of genes induced in the class for which the distribution of metagene expression for the stimulated OFF neurons was the same as or slightly left-shifted (i.e., less expressed) compared to the unstimulated neurons. More specifically, the threshold was set at the number of genes induced in the class that produced the minimum

distance between distributions where $p > 0.1$ by the Kolmogorov–Smirnov test and the stimulated OFF distribution was left-shifted from the unstimulated distribution.

We defined BRIEF neurons as having rPRGs ON and dPRGs OFF, SUSTAINED neurons as having dPRGs ON, and inactive neurons as having rPRGs and dPRGs OFF. For most classification of BRIEF and SUSTAINED neurons, we used the lists of rapid PRGs and delayed PRGs defined in Figure 1 of this paper. We also defined dPRGs among significantly induced genes in the in vivo data: dPRGs showed significant induction at 4h (FDR<0.05, 2-fold induction, unpaired, two-sided rank-sum test on bulk neurons) similar (<1.4 fold different) expression at 1h and 4h following stimulus. In this analysis, we defined genes for each layer individually.

For the analyses to determine whether the population of BRIEF neurons was significant, we asked whether BRIEF neurons were responding to the visual stimulus or reflective of an expected proportion of rapid-PRG-expressing cells among unstimulated neurons. We compared neurons from the stimulated cortex classified as having dPRGs OFF to unstimulated neurons. We used a Fisher's exact test to assess enrichment for rPRG-ON cells among d-PRG-OFF cells compared to unstimulated cells, expecting an odds ratio not equal to 1 if there was a difference in the proportion of BRIEF neurons between dPRG-OFF neurons and unstimulated neurons. We performed this analysis on all excitatory neurons together as well as for each layer individually.

Differential gene expression analysis

Differential gene expression analysis was performed using an unpaired, two-sided Wilcoxon rank-sum test comparing all BRIEF neurons to all SUSTAINED neurons. We confirmed that the package Monocole2 (Trapnell et al., 2014) gave us identical results. We also performed DE analysis using DECENT (Ye et al., 2017) and used it to generate imputed read counts. DECENT had greater power to detect differentially expressed genes, but revealed similar trends (i.e., differential expression of deep layer markers in BREIF neurons).

RNA-seq

Expression analysis

We quantified pre-mRNA transcription using intron reads from total RNA-seq data (Gaidatzis et al., 2015; Gray et al., 2014).

For ARG-seq and total RNA-seq figures, we plotted a mean of the control-normalized expression levels for each gene from several biological replicates. All p-values reported in the figure legends for comparisons between two groups of genes are from an unpaired non-parametric two-tailed Wilcoxon rank-sum test (unless otherwise noted). A paired test was used when comparing between the same set of genes in two conditions. We confirmed significance using a two-tailed Student's T-test (log-normalized if comparing fold-inductions). We also confirmed that the differences observed via analysis of the mean expression levels were replicated in each biological replicate individually ($p<0.05$, rank-sum test).

For ARG-seq and eRNA-seq, we confirmed using the Tukey HSD test in conjunction with ANOVA that expression from control genes or control enhancers in read-depth-normalized

samples and spike-in-normalized samples is not affected by membrane depolarization, visual stimulation, or addition of U0126/SL327 (adjusted p>0.8).

Comparison to other gene lists

Comparison between the genes induced in our study in vitro and the genes induced in three in vivo brain studies was performed with lists generated in a previous study (Cho et al., 2016). Comparison between the genes induced in our study in vitro and the genes induced in mouse macrophages and human cancer cell lines was performed using gene lists of induced genes generated by the authors of the previous studies (Escoubet-Lozach et al., 2011; Tullai et al., 2007). Human cancer cell line genes were converted to their mouse orthologs using the Mouse Genome Database (Blake et al., 2017) prior to analysis.

Analysis of photometry signals

All data analysis of GCaMP6 photometry signals was performed in MATLAB (Mathworks). For estimating the time course of changes in V1 calcium activity during each presentation of a 60-s lights-on stimulus onset (and during the first hour of recording in the dark, during 'pseudo-trials' in which the light was not actually switched on), we first estimated the mean GCaMP6 fluorescence in the 10-s period prior to stimulus onset, F_0. We then calculated the fractional change in fluorescence at each time point from -20 s to 80 s relative to stimulus onset, as $(F(t) - F_0)/F_0$.

ChIP-seq

H3K27ac

We confirmed using the Tukey HSD test in conjunction with ANOVA that read-depth-normalized signal at control enhancers was not affected by stimulation or by addition of U0126 (adjusted $p>0.8$). We also performed one replicate using *Drosophila* spike-in chromatin (Active Motif #61686, #53083) according to the instructions of the manufacturer and observed that U0126 treatment did not result in global H3K27ac changes. The plots shown only include enhancers that should and increase in H3K27ac with neuronal activity: 248 of the 940 putative enhancers reproducibly gain H3K27ac within the first hour of stimulation in two biological replicates (>1.3 fold change). All p-values reported are from the two-tailed non-parametric Wilcoxon rank-sum tests, but we confirmed significance using the Student's t-test. Unpaired tests were used if comparing between two groups of enhancers, and paired tests were used if comparing between the same group of enhancers in two conditions. We also performed a Student's t-test comparing the mean signal across all enhancers from each replicate for each gene class without U0126 to the mean signal across enhancers from each gene class with U0126 and found no significant difference ($p>0.6$). We also compared each enhancer individually, and again found no significant change in H3K27ac signal at any enhancer with U0126 ($p>0.9$, Bonferroni corrected).

Pol2

Additional analysis was performed in R. Given across-sample variability in read-depth- and input-normalized data, the samples were further normalized to Pol2 ChIP-seq density measured at constitutively active, non-activity-regulated control gene promoters—similar to the across-sample ChIP-seq normalization methods adopted by others for quantitative analysis of peaks

(Shao et al., 2012). Specifically, data from each sample was normalized to the median value of a distribution of Pol2 density values occurring at ~800 constitutively active TSSs (-300 to +300bp) with unchanging mRNA levels under KCl as measured by RNA-seq (Kim, et al. 2011). As a separate analysis, rPRG and dPRG TSS lists were filtered for TSS's with mean Pol2 ChIP-seq density greater than a threshold condition defined as two standard deviations above the mean value of un-expressed (Kim, et al. 2011) negative control TSS. For fold change analysis, fold-change was calculated at each TSS using the average unstimulated Pol2 density value obtained from two DMSO- and two U0126- treated samples.

Published ChIP-seq Data

For the enhancer data, in addition to the data shown in the figures, we also compared only those rapid and delayed enhancers near delayed PRGs. In unstimulated neurons, for SRF, CREB, MEF2, MED23, MED1 and NCoR we compared binding -6kb to +6kb from the centers of rapid enhancers compared to delayed enhancers and as reported in the main text found greater binding at rapid enhancers ($p<0.009$, rank-sum test, including only enhancers within 100 kb of delayed PRGs). Active histone marks H3K27ac, H3K4me2, H3K4me1, and H4K16ac were also higher in a comparison of the same rapid compared to delayed enhancers in unstimulated neurons ($p<0.01$, rank-sum test, only enhancers within 100 kb of delayed PRGs).

References

Ackerman, P., Glover, C. V., & Osheroff, N. (1985). Phosphorylation of DNA topoisomerase II by casein kinase II: modulation of eukaryotic topoisomerase II activity in vitro. *Proc Natl Acad Sci U S A, 82*(10), 3164-3168. doi:10.1073/pnas.82.10.3164

Acs, K., Luijsterburg, M. S., Ackermann, L., Salomons, F. A., Hoppe, T., & Dantuma, N. P. (2011). The AAA-ATPase VCP/p97 promotes 53BP1 recruitment by removing L3MBTL1 from DNA double-strand breaks. *Nat Struct Mol Biol, 18*(12), 1345-1350. doi:10.1038/nsmb.2188

Agalioti, T., Lomvardas, S., Parekh, B., Yie, J., Maniatis, T., & Thanos, D. (2000). Ordered recruitment of chromatin modifying and general transcription factors to the IFN-beta promoter. *Cell, 103*(4), 667-678.

Ahn, S., Ginty, D. D., & Linden, D. J. (1999). A late phase of cerebellar long-term depression requires activation of CaMKIV and CREB. *Neuron, 23*(3), 559-568.

Allen, B. L., & Taatjes, D. J. (2015). The Mediator complex: a central integrator of transcription. *Nat Rev Mol Cell Biol, 16*(3), 155-166. doi:10.1038/nrm3951

Amit, I., Citri, A., Shay, T., Lu, Y., Katz, M., Zhang, F., . . . Yarden, Y. (2007). A module of negative feedback regulators defines growth factor signaling. *Nat Genet, 39*(4), 503-512. doi:10.1038/ng1987

Arnold, C. D., Gerlach, D., Stelzer, C., Boryn, L. M., Rath, M., & Stark, A. (2013). Genome-wide quantitative enhancer activity maps identified by STARR-seq. *Science, 339*(6123), 1074-1077. doi:10.1126/science.1232542

Arnold, F. J., Hofmann, F., Bengtson, C. P., Wittmann, M., Vanhoutte, P., & Bading, H. (2005). Microelectrode array recordings of cultured hippocampal networks reveal a simple model for transcription and protein synthesis-dependent plasticity. *J Physiol, 564*(Pt 1), 3-19. doi:10.1113/jphysiol.2004.077446

Atkins, C. M., Selcher, J. C., Petraitis, J. J., Trzaskos, J. M., & Sweatt, J. D. (1998). The MAPK cascade is required for mammalian associative learning. *Nat Neurosci, 1*(7), 602-609. doi:10.1038/2836

Azad, G. K., Ito, K., Sailaja, B. S., Biran, A., Nissim-Rafinia, M., Yamada, Y., . . . Meshorer, E. (2018). PARP1-dependent eviction of the linker histone H1 mediates immediate early gene expression during neuronal activation. *J Cell Biol, 217*(2), 473-481. doi:10.1083/jcb.201703141

Banerjee, S., Bartesaghi, A., Merk, A., Rao, P., Bulfer, S. L., Yan, Y., . . . Subramaniam, S. (2016). 2.3 A resolution cryo-EM structure of human p97 and mechanism of allosteric inhibition. *Science, 351*(6275), 871-875. doi:10.1126/science.aad7974

Blackford, A. N., & Jackson, S. P. (2017). ATM, ATR, and DNA-PK: The Trinity at the Heart of the DNA Damage Response. *Mol Cell, 66*(6), 801-817. doi:10.1016/j.molcel.2017.05.015

Blake, J. A., Eppig, J. T., Kadin, J. A., Richardson, J. E., Smith, C. L., Bult, C. J., & the Mouse Genome Database, G. (2017). Mouse Genome Database (MGD)-2017: community knowledge resource for the laboratory mouse. *Nucleic Acids Res, 45*(D1), D723-D729. doi:10.1093/nar/gkw1040

Bonizec, M., Herissant, L., Pokrzywa, W., Geng, F., Wenzel, S., Howard, G. C., . . . Dargemont, C. (2014). The ubiquitin-selective chaperone Cdc48/p97 associates with Ubx3 to modulate monoubiquitylation of histone H2B. *Nucleic Acids Res, 42*(17), 10975-10986. doi:10.1093/nar/gku786

Bouwman, B. A. M., & Crosetto, N. (2018). Endogenous DNA Double-Strand Breaks during DNA Transactions: Emerging Insights and Methods for Genome-Wide Profiling. *Genes (Basel), 9*(12). doi:10.3390/genes9120632

Bunch, H., Lawney, B. P., Lin, Y. F., Asaithamby, A., Murshid, A., Wang, Y. E., . . . Calderwood, S. K. (2015). Transcriptional elongation requires DNA break-induced signalling. *Nat Commun, 6*, 10191. doi:10.1038/ncomms10191

Calderwood, S. K. (2016). A critical role for topoisomerase IIb and DNA double strand breaks in transcription. *Transcription, 7*(3), 75-83. doi:10.1080/21541264.2016.1181142

Canela, A., Maman, Y., Huang, S. N., Wutz, G., Tang, W., Zagnoli-Vieira, G., . . . Nussenzweig, A. (2019). Topoisomerase II-Induced Chromosome Breakage and Translocation Is Determined by Chromosome Architecture and Transcriptional Activity. *Mol Cell, 75*(2), 252-266 e258. doi:10.1016/j.molcel.2019.04.030

Caruso, M. E., Jenna, S., Bouchecareilh, M., Baillie, D. L., Boismenu, D., Halawani, D., . . . Chevet, E. (2008). GTPase-mediated regulation of the unfolded protein response in Caenorhabditis elegans is dependent on the AAA+ ATPase CDC-48. *Mol Cell Biol, 28*(13), 4261-4274. doi:10.1128/MCB.02252-07

Catic, A., Suh, C. Y., Hill, C. T., Daheron, L., Henkel, T., Orford, K. W., . . . Scadden, D. T. (2013). Genome-wide map of nuclear protein degradation shows NCoR1 turnover as a key to mitochondrial gene regulation. *Cell, 155*(6), 1380-1395. doi:10.1016/j.cell.2013.11.016

Chen, L. F., Lin, Y. T., Gallegos, D. A., Hazlett, M. F., Gomez-Schiavon, M., Yang, M. G., . . . West, A. E. (2019). Enhancer Histone Acetylation Modulates Transcriptional Bursting Dynamics of Neuronal Activity-Inducible Genes. *Cell Rep, 26*(5), 1174-1188 e1175. doi:10.1016/j.celrep.2019.01.032

Chen, R. H., Juo, P. C., Curran, T., & Blenis, J. (1996). Phosphorylation of c-Fos at the C-terminus enhances its transforming activity. *Oncogene, 12*(7), 1493-1502.

Chen, Y., Stevens, B., Chang, J., Milbrandt, J., Barres, B. A., & Hell, J. W. (2008). NS21: re-defined and modified supplement B27 for neuronal cultures. *J Neurosci Methods, 171*(2), 239-247. doi:10.1016/j.jneumeth.2008.03.013

Chepelev, I., Wei, G., Wangsa, D., Tang, Q., & Zhao, K. (2012). Characterization of genome-wide enhancer-promoter interactions reveals co-expression of interacting genes and modes of higher order chromatin organization. *Cell Res, 22*(3), 490-503. doi:10.1038/cr.2012.15

Cho, J. H., Huang, B. S., & Gray, J. M. (2016). RNA sequencing from neural ensembles activated during fear conditioning in the mouse temporal association cortex. *Sci Rep, 6*, 31753. doi:10.1038/srep31753

Cochran, B. H., Reffel, A. C., & Stiles, C. D. (1983). Molecular cloning of gene sequences regulated by platelet-derived growth factor. *Cell, 33*(3), 939-947. doi:10.1016/0092-8674(83)90037-5

Cong, L., Ran, F. A., Cox, D., Lin, S., Barretto, R., Habib, N., . . . Zhang, F. (2013). Multiplex genome engineering using CRISPR/Cas systems. *Science, 339*(6121), 819-823. doi:10.1126/science.1231143

Consortium, E. P. (2012). An integrated encyclopedia of DNA elements in the human genome. *Nature, 489*(7414), 57-74. doi:10.1038/nature11247

Crabtree, G. R. (2001). Calcium, calcineurin, and the control of transcription. *J Biol Chem, 276*(4), 2313-2316. doi:10.1074/jbc.R000024200

Creyghton, M. P., Cheng, A. W., Welstead, G. G., Kooistra, T., Carey, B. W., Steine, E. J., . . . Jaenisch, R. (2010). Histone H3K27ac separates active from poised enhancers and predicts developmental state. *Proc Natl Acad Sci U S A, 107*(50), 21931-21936. doi:10.1073/pnas.1016071107

Crowe, S. L., Tsukerman, S., Gale, K., Jorgensen, T. J., & Kondratyev, A. D. (2011). Phosphorylation of histone H2A.X as an early marker of neuronal endangerment following seizures in the adult rat brain. *J Neurosci, 31*(21), 7648-7656. doi:10.1523/JNEUROSCI.0092-11.2011

Dale, R. K., Matzat, L. H., & Lei, E. P. (2014). metaseq: a Python package for integrative genome-wide analysis reveals relationships between chromatin insulators and associated nuclear mRNA. *Nucleic Acids Res, 42*(14), 9158-9170. doi:10.1093/nar/gku644

Dantuma, N. P., Acs, K., & Luijsterburg, M. S. (2014). Should I stay or should I go: VCP/p97-mediated chromatin extraction in the DNA damage response. *Exp Cell Res, 329*(1), 9-17. doi:10.1016/j.yexcr.2014.08.025

Dantuma, N. P., & van Attikum, H. (2016). Spatiotemporal regulation of posttranslational modifications in the DNA damage response. *EMBO J, 35*(1), 6-23. doi:10.15252/embj.201592595

Davis, S., Vanhoutte, P., Pages, C., Caboche, J., & Laroche, S. (2000). The MAPK/ERK cascade targets both Elk-1 and cAMP response element-binding protein to control long-term potentiation-dependent gene expression in the dentate gyrus in vivo. *J Neurosci, 20*(12), 4563-4572.

De Koninck, P., & Schulman, H. (1998). Sensitivity of CaM kinase II to the frequency of Ca2+ oscillations. *Science, 279*(5348), 227-230.

DeVore, R. F., Corbett, A. H., & Osheroff, N. (1992). Phosphorylation of topoisomerase II by casein kinase II and protein kinase C: effects on enzyme-mediated DNA cleavage/religation and sensitivity to the antineoplastic drugs etoposide and 4'-(9-acridinylamino)methane-sulfon-m-anisidide. *Cancer Res, 52*(8), 2156-2161.

Dobin, A., Davis, C. A., Schlesinger, F., Drenkow, J., Zaleski, C., Jha, S., . . . Gingeras, T. R. (2013). STAR: ultrafast universal RNA-seq aligner. *Bioinformatics, 29*(1), 15-21. doi:10.1093/bioinformatics/bts635

Dolmetsch, R. E., Lewis, R. S., Goodnow, C. C., & Healy, J. I. (1997). Differential activation of transcription factors induced by Ca2+ response amplitude and duration. *Nature, 386*(6627), 855-858. doi:10.1038/386855a0

Dolmetsch, R. E., Pajvani, U., Fife, K., Spotts, J. M., & Greenberg, M. E. (2001). Signaling to the nucleus by an L-type calcium channel-calmodulin complex through the MAP kinase pathway. *Science, 294*(5541), 333-339. doi:10.1126/science.1063395

Dolmetsch, R. E., Xu, K., & Lewis, R. S. (1998). Calcium oscillations increase the efficiency and specificity of gene expression. *Nature, 392*(6679), 933-936. doi:10.1038/31960

Douglas, R. M., Dragunow, M., & Robertson, H. A. (1988). High-frequency discharge of dentate granule cells, but not long-term potentiation, induces c-fos protein. *Brain Res, 464*(3), 259-262.

Dudek, S. M., & Fields, R. D. (2001). Mitogen-activated protein kinase/extracellular signal-regulated kinase activation in somatodendritic compartments: roles of action potentials, frequency, and mode of calcium entry. *J Neurosci, 21*(2), RC122.

Ebert, D. H., & Greenberg, M. E. (2013). Activity-dependent neuronal signalling and autism spectrum disorder. *Nature, 493*(7432), 327-337. doi:10.1038/nature11860

Edwards, D. R., & Mahadevan, L. C. (1992). Protein synthesis inhibitors differentially superinduce c-fos and c-jun by three distinct mechanisms: lack of evidence for labile repressors. *EMBO J, 11*(7), 2415-2424.

Eriksson, M., Taskinen, M., & Leppa, S. (2007). Mitogen activated protein kinase-dependent activation of c-Jun and c-Fos is required for neuronal differentiation but not for growth and stress response in PC12 cells. *J Cell Physiol, 210*(2), 538-548. doi:10.1002/jcp.20907

Escoubet-Lozach, L., Benner, C., Kaikkonen, M. U., Lozach, J., Heinz, S., Spann, N. J., . . . Glass, C. K. (2011). Mechanisms establishing TLR4-responsive activation states of inflammatory response genes. *PLoS Genet, 7*(12), e1002401. doi:10.1371/journal.pgen.1002401

Eshete, F., & Fields, R. D. (2001). Spike frequency decoding and autonomous activation of Ca2+-calmodulin-dependent protein kinase II in dorsal root ganglion neurons. *J Neurosci, 21*(17), 6694-6705.

Esnault, C., Gualdrini, F., Horswell, S., Kelly, G., Stewart, A., East, P., . . . Treisman, R. (2017). ERK-Induced Activation of TCF Family of SRF Cofactors Initiates a Chromatin Modification Cascade Associated with Transcription. *Mol Cell, 65*(6), 1081-1095 e1085. doi:10.1016/j.molcel.2017.02.005

Evans, M. D., Sammons, R. P., Lebron, S., Dumitrescu, A. S., Watkins, T. B., Uebele, V. N., . . . Grubb, M. S. (2013). Calcineurin signaling mediates activity-dependent relocation of the axon initial segment. *J Neurosci, 33*(16), 6950-6963. doi:10.1523/JNEUROSCI.0277-13.2013

Favata, M. F., Horiuchi, K. Y., Manos, E. J., Daulerio, A. J., Stradley, D. A., Feeser, W. S., . . . Trzaskos, J. M. (1998). Identification of a novel inhibitor of mitogen-activated protein kinase kinase. *J Biol Chem, 273*(29), 18623-18632.

Fields, R. D., Eshete, F., Stevens, B., & Itoh, K. (1997). Action potential-dependent regulation of gene expression: temporal specificity in ca2+, cAMP-responsive element binding proteins, and mitogen-activated protein kinase signaling. *J Neurosci, 17*(19), 7252-7266.

Flack, J. E., Mieszczanek, J., Novcic, N., & Bienz, M. (2017). Wnt-Dependent Inactivation of the Groucho/TLE Co-repressor by the HECT E3 Ubiquitin Ligase Hyd/UBR5. *Mol Cell, 67*(2), 181-193 e185. doi:10.1016/j.molcel.2017.06.009

Flavell, S. W., & Greenberg, M. E. (2008). Signaling mechanisms linking neuronal activity to gene expression and plasticity of the nervous system. *Annu Rev Neurosci, 31*, 563-590. doi:10.1146/annurev.neuro.31.060407.125631

Foster, S. L., Hargreaves, D. C., & Medzhitov, R. (2007). Gene-specific control of inflammation by TLR-induced chromatin modifications. *Nature, 447*(7147), 972-978. doi:10.1038/nature05836

Fowler, T., Sen, R., & Roy, A. L. (2011). Regulation of primary response genes. *Mol Cell, 44*(3), 348-360. doi:10.1016/j.molcel.2011.09.014

Franz, A., Ackermann, L., & Hoppe, T. (2016). Ring of Change: CDC48/p97 Drives Protein Dynamics at Chromatin. *Front Genet, 7*, 73. doi:10.3389/fgene.2016.00073

Fujii, H., Inoue, M., Okuno, H., Sano, Y., Takemoto-Kimura, S., Kitamura, K., . . . Bito, H. (2013). Nonlinear decoding and asymmetric representation of neuronal input information by CaMKIIalpha and calcineurin. *Cell Rep, 3*(4), 978-987. doi:10.1016/j.celrep.2013.03.033

Gaidatzis, D., Burger, L., Florescu, M., & Stadler, M. B. (2015). Analysis of intronic and exonic reads in RNA-seq data characterizes transcriptional and post-transcriptional regulation. *Nat Biotechnol, 33*(7), 722-729. doi:10.1038/nbt.3269

Gaughan, L., Logan, I. R., Neal, D. E., & Robson, C. N. (2005). Regulation of androgen receptor and histone deacetylase 1 by Mdm2-mediated ubiquitylation. *Nucleic Acids Res, 33*(1), 13-26. doi:10.1093/nar/gki141

Gilchrist, D. A., Dos Santos, G., Fargo, D. C., Xie, B., Gao, Y., Li, L., & Adelman, K. (2010). Pausing of RNA polymerase II disrupts DNA-specified nucleosome organization to enable precise gene regulation. *Cell, 143*(4), 540-551. doi:10.1016/j.cell.2010.10.004

Gilchrist, D. A., Fromm, G., dos Santos, G., Pham, L. N., McDaniel, I. E., Burkholder, A., . . . Adelman, K. (2012). Regulating the regulators: the pervasive effects of Pol II pausing on stimulus-responsive gene networks. *Genes Dev, 26*(9), 933-944. doi:10.1101/gad.187781.112

Gilmour, D. S., & Lis, J. T. (1986). RNA polymerase II interacts with the promoter region of the noninduced hsp70 gene in Drosophila melanogaster cells. *Mol Cell Biol, 6*(11), 3984-3989.

Gomez-Herreros, F., Schuurs-Hoeijmakers, J. H., McCormack, M., Greally, M. T., Rulten, S., Romero-Granados, R., . . . Caldecott, K. W. (2014). TDP2 protects transcription from abortive topoisomerase activity and is required for normal neural function. *Nat Genet, 46*(5), 516-521. doi:10.1038/ng.2929

Gotoh, Y., Nishida, E., Yamashita, T., Hoshi, M., Kawakami, M., & Sakai, H. (1990). Microtubule-associated-protein (MAP) kinase activated by nerve growth factor and epidermal growth factor in PC12 cells. Identity with the mitogen-activated MAP kinase of fibroblastic cells. *Eur J Biochem, 193*(3), 661-669.

Gray, J. M., Harmin, D. A., Boswell, S. A., Cloonan, N., Mullen, T. E., Ling, J. J., . . . Springer, M. (2014). SnapShot-Seq: a method for extracting genome-wide, in vivo mRNA dynamics from a single total RNA sample. *PLoS One, 9*(2), e89673. doi:10.1371/journal.pone.0089673

Greenberg, M. E., Greene, L. A., & Ziff, E. B. (1985). Nerve growth factor and epidermal growth factor induce rapid transient changes in proto-oncogene transcription in PC12 cells. *J Biol Chem, 260*(26), 14101-14110.

Greenberg, M. E., & Ziff, E. B. (1984). Stimulation of 3T3 cells induces transcription of the c-fos proto-oncogene. *Nature, 311*(5985), 433-438.

Greenberg, M. E., Ziff, E. B., & Greene, L. A. (1986). Stimulation of neuronal acetylcholine receptors induces rapid gene transcription. *Science, 234*(4772), 80-83.

Greer, P. L., & Greenberg, M. E. (2008). From synapse to nucleus: calcium-dependent gene transcription in the control of synapse development and function. *Neuron, 59*(6), 846-860. doi:10.1016/j.neuron.2008.09.002

Hah, N., Danko, C. G., Core, L., Waterfall, J. J., Siepel, A., Lis, J. T., & Kraus, W. L. (2011). A rapid, extensive, and transient transcriptional response to estrogen signaling in breast cancer cells. *Cell, 145*(4), 622-634. doi:10.1016/j.cell.2011.03.042

Hah, N., Murakami, S., Nagari, A., Danko, C. G., & Kraus, W. L. (2013). Enhancer transcripts mark active estrogen receptor binding sites. *Genome Res, 23*(8), 1210-1223. doi:10.1101/gr.152306.112

Hardingham, G. E., Arnold, F. J., & Bading, H. (2001). A calcium microdomain near NMDA receptors: on switch for ERK-dependent synapse-to-nucleus communication. *Nat Neurosci, 4*(6), 565-566. doi:10.1038/88380

Hargreaves, D. C., Horng, T., & Medzhitov, R. (2009). Control of inducible gene expression by signal-dependent transcriptional elongation. *Cell, 138*(1), 129-145. doi:10.1016/j.cell.2009.05.047

Harlen, K. M., Trotta, K. L., Smith, E. E., Mosaheb, M. M., Fuchs, S. M., & Churchman, L. S. (2016). Comprehensive RNA Polymerase II Interactomes Reveal Distinct and Varied Roles for Each Phospho-CTD Residue. *Cell Rep, 15*(10), 2147-2158. doi:10.1016/j.celrep.2016.05.010

Hazzalin, C. A., Cuenda, A., Cano, E., Cohen, P., & Mahadevan, L. C. (1997). Effects of the inhibition of p38/RK MAP kinase on induction of five fos and jun genes by diverse stimuli. *Oncogene, 15*(19), 2321-2331. doi:10.1038/sj.onc.1201403

Heintzman, N. D., Stuart, R. K., Hon, G., Fu, Y., Ching, C. W., Hawkins, R. D., . . . Ren, B. (2007). Distinct and predictive chromatin signatures of transcriptional promoters and enhancers in the human genome. *Nat Genet, 39*(3), 311-318. doi:10.1038/ng1966

Hengen, K. B., Torrado Pacheco, A., McGregor, J. N., Van Hooser, S. D., & Turrigiano, G. G. (2016). Neuronal Firing Rate Homeostasis Is Inhibited by Sleep and Promoted by Wake. *Cell, 165*(1), 180-191. doi:10.1016/j.cell.2016.01.046

Her, N. G., Toth, J. I., Ma, C. T., Wei, Y., Motamedchaboki, K., Sergienko, E., & Petroski, M. D. (2016). p97 Composition Changes Caused by Allosteric Inhibition Are Suppressed by an On-Target Mechanism that Increases the Enzyme's ATPase Activity. *Cell Chem Biol, 23*(4), 517-528. doi:10.1016/j.chembiol.2016.03.012

Herschman, H. R. (1991). Primary response genes induced by growth factors and tumor promoters. *Annu Rev Biochem, 60*, 281-319. doi:10.1146/annurev.bi.60.070191.001433

Hong, J. W., Hendrix, D. A., & Levine, M. S. (2008). Shadow enhancers as a source of evolutionary novelty. *Science, 321*(5894), 1314. doi:10.1126/science.1160631

Hrvatin, S., Hochbaum, D. R., Nagy, M. A., Cicconet, M., Robertson, K., Cheadle, L., . . . Greenberg, M. E. (2018). Single-cell analysis of experience-dependent transcriptomic states in the mouse visual cortex. *Nat Neurosci, 21*(1), 120-129. doi:10.1038/s41593-017-0029-5

Hu, P., Fabyanic, E., Kwon, D. Y., Tang, S., Zhou, Z., & Wu, H. (2017). Dissecting Cell-Type Composition and Activity-Dependent Transcriptional State in Mammalian Brains by Massively Parallel Single-Nucleus RNA-Seq. *Mol Cell, 68*(5), 1006-1015 e1007. doi:10.1016/j.molcel.2017.11.017

Hunter, J. D. (2007). Matplotlib: A 2D graphics environment. *Comput. Sci. Eng., 9*, 99-104.

Ibata, K., Sun, Q., & Turrigiano, G. G. (2008). Rapid synaptic scaling induced by changes in postsynaptic firing. *Neuron, 57*(6), 819-826. doi:10.1016/j.neuron.2008.02.031

Joo, J. Y., Schaukowitch, K., Farbiak, L., Kilaru, G., & Kim, T. K. (2016). Stimulus-specific combinatorial functionality of neuronal c-fos enhancers. *Nat Neurosci, 19*(1), 75-83. doi:10.1038/nn.4170

Ju, B. G., Lunyak, V. V., Perissi, V., Garcia-Bassets, I., Rose, D. W., Glass, C. K., & Rosenfeld, M. G. (2006). A topoisomerase IIbeta-mediated dsDNA break required for regulated transcription. *Science, 312*(5781), 1798-1802. doi:10.1126/science.1127196

Ju, B. G., & Rosenfeld, M. G. (2006). A breaking strategy for topoisomerase IIbeta/PARP-1-dependent regulated transcription. *Cell Cycle, 5*(22), 2557-2560. doi:10.4161/cc.5.22.3497

Jun, J. J., Steinmetz, N. A., Siegle, J. H., Denman, D. J., Bauza, M., Barbarits, B., . . . Harris, T. D. (2017). Fully integrated silicon probes for high-density recording of neural activity. *Nature, 551*(7679), 232-236. doi:10.1038/nature24636

Kaikkonen, M. U., Spann, N. J., Heinz, S., Romanoski, C. E., Allison, K. A., Stender, J. D., . . . Glass, C. K. (2013). Remodeling of the enhancer landscape during macrophage activation is coupled to enhancer transcription. *Mol Cell, 51*(3), 310-325. doi:10.1016/j.molcel.2013.07.010

Kim, T. K., Hemberg, M., Gray, J. M., Costa, A. M., Bear, D. M., Wu, J., . . . Greenberg, M. E. (2010). Widespread transcription at neuronal activity-regulated enhancers. *Nature, 465*(7295), 182-187. doi:10.1038/nature09033

Kim, Y. W., Lee, S., Yun, J., & Kim, A. (2015). Chromatin looping and eRNA transcription precede the transcriptional activation of gene in the beta-globin locus. *Biosci Rep, 35*(2). doi:10.1042/BSR20140126

King, I. F., Yandava, C. N., Mabb, A. M., Hsiao, J. S., Huang, H. S., Pearson, B. L., . . . Zylka, M. J. (2013). Topoisomerases facilitate transcription of long genes linked to autism. *Nature, 501*(7465), 58-62. doi:10.1038/nature12504

Kingsbury, T. J., Bambrick, L. L., Roby, C. D., & Krueger, B. K. (2007). Calcineurin activity is required for depolarization-induced, CREB-dependent gene transcription in cortical neurons. *J Neurochem, 103*(2), 761-770. doi:10.1111/j.1471-4159.2007.04801.x

Koike, M., Fukushi, J., Ichinohe, Y., Higashimae, N., Fujishiro, M., Sasaki, C., . . . Kakizuka, A. (2010). Valosin-containing protein (VCP) in novel feedback machinery between abnormal protein accumulation and transcriptional suppression. *J Biol Chem, 285*(28), 21736-21749. doi:10.1074/jbc.M109.099283

Kuhn, R. M., Haussler, D., & Kent, W. J. (2013). The UCSC genome browser and associated tools. *Brief Bioinform, 14*(2), 144-161. doi:10.1093/bib/bbs038

Lacar, B., Linker, S. B., Jaeger, B. N., Krishnaswami, S. R., Barron, J. J., Kelder, M. J. E., . . . Gage, F. H. (2016). Nuclear RNA-seq of single neurons reveals molecular signatures of activation. *Nat Commun, 7*, 11022. doi:10.1038/ncomms11022

Lafon, A., Taranum, S., Pietrocola, F., Dingli, F., Loew, D., Brahma, S., . . . Papamichos-Chronakis, M. (2015). INO80 Chromatin Remodeler Facilitates Release of RNA Polymerase II from Chromatin for Ubiquitin-Mediated Proteasomal Degradation. *Mol Cell, 60*(5), 784-796. doi:10.1016/j.molcel.2015.10.028

Lam, M. T., Cho, H., Lesch, H. P., Gosselin, D., Heinz, S., Tanaka-Oishi, Y., . . . Glass, C. K. (2013). Rev-Erbs repress macrophage gene expression by inhibiting enhancer-directed transcription. *Nature, 498*(7455), 511-515. doi:10.1038/nature12209

Lam, M. T., Li, W., Rosenfeld, M. G., & Glass, C. K. (2014). Enhancer RNAs and regulated transcriptional programs. *Trends Biochem Sci, 39*(4), 170-182. doi:10.1016/j.tibs.2014.02.007

Langmead, B., & Salzberg, S. L. (2012). Fast gapped-read alignment with Bowtie 2. *Nat Methods, 9*(4), 357-359. doi:10.1038/nmeth.1923

Lau, L. F., & Nathans, D. (1987). Expression of a set of growth-related immediate early genes in BALB/c 3T3 cells: coordinate regulation with c-fos or c-myc. *Proc Natl Acad Sci U S A, 84*(5), 1182-1186. doi:10.1073/pnas.84.5.1182

Lee, P. R., Cohen, J. E., Iacobas, D. A., Iacobas, S., & Fields, R. D. (2017). Gene networks activated by specific patterns of action potentials in dorsal root ganglia neurons. *Sci Rep, 7*, 43765. doi:10.1038/srep43765

Li, H., Handsaker, B., Wysoker, A., Fennell, T., Ruan, J., Homer, N., . . . Genome Project Data Processing, S. (2009). The Sequence Alignment/Map format and SAMtools. *Bioinformatics, 25*(16), 2078-2079. doi:10.1093/bioinformatics/btp352

Li, W., Hu, Y., Oh, S., Ma, Q., Merkurjev, D., Song, X., . . . Rosenfeld, M. G. (2015). Condensin I and II Complexes License Full Estrogen Receptor alpha-Dependent Enhancer Activation. *Mol Cell, 59*(2), 188-202. doi:10.1016/j.molcel.2015.06.002

Li, W., Notani, D., Ma, Q., Tanasa, B., Nunez, E., Chen, A. Y., . . . Rosenfeld, M. G. (2013). Functional roles of enhancer RNAs for oestrogen-dependent transcriptional activation. *Nature, 498*(7455), 516-520. doi:10.1038/nature12210

Li, Y., Rivera, C. M., Ishii, H., Jin, F., Selvaraj, S., Lee, A. Y., . . . Ren, B. (2014). CRISPR reveals a distal super-enhancer required for Sox2 expression in mouse embryonic stem cells. *PLoS One, 9*(12), e114485. doi:10.1371/journal.pone.0114485

Lin, C., Yang, L., Tanasa, B., Hutt, K., Ju, B. G., Ohgi, K., . . . Rosenfeld, M. G. (2009). Nuclear receptor-induced chromosomal proximity and DNA breaks underlie specific translocations in cancer. *Cell, 139*(6), 1069-1083. doi:10.1016/j.cell.2009.11.030

Local, A., Huang, H., Albuquerque, C. P., Singh, N., Lee, A. Y., Wang, W., . . . Ren, B. (2018). Identification of H3K4me1-associated proteins at mammalian enhancers. *Nat Genet, 50*(1), 73-82. doi:10.1038/s41588-017-0015-6

Lutz, H., Nguyen, T. A., Joswig, J., Rau, K., & Laube, B. (2019). NMDA Receptor Signaling Mediates cFos Expression via Top2beta-Induced DSBs in Glioblastoma Cells. *Cancers (Basel), 11*(3). doi:10.3390/cancers11030306

Ma, B., & Tanese, N. (2013). Combined FISH and immunofluorescent staining methods to co-localize proteins and mRNA in neurons and brain tissue. *Methods Mol Biol, 1010*, 123-138. doi:10.1007/978-1-62703-411-1_9

Ma, H., Groth, R. D., Wheeler, D. G., Barrett, C. F., & Tsien, R. W. (2011). Excitation-transcription coupling in sympathetic neurons and the molecular mechanism of its initiation. *Neurosci Res, 70*(1), 2-8. doi:10.1016/j.neures.2011.02.004

Mabb, A. M., Simon, J. M., King, I. F., Lee, H. M., An, L. K., Philpot, B. D., & Zylka, M. J. (2016). Topoisomerase 1 Regulates Gene Expression in Neurons through Cleavage

Complex-Dependent and -Independent Mechanisms. *PLoS One, 11*(5), e0156439. doi:10.1371/journal.pone.0156439

Madabhushi, R. (2018). The Roles of DNA Topoisomerase IIbeta in Transcription. *Int J Mol Sci, 19*(7). doi:10.3390/ijms19071917

Madabhushi, R., Gao, F., Pfenning, A. R., Pan, L., Yamakawa, S., Seo, J., . . . Tsai, L. H. (2015). Activity-Induced DNA Breaks Govern the Expression of Neuronal Early-Response Genes. *Cell, 161*(7), 1592-1605. doi:10.1016/j.cell.2015.05.032

Magnaghi, P., D'Alessio, R., Valsasina, B., Avanzi, N., Rizzi, S., Asa, D., . . . Isacchi, A. (2013). Covalent and allosteric inhibitors of the ATPase VCP/p97 induce cancer cell death. *Nat Chem Biol, 9*(9), 548-556. doi:10.1038/nchembio.1313

Mandemaker, I. K., van Cuijk, L., Janssens, R. C., Lans, H., Bezstarosti, K., Hoeijmakers, J. H., . . . Marteijn, J. A. (2017). DNA damage-induced histone H1 ubiquitylation is mediated by HUWE1 and stimulates the RNF8-RNF168 pathway. *Sci Rep, 7*(1), 15353. doi:10.1038/s41598-017-15194-y

Marais, R., Wynne, J., & Treisman, R. (1993). The SRF accessory protein Elk-1 contains a growth factor-regulated transcriptional activation domain. *Cell, 73*(2), 381-393.

Marshall, C. J. (1995). Specificity of receptor tyrosine kinase signaling: transient versus sustained extracellular signal-regulated kinase activation. *Cell, 80*(2), 179-185.

Marza, E., Taouji, S., Barroso, K., Raymond, A. A., Guignard, L., Bonneu, M., . . . Chevet, E. (2015). Genome-wide screen identifies a novel p97/CDC-48-dependent pathway regulating ER-stress-induced gene transcription. *EMBO Rep, 16*(3), 332-340. doi:10.15252/embr.201439123

Maze, I., Wenderski, W., Noh, K. M., Bagot, R. C., Tzavaras, N., Purushothaman, I., . . . Allis, C. D. (2015). Critical Role of Histone Turnover in Neuronal Transcription and Plasticity. *Neuron, 87*(1), 77-94. doi:10.1016/j.neuron.2015.06.014

McFedries, A., Schwaid, A., & Saghatelian, A. (2013). Methods for the elucidation of protein-small molecule interactions. *Chem Biol, 20*(5), 667-673. doi:10.1016/j.chembiol.2013.04.008

Meerang, M., Ritz, D., Paliwal, S., Garajova, Z., Bosshard, M., Mailand, N., . . . Ramadan, K. (2011). The ubiquitin-selective segregase VCP/p97 orchestrates the response to DNA double-strand breaks. *Nat Cell Biol, 13*(11), 1376-1382. doi:10.1038/ncb2367

Melo, C. A., Drost, J., Wijchers, P. J., van de Werken, H., de Wit, E., Oude Vrielink, J. A., . . . Agami, R. (2013). eRNAs are required for p53-dependent enhancer activity and gene transcription. *Mol Cell, 49*(3), 524-535. doi:10.1016/j.molcel.2012.11.021

Mi, H., Huang, X., Muruganujan, A., Tang, H., Mills, C., Kang, D., & Thomas, P. D. (2017). PANTHER version 11: expanded annotation data from Gene Ontology and Reactome pathways, and data analysis tool enhancements. *Nucleic Acids Res, 45*(D1), D183-D189. doi:10.1093/nar/gkw1138

Miyashita, T., Kubik, S., Haghighi, N., Steward, O., & Guzowski, J. F. (2009). Rapid activation of plasticity-associated gene transcription in hippocampal neurons provides a mechanism for encoding of one-trial experience. *J Neurosci, 29*(4), 898-906. doi:10.1523/JNEUROSCI.4588-08.2009

Mohammed, A. I., Gritton, H. J., Tseng, H. A., Bucklin, M. E., Yao, Z., & Han, X. (2016). An integrative approach for analyzing hundreds of neurons in task performing mice using wide-field calcium imaging. *Sci Rep, 6*, 20986. doi:10.1038/srep20986

Mousavi, K., Zare, H., Dell'orso, S., Grontved, L., Gutierrez-Cruz, G., Derfoul, A., . . . Sartorelli, V. (2013). eRNAs promote transcription by establishing chromatin accessibility at defined genomic loci. *Mol Cell, 51*(5), 606-617. doi:10.1016/j.molcel.2013.07.022

Murphy, T. H., Blatter, L. A., Bhat, R. V., Fiore, R. S., Wier, W. G., & Baraban, J. M. (1994). Differential regulation of calcium/calmodulin-dependent protein kinase II and p42 MAP kinase activity by synaptic transmission. *J Neurosci, 14*(3 Pt 1), 1320-1331.

Nakazawa, K., Sun, L. D., Quirk, M. C., Rondi-Reig, L., Wilson, M. A., & Tonegawa, S. (2003). Hippocampal CA3 NMDA receptors are crucial for memory acquisition of one-time experience. *Neuron, 38*(2), 305-315.

Ndoja, A., Cohen, R. E., & Yao, T. (2014). Ubiquitin signals proteolysis-independent stripping of transcription factors. *Mol Cell, 53*(6), 893-903. doi:10.1016/j.molcel.2014.02.002

Nguyen, P. V., Abel, T., & Kandel, E. R. (1994). Requirement of a critical period of transcription for induction of a late phase of LTP. *Science, 265*(5175), 1104-1107.

Nguyen, T. V., Li, J., Lu, C. J., Mamrosh, J. L., Lu, G., Cathers, B. E., & Deshaies, R. J. (2017). p97/VCP promotes degradation of CRBN substrate glutamine synthetase and neosubstrates. *Proc Natl Acad Sci U S A, 114*(14), 3565-3571. doi:10.1073/pnas.1700949114

Nitiss, J. L. (2009). DNA topoisomerase II and its growing repertoire of biological functions. *Nat Rev Cancer, 9*(5), 327-337. doi:10.1038/nrc2608

Puc, J., Kozbial, P., Li, W., Tan, Y., Liu, Z., Suter, T., . . . Rosenfeld, M. G. (2015). Ligand-dependent enhancer activation regulated by topoisomerase-I activity. *Cell, 160*(3), 367-380. doi:10.1016/j.cell.2014.12.023

Qiu, Z., & Ghosh, A. (2008). A calcium-dependent switch in a CREST-BRG1 complex regulates activity-dependent gene expression. *Neuron, 60*(5), 775-787. doi:10.1016/j.neuron.2008.09.040

Quinlan, A. R., & Hall, I. M. (2010). BEDTools: a flexible suite of utilities for comparing genomic features. *Bioinformatics, 26*(6), 841-842. doi:10.1093/bioinformatics/btq033

Rada-Iglesias, A., Bajpai, R., Swigut, T., Brugmann, S. A., Flynn, R. A., & Wysocka, J. (2011). A unique chromatin signature uncovers early developmental enhancers in humans. *Nature, 470*(7333), 279-283. doi:10.1038/nature09692

Ramanan, N., Shen, Y., Sarsfield, S., Lemberger, T., Schutz, G., Linden, D. J., & Ginty, D. D. (2005). SRF mediates activity-induced gene expression and synaptic plasticity but not neuronal viability. *Nat Neurosci, 8*(6), 759-767. doi:10.1038/nn1462

Ramirez-Carrozzi, V. R., Braas, D., Bhatt, D. M., Cheng, C. S., Hong, C., Doty, K. R., . . . Smale, S. T. (2009). A unifying model for the selective regulation of inducible transcription by CpG islands and nucleosome remodeling. *Cell, 138*(1), 114-128. doi:10.1016/j.cell.2009.04.020

Ramirez-Carrozzi, V. R., Nazarian, A. A., Li, C. C., Gore, S. L., Sridharan, R., Imbalzano, A. N., & Smale, S. T. (2006). Selective and antagonistic functions of SWI/SNF and Mi-2beta nucleosome remodeling complexes during an inflammatory response. *Genes Dev, 20*(3), 282-296. doi:10.1101/gad.1383206

Rao, S. S. P., Huang, S. C., Glenn St Hilaire, B., Engreitz, J. M., Perez, E. M., Kieffer-Kwon, K. R., . . . Aiden, E. L. (2017). Cohesin Loss Eliminates All Loop Domains. *Cell, 171*(2), 305-320 e324. doi:10.1016/j.cell.2017.09.026

Rialdi, A., Campisi, L., Zhao, N., Lagda, A. C., Pietzsch, C., Ho, J. S. Y., . . . Marazzi, I. (2016). Topoisomerase 1 inhibition suppresses inflammatory genes and protects from death by inflammation. *Science, 352*(6289), aad7993. doi:10.1126/science.aad7993

Ripke, S., O'Dushlaine, C., Chambert, K., Moran, J. L., Kahler, A. K., Akterin, S., . . . Sullivan, P. F. (2013). Genome-wide association analysis identifies 13 new risk loci for schizophrenia. *Nat Genet, 45*(10), 1150-1159. doi:10.1038/ng.2742

Rivera, V. M., Sheng, M., & Greenberg, M. E. (1990). The inner core of the serum response element mediates both the rapid induction and subsequent repression of c-fos transcription following serum stimulation. *Genes Dev, 4*(2), 255-268.

Robinson, M. D., McCarthy, D. J., & Smyth, G. K. (2010). edgeR: a Bioconductor package for differential expression analysis of digital gene expression data. *Bioinformatics, 26*(1), 139-140. doi:10.1093/bioinformatics/btp616

Roux, P. P., & Blenis, J. (2004). ERK and p38 MAPK-activated protein kinases: a family of protein kinases with diverse biological functions. *Microbiol Mol Biol Rev, 68*(2), 320-344. doi:10.1128/MMBR.68.2.320-344.2004

Saha, R. N., & Dudek, S. M. (2013). Splitting hares and tortoises: a classification of neuronal immediate early gene transcription based on poised RNA polymerase II. *Neuroscience, 247*, 175-181. doi:10.1016/j.neuroscience.2013.04.064

Saha, R. N., Wissink, E. M., Bailey, E. R., Zhao, M., Fargo, D. C., Hwang, J. Y., . . . Dudek, S. M. (2011). Rapid activity-induced transcription of Arc and other IEGs relies on poised RNA polymerase II. *Nat Neurosci, 14*(7), 848-856. doi:10.1038/nn.2839

Santos, S. D., Verveer, P. J., & Bastiaens, P. I. (2007). Growth factor-induced MAPK network topology shapes Erk response determining PC-12 cell fate. *Nat Cell Biol, 9*(3), 324-330. doi:10.1038/ncb1543

Schaukowitch, K., Joo, J. Y., Liu, X., Watts, J. K., Martinez, C., & Kim, T. K. (2014). Enhancer RNA facilitates NELF release from immediate early genes. *Mol Cell, 56*(1), 29-42. doi:10.1016/j.molcel.2014.08.023

Segala, G., Bennesch, M. A., Pandey, D. P., Hulo, N., & Picard, D. (2016). Monoubiquitination of Histone H2B Blocks Eviction of Histone Variant H2A.Z from Inducible Enhancers. *Mol Cell, 64*(2), 334-346. doi:10.1016/j.molcel.2016.08.034

Sgambato, V., Vanhoutte, P., Pages, C., Rogard, M., Hipskind, R., Besson, M. J., & Caboche, J. (1998). In vivo expression and regulation of Elk-1, a target of the extracellular-regulated kinase signaling pathway, in the adult rat brain. *J Neurosci, 18*(1), 214-226.

Shao, Z., Zhang, Y., Yuan, G. C., Orkin, S. H., & Waxman, D. J. (2012). MAnorm: a robust model for quantitative comparison of ChIP-Seq data sets. *Genome Biol, 13*(3), R16. doi:10.1186/gb-2012-13-3-r16

Sheng, H. Z., Fields, R. D., & Nelson, P. G. (1993). Specific regulation of immediate early genes by patterned neuronal activity. *J Neurosci Res, 35*(5), 459-467. doi:10.1002/jnr.490350502

Shepherd, J. D., & Bear, M. F. (2011). New views of Arc, a master regulator of synaptic plasticity. *Nat Neurosci, 14*(3), 279-284. doi:10.1038/nn.2708

Shepherd, J. D., Rumbaugh, G., Wu, J., Chowdhury, S., Plath, N., Kuhl, D., . . . Worley, P. F. (2006). Arc/Arg3.1 mediates homeostatic synaptic scaling of AMPA receptors. *Neuron, 52*(3), 475-484. doi:10.1016/j.neuron.2006.08.034

Shi, L., Qiu, D., Zhao, G., Corthesy, B., Lees-Miller, S., Reeves, W. H., & Kao, P. N. (2007). Dynamic binding of Ku80, Ku70 and NF90 to the IL-2 promoter in vivo in activated T-cells. *Nucleic Acids Res, 35*(7), 2302-2310. doi:10.1093/nar/gkm117

Smith-Hicks, C., Xiao, B., Deng, R., Ji, Y., Zhao, X., Shepherd, J. D., . . . Linden, D. J. (2010). SRF binding to SRE 6.9 in the Arc promoter is essential for LTD in cultured Purkinje cells. *Nat Neurosci, 13*(9), 1082-1089. doi:10.1038/nn.2611

Spiegel, I., Mardinly, A. R., Gabel, H. W., Bazinet, J. E., Couch, C. H., Tzeng, C. P., . . . Greenberg, M. E. (2014). Npas4 regulates excitatory-inhibitory balance within neural circuits through cell-type-specific gene programs. *Cell, 157*(5), 1216-1229. doi:10.1016/j.cell.2014.03.058

Stach, L., & Freemont, P. S. (2017). The AAA+ ATPase p97, a cellular multitool. *Biochem J, 474*(17), 2953-2976. doi:10.1042/BCJ20160783

Suberbielle, E., Sanchez, P. E., Kravitz, A. V., Wang, X., Ho, K., Eilertson, K., . . . Mucke, L. (2013). Physiologic brain activity causes DNA double-strand breaks in neurons, with exacerbation by amyloid-beta. *Nat Neurosci, 16*(5), 613-621. doi:10.1038/nn.3356

Subramaniam, M., Schmidt, L. J., Crutchfield, C. E., 3rd, & Getz, M. J. (1989). Negative regulation of serum-responsive enhancer elements. *Nature, 340*(6228), 64-66. doi:10.1038/340064a0

Sucharov, C. C., Helmke, S. M., Langer, S. J., Perryman, M. B., Bristow, M., & Leinwand, L. (2004). The Ku protein complex interacts with YY1, is up-regulated in human heart failure, and represses alpha myosin heavy-chain gene expression. *Mol Cell Biol, 24*(19), 8705-8715. doi:10.1128/MCB.24.19.8705-8715.2004

Sullivan, J. M., Badimon, A., Schaefer, U., Ayata, P., Gray, J., Chung, C. W., . . . Schaefer, A. (2015). Autism-like syndrome is induced by pharmacological suppression of BET proteins in young mice. *J Exp Med, 212*(11), 1771-1781. doi:10.1084/jem.20151271

Szutorisz, H., Dillon, N., & Tora, L. (2005). The role of enhancers as centres for general transcription factor recruitment. *Trends Biochem Sci, 30*(11), 593-599. doi:10.1016/j.tibs.2005.08.006

Tasic, B., Menon, V., Nguyen, T. N., Kim, T. K., Jarsky, T., Yao, Z., . . . Zeng, H. (2016). Adult mouse cortical cell taxonomy revealed by single cell transcriptomics. *Nat Neurosci, 19*(2), 335-346. doi:10.1038/nn.4216

Telese, F., Ma, Q., Perez, P. M., Notani, D., Oh, S., Li, W., . . . Rosenfeld, M. G. (2015). LRP8-Reelin-Regulated Neuronal Enhancer Signature Underlying Learning and Memory Formation. *Neuron, 86*(3), 696-710. doi:10.1016/j.neuron.2015.03.033

Thomas, G. M., & Huganir, R. L. (2004). MAPK cascade signalling and synaptic plasticity. *Nat Rev Neurosci, 5*(3), 173-183. doi:10.1038/nrn1346

Thompson, M. A., Ginty, D. D., Bonni, A., & Greenberg, M. E. (1995). L-type voltage-sensitive Ca2+ channel activation regulates c-fos transcription at multiple levels. *J Biol Chem, 270*(9), 4224-4235.

Tiwari, V. K., Burger, L., Nikoletopoulou, V., Deogracias, R., Thakurela, S., Wirbelauer, C., . . . Schubeler, D. (2012). Target genes of Topoisomerase IIbeta regulate neuronal survival and are defined by their chromatin state. *Proc Natl Acad Sci U S A, 109*(16), E934-943. doi:10.1073/pnas.1119798109

Toettcher, J. E., Weiner, O. D., & Lim, W. A. (2013). Using optogenetics to interrogate the dynamic control of signal transmission by the Ras/Erk module. *Cell, 155*(6), 1422-1434. doi:10.1016/j.cell.2013.11.004

Trapnell, C., Cacchiarelli, D., Grimsby, J., Pokharel, P., Li, S., Morse, M., . . . Rinn, J. L. (2014). The dynamics and regulators of cell fate decisions are revealed by pseudotemporal ordering of single cells. *Nat Biotechnol, 32*(4), 381-386. doi:10.1038/nbt.2859

Treisman, R. (1996). Regulation of transcription by MAP kinase cascades. *Curr Opin Cell Biol, 8*(2), 205-215.

Trotter, K. W., King, H. A., & Archer, T. K. (2015). Glucocorticoid Receptor Transcriptional Activation via the BRG1-Dependent Recruitment of TOP2beta and Ku70/86. *Mol Cell Biol, 35*(16), 2799-2817. doi:10.1128/MCB.00230-15

Tullai, J. W., Schaffer, M. E., Mullenbrock, S., Sholder, G., Kasif, S., & Cooper, G. M. (2007). Immediate-early and delayed primary response genes are distinct in function and genomic architecture. *J Biol Chem, 282*(33), 23981-23995. doi:10.1074/jbc.M702044200

Turrigiano, G. (2011). Too many cooks? Intrinsic and synaptic homeostatic mechanisms in cortical circuit refinement. *Annu Rev Neurosci, 34*, 89-103. doi:10.1146/annurev-neuro-060909-153238

Uuskula-Reimand, L., Hou, H., Samavarchi-Tehrani, P., Rudan, M. V., Liang, M., Medina-Rivera, A., . . . Wilson, M. D. (2016). Topoisomerase II beta interacts with cohesin and CTCF at topological domain borders. *Genome Biol, 17*(1), 182. doi:10.1186/s13059-016-1043-8

van den Boom, J., Wolf, M., Weimann, L., Schulze, N., Li, F., Kaschani, F., . . . Meyer, H. (2016). VCP/p97 Extracts Sterically Trapped Ku70/80 Rings from DNA in Double-Strand Break Repair. *Mol Cell, 64*(1), 189-198. doi:10.1016/j.molcel.2016.08.037

Van Der Walt, S., Colbert, S.C., and Varoquaux, G. (2011). The NumPy array: A structure for efficient numerical computation. *Comput. Sci. Eng., 13*, 22-30.

Verma, R., Oania, R., Fang, R., Smith, G. T., & Deshaies, R. J. (2011). Cdc48/p97 mediates UV-dependent turnover of RNA Pol II. *Mol Cell, 41*(1), 82-92. doi:10.1016/j.molcel.2010.12.017

Verma, R., Oania, R. S., Kolawa, N. J., & Deshaies, R. J. (2013). Cdc48/p97 promotes degradation of aberrant nascent polypeptides bound to the ribosome. *Elife, 2*, e00308. doi:10.7554/eLife.00308

Vierbuchen, T., Ling, E., Cowley, C. J., Couch, C. H., Wang, X., Harmin, D. A., . . . Greenberg, M. E. (2017). AP-1 Transcription Factors and the BAF Complex Mediate Signal-Dependent Enhancer Selection. *Mol Cell, 68*(6), 1067-1082 e1012. doi:10.1016/j.molcel.2017.11.026

Wall, R., Briskin, M., Carter, C., Govan, H., Taylor, A., & Kincade, P. (1986). A labile inhibitor blocks immunoglobulin kappa-light-chain-gene transcription in a pre-B leukemic cell line. *Proc Natl Acad Sci U S A, 83*(2), 295-298. doi:10.1073/pnas.83.2.295

Wang, D., Garcia-Bassets, I., Benner, C., Li, W., Su, X., Zhou, Y., . . . Fu, X. D. (2011). Reprogramming transcription by distinct classes of enhancers functionally defined by eRNA. *Nature, 474*(7351), 390-394. doi:10.1038/nature10006

Wang, G., Balamotis, M. A., Stevens, J. L., Yamaguchi, Y., Handa, H., & Berk, A. J. (2005). Mediator requirement for both recruitment and postrecruitment steps in transcription initiation. *Mol Cell, 17*(5), 683-694. doi:10.1016/j.molcel.2005.02.010

Wei, J., Dong, S., Bowser, R. K., Khoo, A., Zhang, L., Jacko, A. M., . . . Zhao, J. (2017). Regulation of the ubiquitylation and deubiquitylation of CREB-binding protein modulates histone acetylation and lung inflammation. *Sci Signal, 10*(483). doi:10.1126/scisignal.aak9660

West, A. E., & Greenberg, M. E. (2011). Neuronal activity-regulated gene transcription in synapse development and cognitive function. *Cold Spring Harb Perspect Biol, 3*(6). doi:10.1101/cshperspect.a005744

Whitney, O., Pfenning, A. R., Howard, J. T., Blatti, C. A., Liu, F., Ward, J. M., . . . Jarvis, E. D. (2014). Core and region-enriched networks of behaviorally regulated genes and the singing genome. *Science, 346*(6215), 1256780. doi:10.1126/science.1256780

Worley, P. F., Bhat, R. V., Baraban, J. M., Erickson, C. A., McNaughton, B. L., & Barnes, C. A. (1993). Thresholds for synaptic activation of transcription factors in hippocampus: correlation with long-term enhancement. *J Neurosci, 13*(11), 4776-4786.

Wu, G. Y., Deisseroth, K., & Tsien, R. W. (2001a). Activity-dependent CREB phosphorylation: convergence of a fast, sensitive calmodulin kinase pathway and a slow, less sensitive mitogen-activated protein kinase pathway. *Proc Natl Acad Sci U S A, 98*(5), 2808-2813. doi:10.1073/pnas.051634198

Wu, G. Y., Deisseroth, K., & Tsien, R. W. (2001b). Spaced stimuli stabilize MAPK pathway activation and its effects on dendritic morphology. *Nat Neurosci, 4*(2), 151-158. doi:10.1038/83976

Wu, Y. E., Pan, L., Zuo, Y., Li, X., & Hong, W. (2017). Detecting Activated Cell Populations Using Single-Cell RNA-Seq. *Neuron, 96*(2), 313-329 e316. doi:10.1016/j.neuron.2017.09.026

Xia, Z., Dudek, H., Miranti, C. K., & Greenberg, M. E. (1996). Calcium influx via the NMDA receptor induces immediate early gene transcription by a MAP kinase/ERK-dependent mechanism. *J Neurosci, 16*(17), 5425-5436.

Yang, Y., Yamada, T., Hill, K. K., Hemberg, M., Reddy, N. C., Cho, H. Y., . . . Bonni, A. (2016). Chromatin remodeling inactivates activity genes and regulates neural coding. *Science, 353*(6296), 300-305. doi:10.1126/science.aad4225

Ye, C., Speed, T.P., and Salim, A. . (2017). DECENT : Differential Expression with Capture Efficiency AdjustmeNT for Single-Cell RNA-seq Data. *bioRxiv, doi:* http://dx.doi.org/10.1101/225177.

Ye, Y., Meyer, H. H., & Rapoport, T. A. (2001). The AAA ATPase Cdc48/p97 and its partners transport proteins from the ER into the cytosol. *Nature, 414*(6864), 652-656. doi:10.1038/414652a

Yu, Y., Oberlaender, K., Bengtson, C. P., & Bading, H. (2017). One nuclear calcium transient induced by a single burst of action potentials represents the minimum signal strength in activity-dependent transcription in hippocampal neurons. *Cell Calcium, 65*, 14-21. doi:10.1016/j.ceca.2017.03.003

Yuan, Z., Gong, S., Luo, J., Zheng, Z., Song, B., Ma, S., . . . Li, M. (2009). Opposing roles for ATF2 and c-Fos in c-Jun-mediated neuronal apoptosis. *Mol Cell Biol, 29*(9), 2431-2442. doi:10.1128/MCB.01344-08

Zhai, S., Ark, E. D., Parra-Bueno, P., & Yasuda, R. (2013). Long-distance integration of nuclear ERK signaling triggered by activation of a few dendritic spines. *Science, 342*(6162), 1107-1111. doi:10.1126/science.1245622

Zheng, F., Luo, Y., & Wang, H. (2009). Regulation of brain-derived neurotrophic factor-mediated transcription of the immediate early gene Arc by intracellular calcium and calmodulin. *J Neurosci Res, 87*(2), 380-392. doi:10.1002/jnr.21863

Zhou, H. L., Geng, C., Luo, G., & Lou, H. (2013). The p97-UBXD8 complex destabilizes mRNA by promoting release of ubiquitinated HuR from mRNP. *Genes Dev, 27*(9), 1046-1058. doi:10.1101/gad.215681.113

Zhu, Y., Sun, L., Chen, Z., Whitaker, J. W., Wang, T., & Wang, W. (2013). Predicting enhancer transcription and activity from chromatin modifications. *Nucleic Acids Res, 41*(22), 10032-10043. doi:10.1093/nar/gkt826

Supplemental Figures

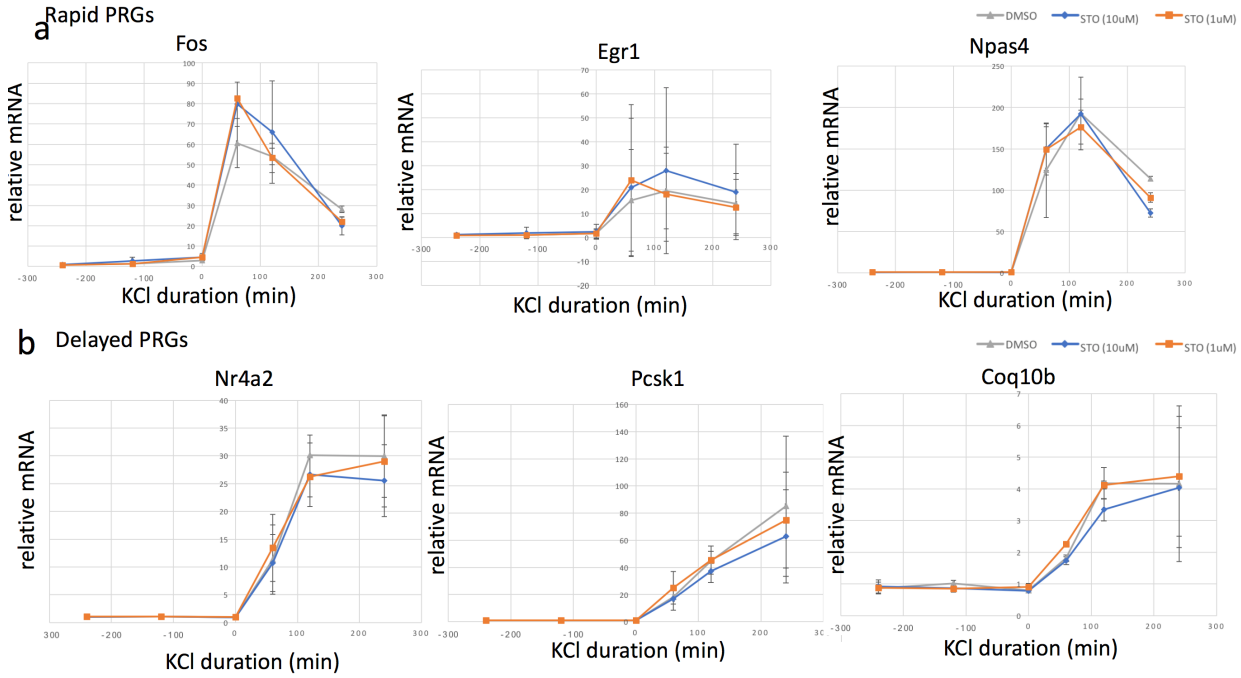

Supplemental Figure 1. Pharmacologic inhibition of CaMKIV by STO-609 does not affect early or delayed gene transcription in response to depolarizing KCl .

a) qPCR mRNA measurements for three representative MAPK-dependent rPRGs following 60, 120, or 240 minutes of continuous depolarization (KCl). Stimulation conducted following pre-treatment with vehicle (grey) or STO609 (1uM in orange or 10uM in blue), with pre-treatment mRNA levels shown in the negative portion of each plot. Traces colored by treatment condition (see top right). Shown are arithmetic mean (n=2) with standard deviation. b) as in (a) but for three representative delayed genes which are MAPK-independent (Nr4a2, Pcsk1, Coq10b).

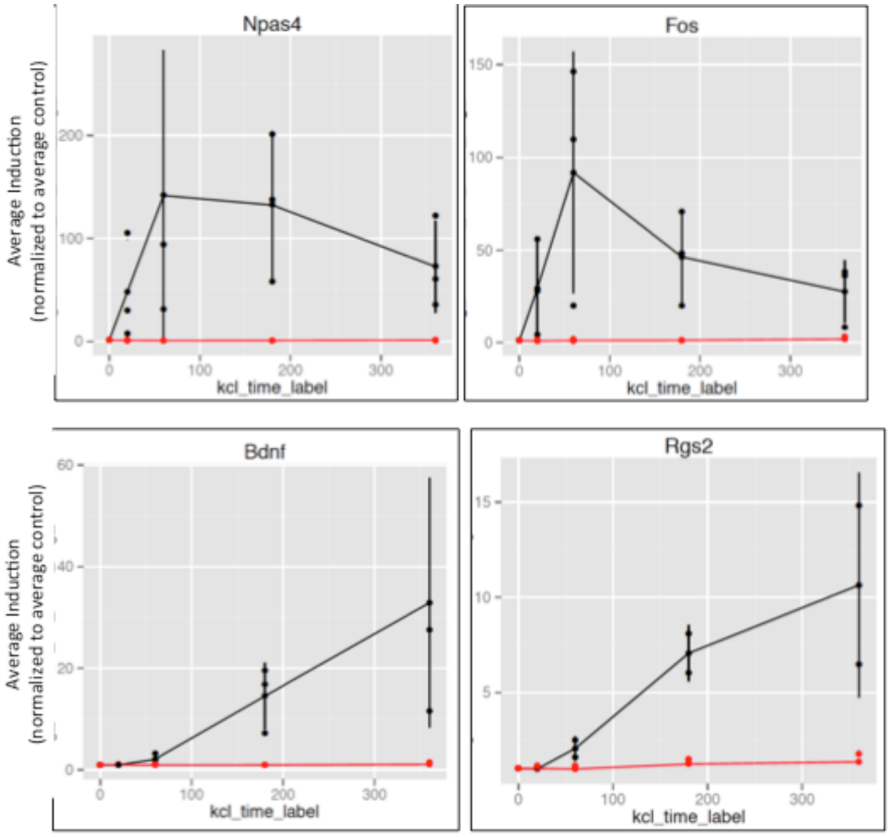

Supplemental Figure 2. NMS-873 blocks depolarization-dependent induction of neuronal rapid- and delayed- genes. qPCR measurements of representative IEG (*top—Fos, Npas4)* and dPRG (*bottom—Bdnf, Rgs2)* mRNA levels following application of depolarizing KCl for 0', 20', 60', 180' and 360' minutes, to primary neuronal cultures. Cultures were pre-treated for 30-minutes with either NMS-873 (10uM, *red)* or DMSO vehicle (*black)*. Plotted values are normalized to average unstimulated levels of two control mRNAs (Calm1 and Tubb3) and are shown relative to the un-stimulated 0' time-point (0', an average of two independent un-stimulated samples per treatment condition). Connected points represent the mean of three independent replicates (with replicate points plotted as separate points); mean values are connected by solid line and error-bars represent standard-error.

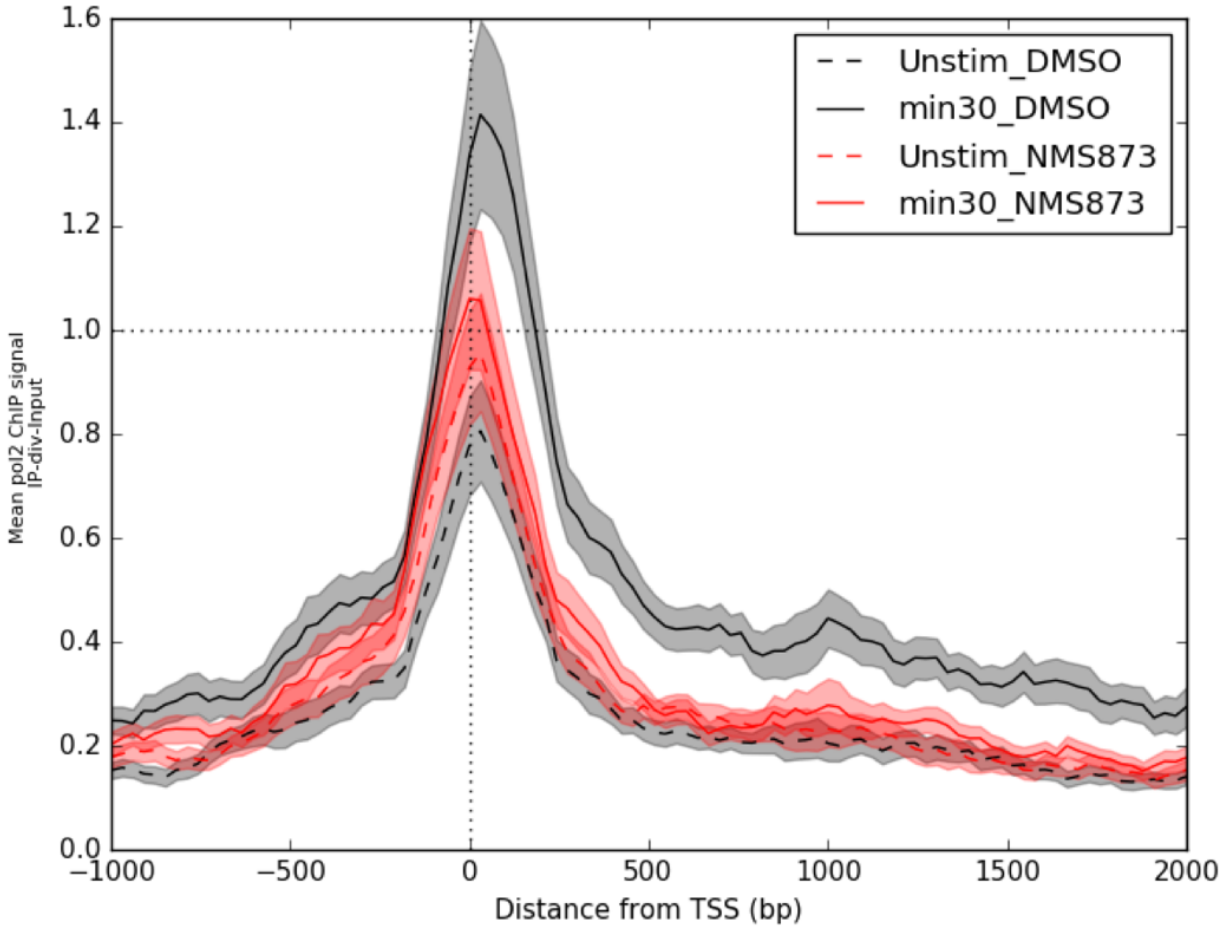

Supplemental Figure 3. Meta gene profiles of RNAPII ChIPseq density at rapid primary response gene (rPRG) TSSs (right). Data represent RNAPII ChIP-seq density (IP/Input) at neuronal immediate early genes, normalized by read-depth and by the median RNAPII density found at constitutively active neuronal TSS's. Data represent single biological replicate. Vehicle-treated shown in grey, NMS873 shown in red. Unstimulated by hashed-line, 30-minutes KCl by solid line. Shading represents SEM.

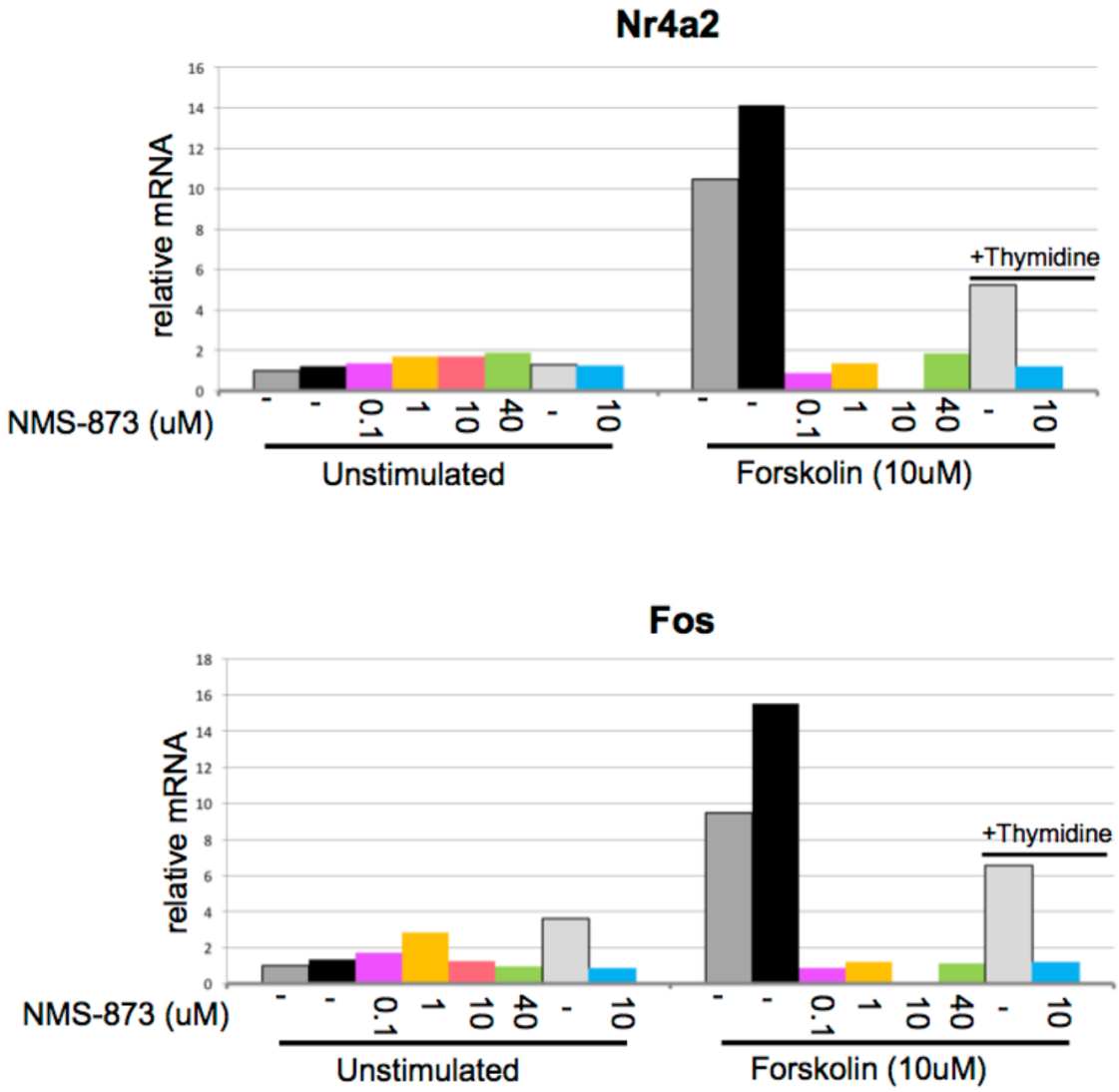

Supplemental Figure 4. NMS-873 inhibits Forskolin-induced transcription in HEK293T cells.

(top) Nr4a2 mRNA levels under un- and Forskolin- stimulated (30-minutes) following pre-incubation with NMS-873 at the indicated concentrations. (bottom) as in (top) but for Fos mRNA. (n=1 replicate). Bars beneath "+Thymidine" are from samples in which cells were treated with 2.5mM thymidine to arrest cellular division.

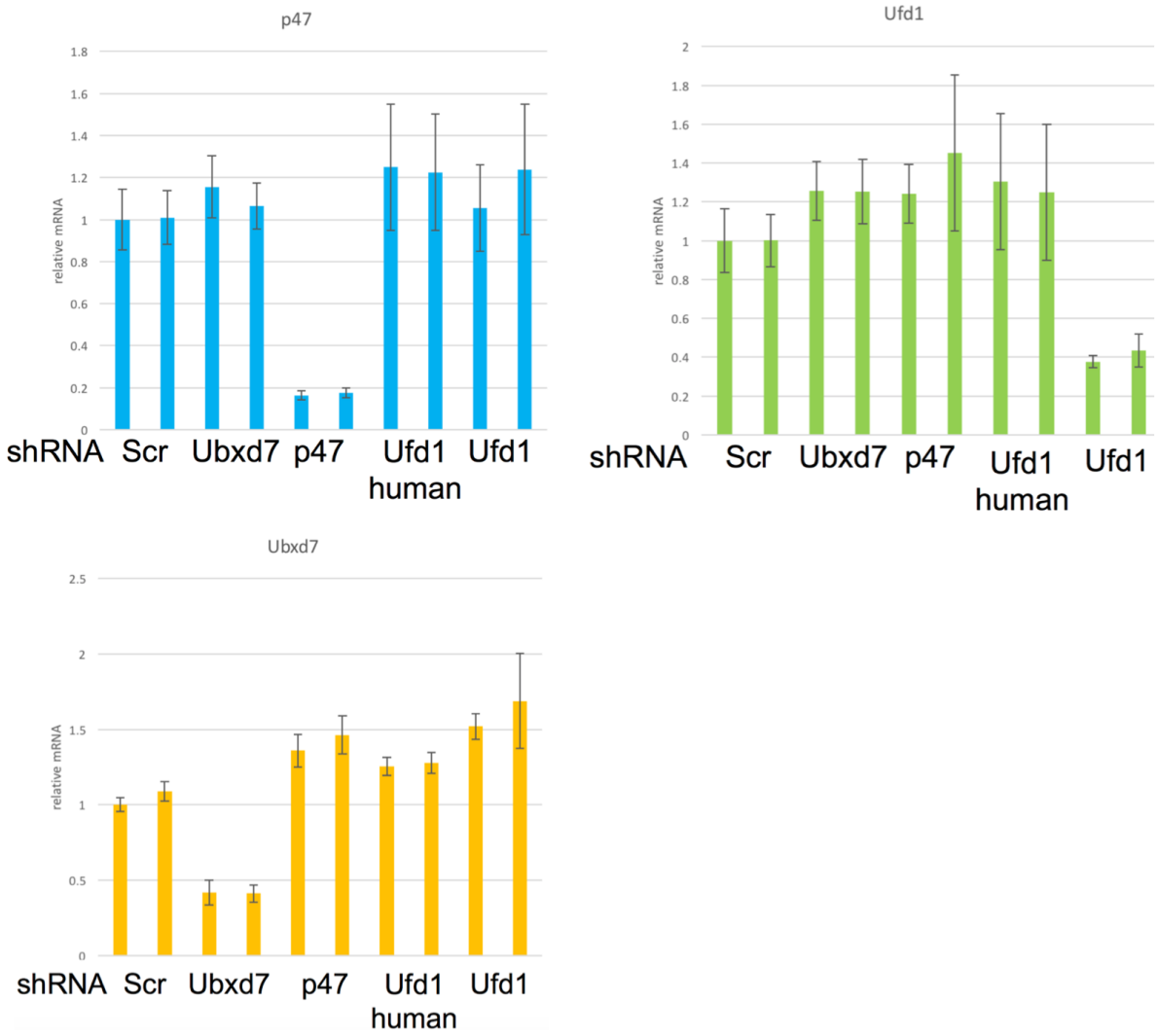

Supplemental Figure 5. shRNA knockdown of p97/VCP co-factors and UBX-adaptor proteins.

qPCR measurements of target mRNAs (top left = p47 ; top right = Ufd1l ; bot left = Ubxd7), normalized to Tubb3 control mRNA. Shown are mean values +/- SEM. (n=4 replicates).

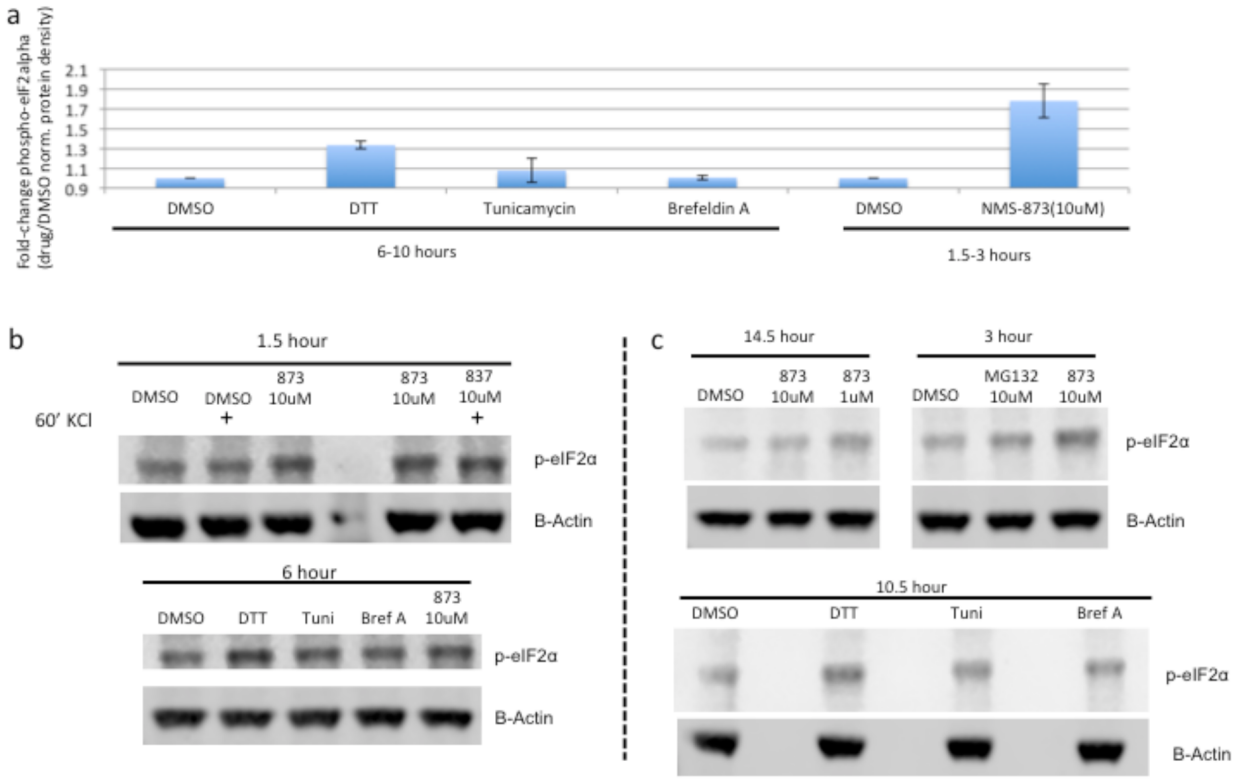

Supplemental Figure 6. Comparison of phospho-eIF2alpha induction between NMS-873 and UPR activators.

Summary Western blot values, normalized protein density presented as mean +/- SEM (n=3 replicates DMSO/DTT/Tuni/Bref, n=2 replicates DMSO/NMS-873). Values shown relative to average of DMSO condition. Duration of drug treatment shown beneath treatment labels. (b,c) Representative images of p-eIF2alpha blotting across UPR-activators and NMS-873. (b) and (c) represent independent biological replicates.

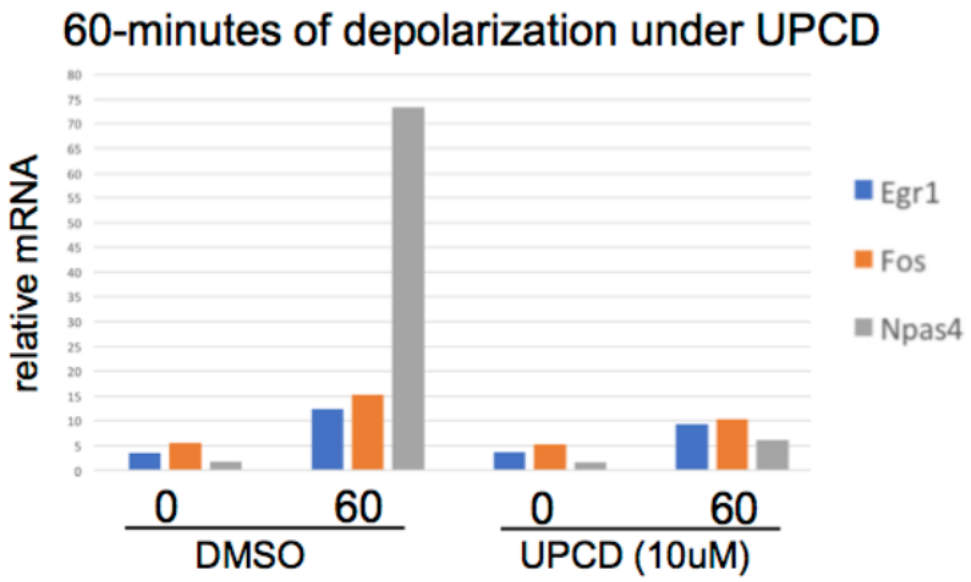

Supplemental Figure 7. Allosteric P97 inhibitor UPCD30245 inhibits neuronal activity-dependent transcription of immediate early genes.

As in Figure 30, but under 60-minutes KCl and with 5-min. pre-treatment with 10uM UPCD (n=1 replicate).

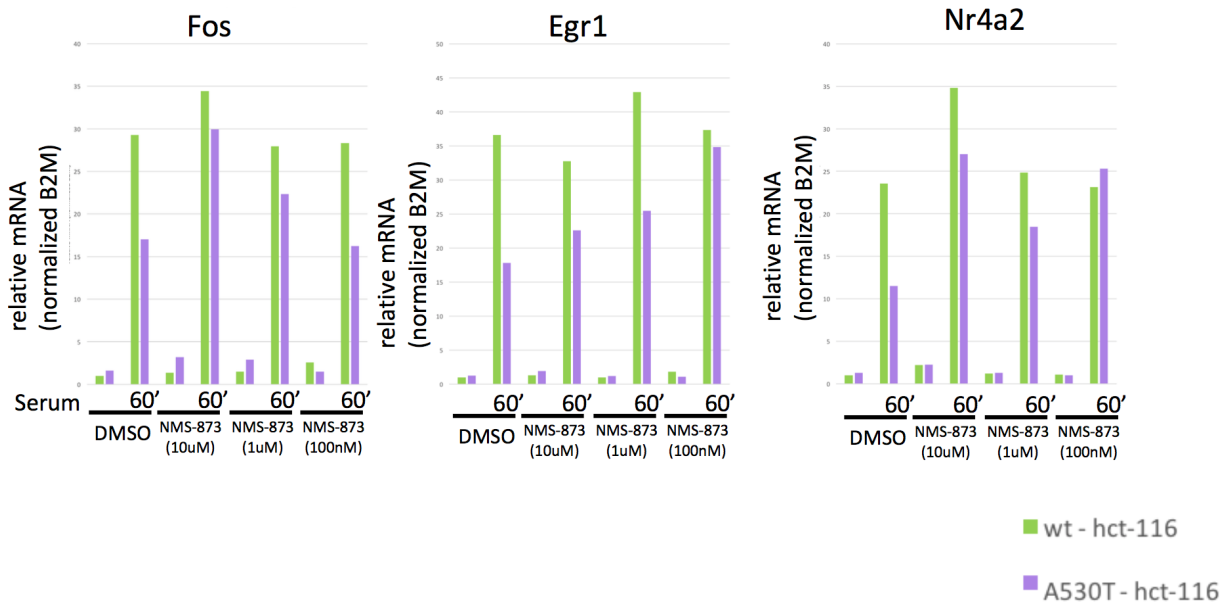

Supplemental Figure 8. Effects of NMS-873 treatment on immediate-early gene transcription following serum-stimulation of HCT-116 cells.

Wild-type and NMS-873-resistant (A530T-VCP) HCT-116 cell lines were pre-treated with NMS-873 and then stimulated with 10% FBS for 60-minutes. Shown are relative mRNA levels for three stimulus-dependent genes (Fos, Egr1, and Nr4a2). Values are normalized to B2M control mRNA and shown relative to unstimulated vehicle condition of the wild-type (wt) line. (n=1 replicate).

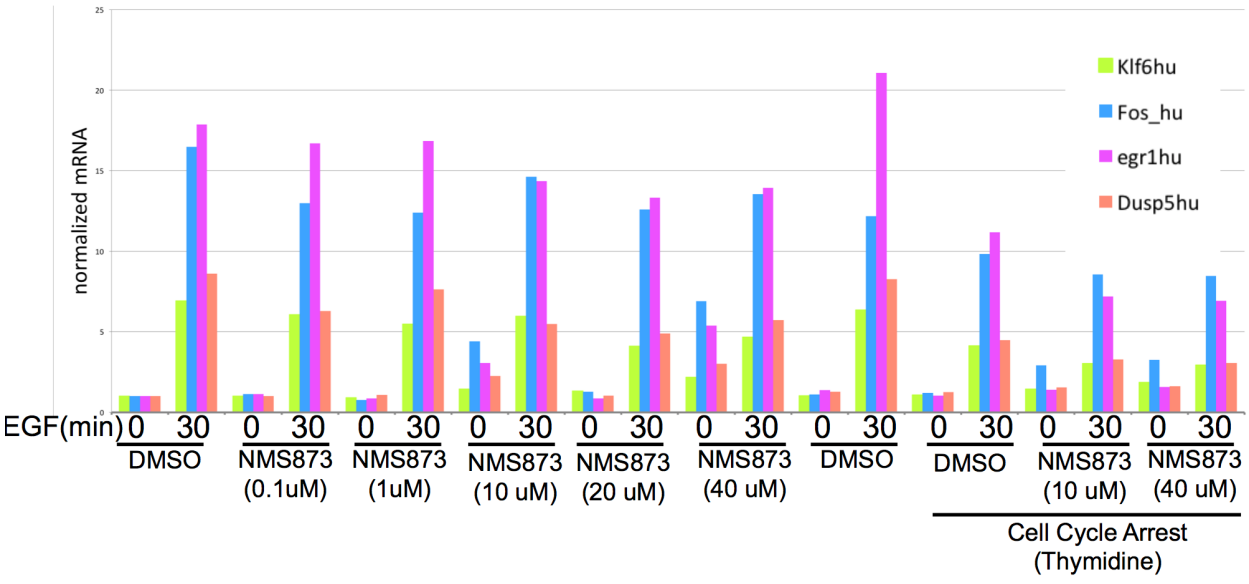

Supplemental Figure 9. Effect of NMS-873 on EGF-induced gene expression in HeLa cells.

Supplemental Figure 9. (Continued) Effect of NMS-873 on EGF-induced gene expression in HeLa cells. HeLa cells were pre-treated for 30-minutes with vehicle or NMS-873 at the indicated dose. They were then stimulated with epidermal growth factor (EGF) for 30-minutes. Shown are qPCR measurements of indicated mRNAs (Klf6, Fos, Egr1, Dusp5). On right, cells were pre-treated with thymidine to arrest cell cycle. (n=1 replicate).

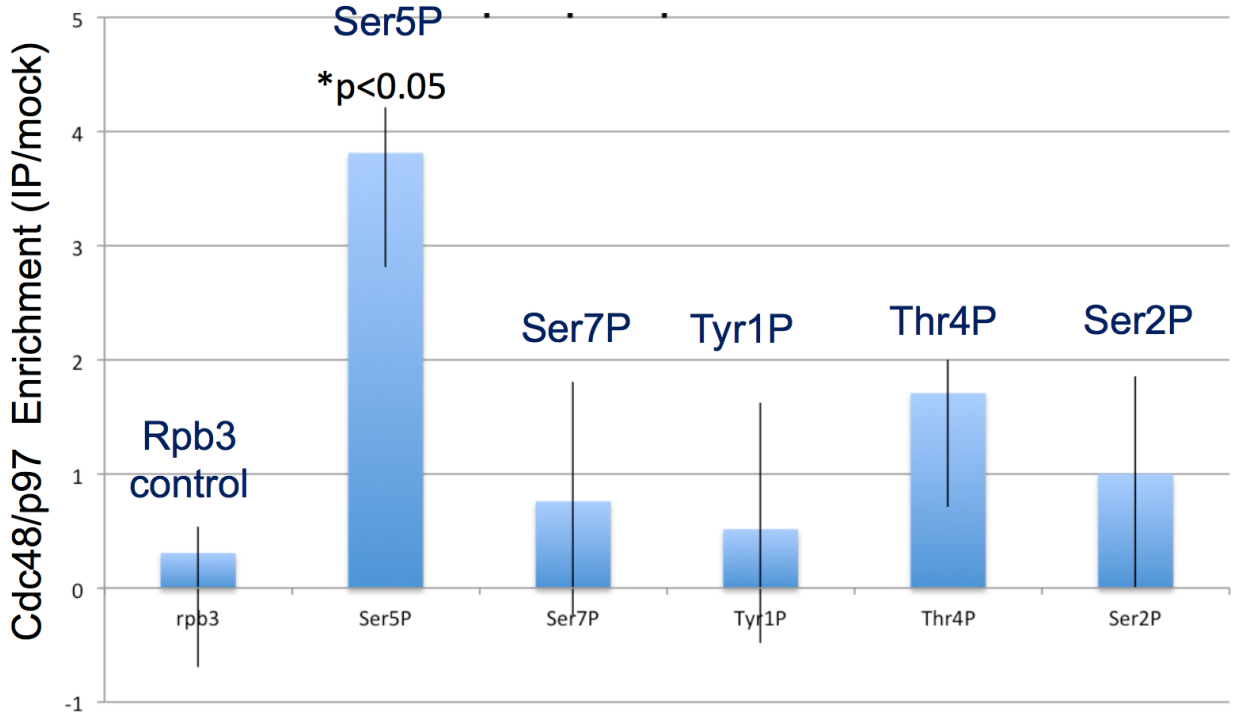

Supplemental Figure 10. yeast Cdc48/p97 immuno-precipitates selectively with RNA Polymerase II complexes possessing Serine-5 phosphorylation of the RNA Polymerase II CTD.

Relative enrichment of Cdc48 in the indicated RNAPII complexes, from immune-precipitates generated using antibodies selective for the indicated CTD phosphorylation or Rpb3 control. Data from (Harlen et al., 2016)**.**